POLITECNICO DI TORINO

Corso di Laurea Magistrale in
Ingegneria Energetica e Nucleare

Tesi di Laurea Magistrale

Lunar Base: power generation and thermal control system design

Relatore
Prof. Marco Carlo Masoero

Secondo Relatore
Ing. Giuseppe Gervasio

Co-relatori
Ing. Marco Cimino
Ing. Gabriele Cecchini

Candidato
Angelica Peressotti

Politecnico di Torino
6 Dicembre 2018

Abstract

This thesis is a preliminary study for a future human return to the Moon and a construction of a lunar base. The reasons are multiple, but the most important one is a scientific objective. This can lead to a deeper knowledge of our natural satellite, how it was created, what is evolution of Earth-Moon system and the origin of rocky planets. The lunar surface also contains information of inner Solar system process, linked for example to the water analysis. Water was in fact deposited on the Moon about 4 billion years ago from the impact of comets and asteroids and this happens also for Earth. Some of these objectives can be achieved robotically with in situ measurements and experiments, but the perspective is also a human contribution. Obviously, there will be different construction phases that will bring to the operative and autonomous lunar base. The scope of this work is the analysis of a power generation and thermal control system for a fully operative Moon base.

First of all, it was done a data collection of power and thermal system for different space mission in order to understand what the most used ones are. Then it was performed the system power budget, based on International Space Station to have a better feeling of how much power is necessary to sustain life and perform scientific objectives, that is about 54 kW_e for the day and 17 kW_e for the night. The power source selection was done once having defined the time mission and, for a 10-year period with that power requirements, the suggested solution is solar photovoltaic and nuclear source.

It is then presented a state of art of the main nuclear power technologies used for space applications. They can be divided into two main categories: Radioisotope Power System (RPS) and Fission Power System (FPS). The first one relies on radioactive material heat release, the second one on fission reaction. In both cases, the heat is converted into electricity with a static or dynamic conversion system. The static energy conversion, i.e. no moving parts, involves the use of thermocouples that exploit Seebeck Effect: in an electrical circuit formed by two different conductors, or semiconductors, a temperature gradient can generate a current. In this case, the system is known as RTG, or Radioisotope Thermoelectric Generator. The dynamic energy conversion involves the use of a working fluid and a heat engine. The heat is converted into mechanical energy

and then into electricity. The most used thermodynamic cycles are Rankine, Bryton or Stirling. In space application, Stirling cycle is the most common, and the system is named therefore Stirling Radioisotope Generator (SRG).

Once having defined the landing site (South Pole – North Haworth in this case), it is possible to establish the night length and minimum and maximum temperature. The project data are therefore T_{max}=300 K, T_{min}=120 K and 180 hours night duration. The so low temperature and the relatively long night duration are the constrains that mostly influences the selection of the power sources, the energy storage and the Thermal Control System (TCS) design. For the Electrical Power System design a combination of Advanced Stirling Radioisotope Generator (ASRG) and solar cells were chosen.

One of the most important figures of merit in space applications is the mass of the system, and for each project the maximum launchable mass is established by the capability of the chosen launcher. In terms of power system dimensioning, the sizing case for the selected mission profile is represented by the power demand of the overall system during the night period, due to the fact that the solar array is not working. The analysis was performed varying the power supplied from the ASRG from 0 to 17.2 kW, the night maximum electrical power load required, and calculate, consequently, the number of batteries required and the PV area. At the end, it was obtained the mass budget of the EPS power and storage. The PV mass is almost constant, and the ASRG mass increases less than the decrease of batteries mass curve. It is clear that, by taking into account only the mass as figure of merit, the best configuration would be the one without considering the presence of batteries. However, it is fundamental to highlight that the ASRG technology is relatively new for the space market, while the energy storage based on batteries has a strong heritage. These considerations bring to the conclusion that a power system design based only on ASRG without any energy storage capability would be a too risky design option. The working point was chosen at 93 % of power supplied by ASRG, where the battery and radioisotope generator masses are almost the same. The mass budget is 5 tons and the 40.8% is due to batteries, 44.7 % to ASRG and 14.5 % to PV cells. This can permit a diversification in the power system. To compensate a possible ASRG failure (20 % power loss as hypothesis) and a peak power demand, the batteries were oversized, and the results is a 10 tons total mass, where the 70 % is due to batteries. It was also investigated the flywheel storage technologies. The energy density is bigger, and a 62 % mass reduction can be provided but the technology is not enough mature and needs further studies and investigations.

The last chapter is dedicated to the thermal control system. The idea behind that is to use the waste ASRG heat at 90 °C, coming from Stirling engine, to cover totally or partially the heat base load. The structure and stratigraphy were taken by ESA Aurora program. The thermal load was calculated, and results is 4.3 kW_{th} in the worst case, when the outer temperature is 120 K and no internal gains are considered. The ASRG has a 30% efficiency and, therefore, the heat rejected is around 37.3 kW. Supposing to be able to harvest the 50% of that power, a feasibility study was carried out to understand how much power and at what temperature the heat can be transfer. The

layout consists of two loops. The first one links the source with a heat exchanger which interfaces with the moon base, the second one with radiator panels. This configuration permits to reject all the excess ASRG heat in case if it's not necessary to provide that. The study was carried out as a parametric analysis, varying the heat transfer fluid flowrate. A minimum quantity must circulate in the radiators' loop to prevent fluid from freezing inside that. A lumped parameter model was used to calculate the outlet fluid temperature. With these hypotheses, investigating different heat transfer fluids, it's possible to see if the requirements are covered and in what percentage. The most used Thermal Control System fluids in space applications are Ammonia, Ethoxy-nonafluorobutane (HFE), water and a mixture of water and glycol (47 % by volume of $C_3H_6(OH)_2$). The first was excluded due to its toxicity and its boiling point at ambient pressure (-33.4 °C), the second because boils at 76 °C at 1 atm. The loop was considered not buried, due to accessibility in case of failure. From the calculus it's possible to see that water and a mixture of water and glycol are almost equivalent. The difference is the freezing temperature, -56 °C for the mixture and 0°C for pure water, both at ambient pressure. Therefore, it's reasonable to choose the mixture of water and glycol. In this way, if a minimum flowrate is guaranteed, the thermal load can be covered at all. With a 600 kg/h flowrate, the outlet fluid temperature is 75.9 °C, and the power loss is 24.3 W/m. In addition to this preliminary study, for the complete Thermal Control System design, it will be necessary to investigate operative temperature range of the electronic equipment and associated thermal power. Once having choose the secondary heat transfer fluid (air/water), it will be possible to size the heat exchanger between source and base, the return pipe and the radiator panels at the nominal flow rate. Final step would be to dimension the pump electrical power demand with the end-to-end TCS mass and power budget.

This is a preliminary model, and further considerations should be done, also in terms of safety and reliability. Some assumptions have to be confirmed with other investigations, for example the presence of water and its distribution at South pole. Therefore, this is possible only with Moon exploration and data collection. Surely, in the next future, technologies will improve mainly in energy and power density with a consequent significant mass reduction. This thesis can represent a starting point in Moon manned missions. Other power configurations must be studied in order to understand what the best solution is.

Acknowledgment

I would like to thank Prof. M. Masoero of the Energy Department at Politecnico di Torino for his time and courtesy. I would like to acknowledge Ing. Giuseppe Gervasio and Ing. Marco Cimino for assisting me in this work thesis. I would also to thank Ing. Gabriele Cecchini for helping me and for having find always a solution at my problems, and Ing. Paolo Vaccaneo for the precious time spent with me. Last, but not least, I want to acknowledge my parents for the encouragement and for having always supported me, and my sister Fabiana for stimulating me in every situation. I would also thank Alessandro, for his infinite patience and for having always been with me these years.

That's one small step for a man, one giant leap for mankind.
Neil Armstrong

Contents

List of Tables

List of Figures

Acronyms

AC	Alternating Current
AM	Air Mass
ARTG	Advanced Radioistope Thermoelectric Generator
ASRG	Advanced Stirling Radioisotope Generator
AU	Astronomical Unit
BCDU	Battery Charge/Discharge Unit
BGA	Beta Gimbal Assembly
BOL	Begin of life
CNSA	China National Space Administration
DC	Direct Current
DCSU	Direct Current Switching Unit
DDCU	Dc/Dc Converter Unit
DOD	Depth of Discharge
DOE	Department of Energy
e-MMRTG	Enhanced-Multi Mission RTG
EOCV	End Of Charge Voltage
EOL	End of life
EPS	Electrical Power System
FPS	Fission Power System
FW	Flywheel
GPHS-RTG	General Purpose RTG
ISS	International Space Station
JAXA	Japan Aerospace Exploration Agency
MBSU	Main Bus Switching Unit
MLI	Multi-Layer Insulation

NASA	National Aeronautics and Space Administration
NPS	Nuclear Power System
ORU	Orbital Replacement Unit
PCDU	Power Conditioning and Distribution Unit
PV	Photovoltaic
PVA	Photovoltaic Assembly
RHU	Radioisotope Heater Unit
RPDA	Remote Power Distribution Assembly
RPS	Radioisotope Power system
RTG	Radioisotope Thermoelectric Generator
SA	Solar Array
SoA	State of Art
SPDA	Secondary Power Distribution Assembly
SSU	Sequential Shunt Unit
TBD	To Be Determined
TCS	Thermal Control Subsystem
TCS	Thermal Control System
WEB	Warm Electronic Box
WRC	World Radiometric Center

Nomenclature

A_{sa}	Solar array area
c_p	Specific heat
E_{bat}	Battery energy
E_{BTA}	Stored energy
E_{cell}	Cell energy
E_{FW}	Flywheel energy
h	convective heat transfer coefficient
h_{in}	Internal heat transfer coeffcient
h_{night}	Night hours
I_d	Inherent degradation
I_{mp}	Maximum Power current
I_{sc}	Short Circuit voltage
k	Thermal conductivity
L_d	Power degradation factor
m_{cel}	Cell mass
$\dot{m}$	Mass flowrate
N_p	Number of parallel cells
N_s	Number of series cells
Nu	Nusselt number
P_{el}	Electrical power
Pr	Prandtl number
P_s	Specific power
P_{sa}	Solar array power
P_{tot}	Total power
Q_{lin}	Linear power

Q_{rad}	Radiative power
Q_{tot}	Total power dissipated
$\dot{Q}_{th}$	Thermal power
Re	Reynolds number
T_{amb}	Ambient temperature
T_c	Temperature cold
$T_{f,o}$	Outlet fluid temperature
T_h	Temperature hot
T_{in}	Internal temperature
T_{in}	Inlet temperature
T_{max}	Maximum Temperature
T_{min}	Minimum Temparture
$T_{MLI,e}$	MLI external temperature
$T_{out,wc}$	Outlet temperature – worst case
v	Velocity
V_{bus}	Bus tension
V_{mp}	Maximum Power voltage
V_{oc}	Open Circuit voltage
W_e	Electrical Watt
W_{th}	Thermal Watt
ΔT_{max}	Maximum temperature gradient
η_{th}	Thermal efficiency
μ	Dynamic viscosity
ρ	Density

Introduction

Space exploration permits to humankind to understand the history of the Universe and of our solar system, but also the development of new technologies and instrumentations that helps to improve life on Earth. The first step towards the space was done with the launch of a soviet satellite, the Sputnik, in 1957. The first man to journey in outer space was Jurij Gagarin in 1961, who completed an entire elliptical orbit of the Earth. After about 50 years from the Apollo 11 mission that lead the first man on the Moon, the next significant milestone will be to come back and establish a permanently manned lunar base. The implementation of different technologies to support human life in low Earth orbit, as the International Space Station, is the first step towards the Moon, or maybe Mars. Lunar environment is hostile, and this is the bigger challenge to overcome. The development of a lunar base can permit scientific research and better understanding of how our closest neighbour was formed, what is the composition and structure of the crust and if it is internally active or not. Moreover, it will lead to the technology's evolution in space transportation.

The thesis was developed at Thales Alenia Space in Turin in the period May-November 2018. The objective is the design of a power system (in charge of power generation, conditioning, storage and distribution) and thermal harvesting system for a lunar outpost. It was assumed that a previous robotic phase was already been implemented. The power system design flow was carried out through the following steps:

1. Requirement consolidation: collect relevant requirements from several types of missions
2. Compilation of technology and capability inventory: technologies relevant for low temperature power system design and long mission duration
3. Power system trade offs, simulation and selection of the final option
4. Thermal control system design

The thesis is divided into the following chapters.

Chapter 1: Mission analysis
The first chapter is an analysis of some relevant interplanetary missions, from the Moon to Pluto, comets and asteroids, studying the power generation systems, electrical storage and thermal control system used for the mission.

Chapter 2: Electrical Power Systems
In the second chapter there are presented the basic concepts of the Electrical Power System, with a focus on Power Conditioning and Distribution Units, the main part of whatever space Electrical system.

Chapter 3: Moonbase design
In the third chapter are presented the power budget of a lunar base and the power sources options suitable for the mission.

Chapter 4: Nuclear power technology
The fourth chapter it's presented the state of art of nuclear power systems for space applications, useful for the power design.

Chapter 5: Power source and energy storage sizing
In this chapter, it's performed the design of the electrical power system, mainly focusing on the power generation and electrical storage architecture.

Chapter 6: Thermal control system
The sixth chapter is on the lunar base thermal control system, with the hypothesis of harvest heat from the nuclear system used for the power generation.

Chapter 7: Conclusion

Chapter 1

Mission analysis

The analysis was performed with two main purposes:

- to collect data of the technologies used in space application for power generation and thermal control.
- To collect the major environmental parameters which will drive the design phase once the mission profile will be selected

It involves some relevant interplanetary missions, such as the Moon, Mars, the outer planets (Jupiter, Saturn, Uranus, Neptune), Pluto, comets and asteroids.

1.1 Moon

The Moon exploration began with the impact of a soviet probe, Luna 2 in 1959. The first mission that successfully land human on the lunar soil was the NASA's Apollo in 1969. From this point, an increasing interest was developed for our natural satellite.

	Moon	**Earth**
Mass (10^{24} kg)	0.07346	5.9724
Equatorial radius (km)	1738.1	6378.1
Mean density (kg/m^3)	3344	5514
Surface gravity (m/s^2)	1.62	9.80
Bond albedo	0.11	0.306
Geometric albedo	0.12	0.434
Solar irradiance (W/m^2)	1361.0	1361.0
Black body Temperature (K)	270.4	254.0
Length of day (hours)	708.0	24.000
Length of night (hours)	354	12
Average Temperature (K)	147	288

Table 1 - Moon bulk parameters

The atmosphere is mainly composed by Helium (40000 particles/ cm^3), Neon (40000 particles/ cm^3), Hydrogen (35000 particles/ cm^3) and Argon (particles/ cm^3).

The missions analysed are:

- Apollo Program (Apollo 13, Apollo 14, Apollo 15) – NASA, 1969-1972
- Chang'e Program (Chang'e 3) – CNSA, 2013
- Next Lunar Lander and Rover
- Lunar Polar Volatile Explorer – NASA, 2018-2023
- Sample and Return mission
- Selene (Selene 2) – JAXA, TBD

The results are summarized in Figure 1 and Figure 2.

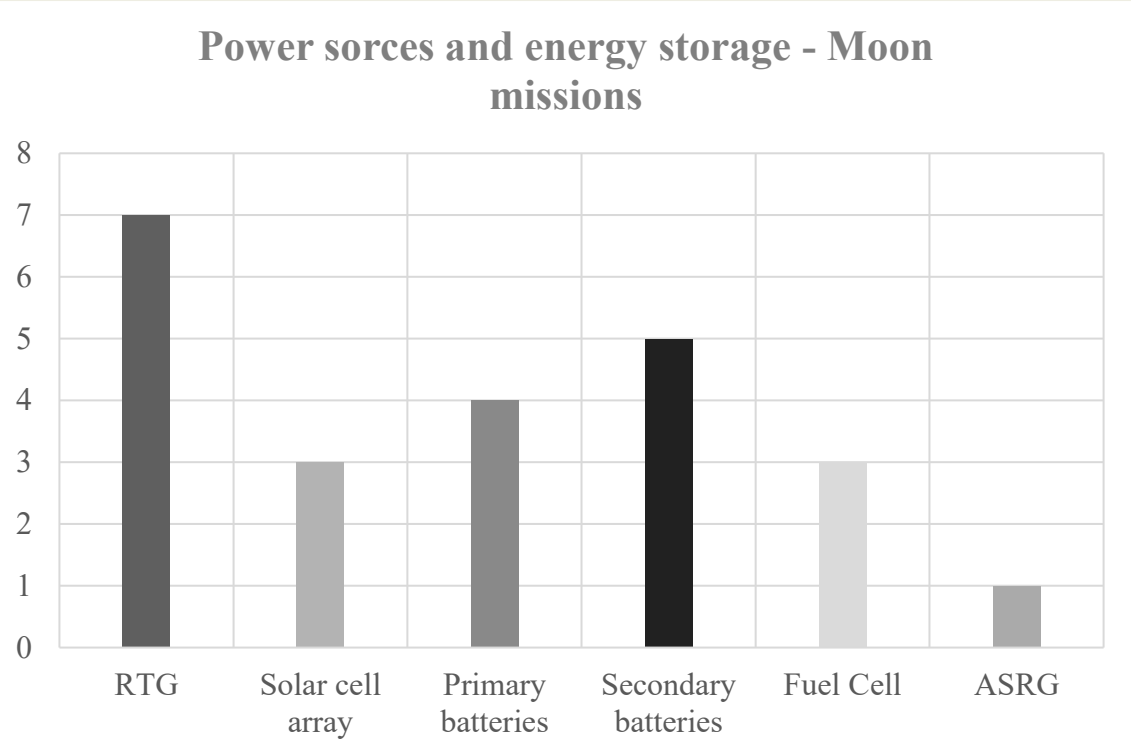

Figure 1 - Moon mission power source and storage

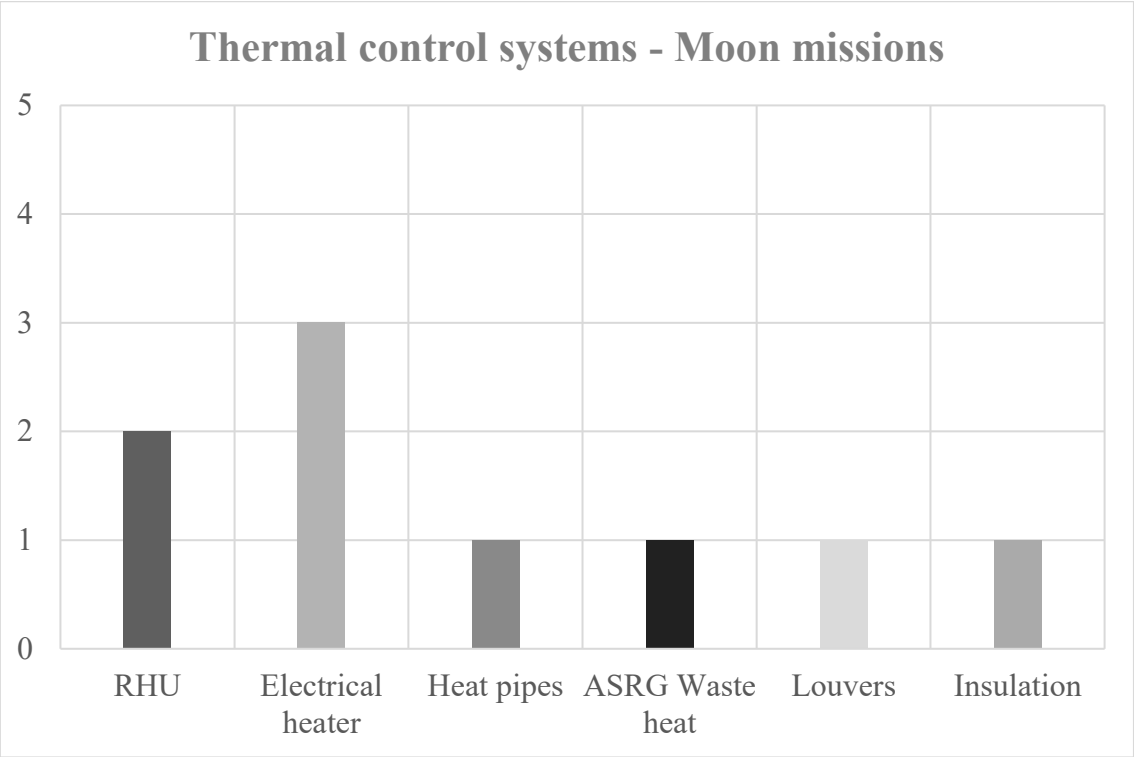

Figure 2 - Moon missions Thermal Control Systems

1.2 Mars

Mars has a harsh environment, with extremes temperature, dust storms and high radiation levels from space. The exploration of the red planet began in the late 20th century, when different probes were sent to the red planet. The main focus is the understanding of Mars geology and the habitability potential. The first landing probes were Mars 2 and Mars 3 lander by Soviet Union in 1971.
The atmosphere is mainly composed by Carbon Dioxide (95.32 % by volume). The rest is a mixture of Nitrogen, Oxygen, Argon and Carbon Monoxide.

	Mars	**Earth**
Mass (10^{24} kg)	0.64171	5.9724
Equatorial radius (km)	3396.2	6378.1
Mean density (kg/m^3)	3933	5514
Surface gravity (m/s^2)	3.71	9.80
Bond albedo	0.250	0.306
Geometric albedo	0.170	0.434
Solar irradiance (W/m^2)	586.2	1361.0
Black body Temperature (K)	209.8	254.0
Length of day (hours)	24.6597	24.0000
Length of night (hours)	12	12
Average Temperature (K)	210	288
Diurnal Temperature range (K)	184-242	283-293
T_{min} (K)	150	185
T_{max} (K)	303	331

Table 2 - Mars bulk parameters

The analysis was performed for:

- Vikings 1 & 2 – NASA, 1972
- Mars Pathfinder – NASA, 1997
- Mars Exploration Rover – NASA, 2003 but still active
- Phoenix – NASA, 2007
- Mars Science Laboratory (Curiosity Rover) – NASA, 2011 but still active
- Mars Express (Beagle 2 rover) – ESA, 2003 but still active
- Exo Mars (Schiaparelli lander) – ESA & Roscosmos, 2016

1.3 Jupiter

Jupiter, known as the gas giant planet, is the biggest object in the solar system, with the sun exception. The equator radius is more than 10 times the Earth one. Jupiter is five times farther from the sun than Earth's location. This implies a sun sunlight reduction of 25 times. Due to high pressure inside its atmosphere, the latter is made up of mostly hydrogen gas and helium gas, like the sun: the composition in average is 89.8 % by volume of Hydrogen and 10.2 by volume of Helium. Jupiter has a powerful magnetic field, like a giant magnet.
From 1979 to 2007, eight NASA spacecrafts studied Jupiter: Pioneer 10, Pioneer-Saturn, Voyager 1, Voyager 2, Ulysses, Galileo, Cassini and New Horizons.
The Ulysses, Cassini and New Horizons missions flew by Jupiter on their way to planets and locations farther in the solar system.

	Jupiter	**Earth**
Mass (10^{24} kg)	1898	5.9724
Equatorial radius (km)	71492	6378.1
Mean density (kg/m^3)	1326	5514
Surface gravity (m/s^2)	24.79	9.80
Bond albedo	0.343	0.306
Geometric albedo	0.538	0.434
Solar irradiance (W/m^2)	50.26	1361.0
Black body Temperature (K)	109.9	254.0
Length of day (hrs)	9.9259	24.0000
Average Temperature (K) @ 1 bar	165	288
Average Temperature (K) @ 0.1 bar	112	-

Table 3 - Jupiter bulk parameters

The analysis was performed for:

- Pioneer 10 & 11 – NASA, 1972
- Voyager 1 & 2 – NASA, 1977
- Galileo – NASA, 1989
- Ulysses – NASA & ESA, 1990
- Cassini-Huygens – NASA/ESA/ASI, 1997
- New Horizons – NASA, 2006
- Juno – NASA, 2011
- Juice – ESA, 2022

1.4 Saturn

Saturn is the second largest planet, after Jupiter. The radius is about 9 times the one of Earth. Being a gas giant, it is characterized by a density smaller than Earth one. It' s mainly known for its big ring system, mainly composed by icy particles.

	Saturn	**Earth**
Mass (10^{24} kg)	568	5.9724
Equatorial radius (km)	60268	6378.1
Mean density (kg/m^3)	687	5514
Surface gravity (m/s^2)	10.44	9.80
Bond albedo	0.342	0.306
Geometric albedo	0.499	0.434
Solar irradiance (W/m^2)	14.82	1361.0
Black body Temperature (K)	81	254.0
Length of day (hours)	10.7	24.0000

Table 4 - Saturn bulk parameters

The missions considered are:

- Pioneer 11 – NASA, 1972
- Voyager – NASA, 1977
- Cassini-Huygens – NASA/ESA/ASI, 1997

1.5 Uranus

Uranus is the third largest planet in the solar system. The atmosphere is mostly composed by Hydrogen (85.5 % by volume), Helium (15.2 % by volume) and Methane (2.3 % by volume).

	Uranus	Earth
Mass (10^{24} kg)	86.813	5.9724
Equatorial radius (km)	25559	6378.1
Mean density (kg/m^3)	1271	5514
Surface gravity (m/s^2)	8.87	9.80
Bond albedo	0.3	0.306
Geometric albedo	0.488	0.434
Solar irradiance (W/m^2)	3.69	1361.0
Black body Temperature (K)	58.1	254.0
Length of day (hours)	17	24.0000

Table 5 - Uranus bulk parameters

The analysis was based on the following missions:

- Voyager – NASA, 1977
- Pathfinder – ESA, 2021
- Upsilon – NASA, 2021
- Oceanus – NASA, 2030
- Muse – ESA, 2019

1.6 Neptune

Neptune is the fourth largest planet in the solar system and it's the farthest one. The atmosphere is composed mainly by Hydrogen (80 % by volume). The rest is Helium (19 % by volume) and Methane (1.5 % by volume). NASA, ESA and independent academic groups have proposed future scientific missions to visit Neptune. Some mission plans are still active, while others have been abandoned or put on hold. Voyager 2 is the only spacecraft to visit Neptune, in 1989.

	Neptune	Earth
Mass (10^{24} kg)	102.413	5.9724
Equatorial radius (km)	24764	6378.1
Mean density (kg/m^3)	1638	5514
Surface gravity (m/s^2)	11.15	9.80
Bond albedo	0.290	0.306
Geometric albedo	0.442	0.434
Solar irradiance (W/m^2)	1.508	1361.0
Black body Temperature (K)	46.6	254.0
Length of day (hrs)	16.11	24.0000
Length of night (hrs)	8	12
Average Temperature (K) @ 1 bar	72	288
Average Temperature (K) @ 0.1 bar	55	

Table 6 - Neptune bulk parameters

The past and future missions analysed are:

- Voyager – NASA, 1977
- Neptune orbiter – NASA, TBD
- Triton hopper – NASA,TBD
- Argo – NASA, TBD
- OSS mission – ESA/NASA, TBD

1.7 Pluto

Originally classified as planet, Pluto was discovered in 1930. In 2006 it has been classified as a dwarf planet, following the introduction of a formal definition of "planet". With a mean distance from the sun bigger than 5 billion kilometres, exploring Pluto is always a challenge. New Horizons is the only space probe to have reached it, in 2015 as part of NASA program.

	Pluto	**Earth**
Mass (10^{24} kg)	0.01303	5.9724
Equatorial radius (km)	1187	6378.1
Mean density (kg/m^3)	1860	5514
Surface gravity (m/s^2)	0.62	9.80
Bond albedo	0.72	0.306
Geometric albedo	0.52	0.434
Solar irradiance (W/m^2)	0.873	1361.0
Black body Temperature (K)	37.5	254.0
Length of day (hours)	153.2820	24.0000
Length of night (hours)	76.5	12

Table 7 - Pluto bulk parameters

1.8 Comets and Asteroids

Comets and asteroids have always fascinated the human kind. Their exploration began in late 20th century and, thanks to the study of their dimensions, chemical composition and spatial distribution, we can have more information about our solar system and its origin. The missions analysed are:

- Clementine (Asteroid) – NASA, 1994
- Near Shoemaker (Asteroid) – NASA, 1996
- Hayabusa (Asteroid) – JAXA, 2003
- Minerva (Asteroid) – JAXA, 2003
- Osirix-Rex (Asteroid) – NASA, 2016
- Psyche (Asteroid) – NASA, 2022

- ISEE-3 (Comet) – NASA, 1978
- VEGA (Comet) – Soviet Union et al., 1985
- Giotto (Comet) – ESA, 1985
- Deep space 1 (Comet) – NASA, 1998
- Stardust (Comet) – NASA, 1999
- Contour (Comet) – NASA, 2002
- Rosetta (Comet) – ESA, 2004
- Philae – Rosetta's lander (Comet) – ESA, 2004
- Deep Impact (Comet) – NASA, 2005

1.9 Outcomes of the missions' survey

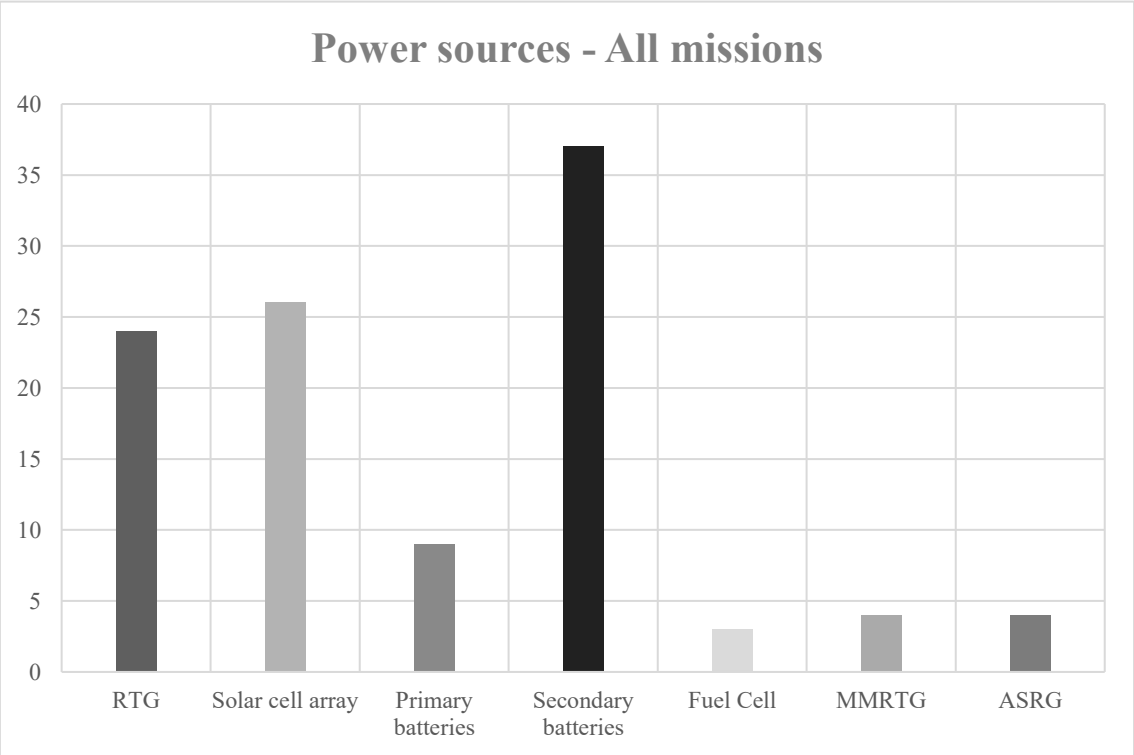

Figure 3 - Histogram power sources

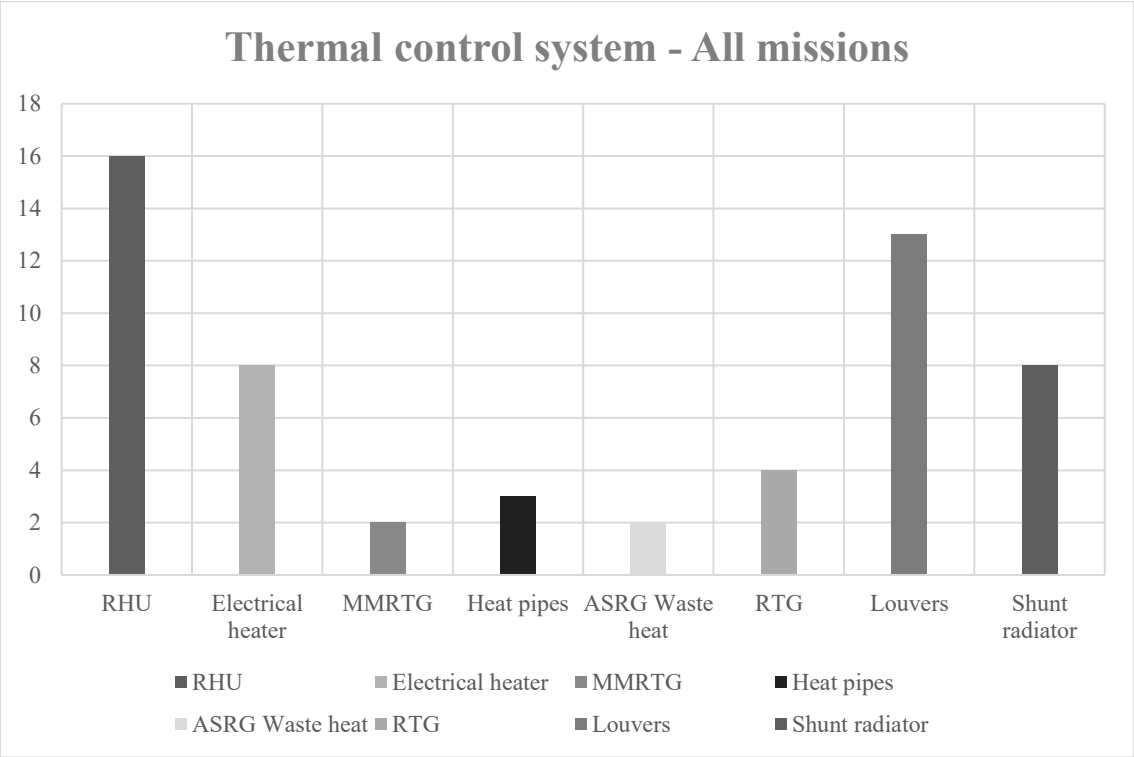

Figure 4 - Thermal control systems histogram

It is possible to see, from Figure 3, that the most used power generation technologies are solar panels and RTGs. For the electrical storage, the secondary batteries are the only technology employed till now. Figure 4 shows how thermal control system is mainly performed. To guarantee the optimal temperature conditions for batteries, payload and whatever technological instrument, the most common system used is RHU. The main reason is that it doesn't have impact on power budget. The second most used is electrical heater, mainly because of its higher flexibility and commandability, but with impact on system power demand. Louvers and shunt radiators permit to dissipate the excess heat. Only a little fraction of the missions takes in consideration the waste heat to keep everything in the optimal temperature range.

Chapter 2

Electrical power system (EPS)

Every space system and subsystem need to be fed by electrical power to implement the functions for what they are designed. The EPS is responsible for providing a safeguarded source of uninterrupted electrical power. It must also store, distribute and condition electrical energy and plays an important role in protecting both the system and the users (i.e. electrical equipments) from electrical hazards. In addition, it supports to manage the power/energy resource budget and the thermal control, and it provides the system grounding reference point.

2.1 EPS basic concepts

A space power system is similar to a terrestrial architecture to generate, store, control and distribute power to industrial or domestic users. The four main sections are:

- Power source
- Energy storage
- Power distribution
- Power regulation and control

The power distribution, regulation and control can be embedded in a unique item, known as PCDU (Power Conditioning and Distribution Unit). The power system functions are typically grouped into three main subsystems: primary power system, secondary power system and support system. As an example, it is reported the EPS architecture of ISS in Figure 5. When a typical satellite is considered, the EPS usually includes only the primary power system. This is due to the fact that a satellite is smaller and less power requiring; in this case, the functions belonging to the secondary power system are generated/distributed by the other subsystem and payloads.

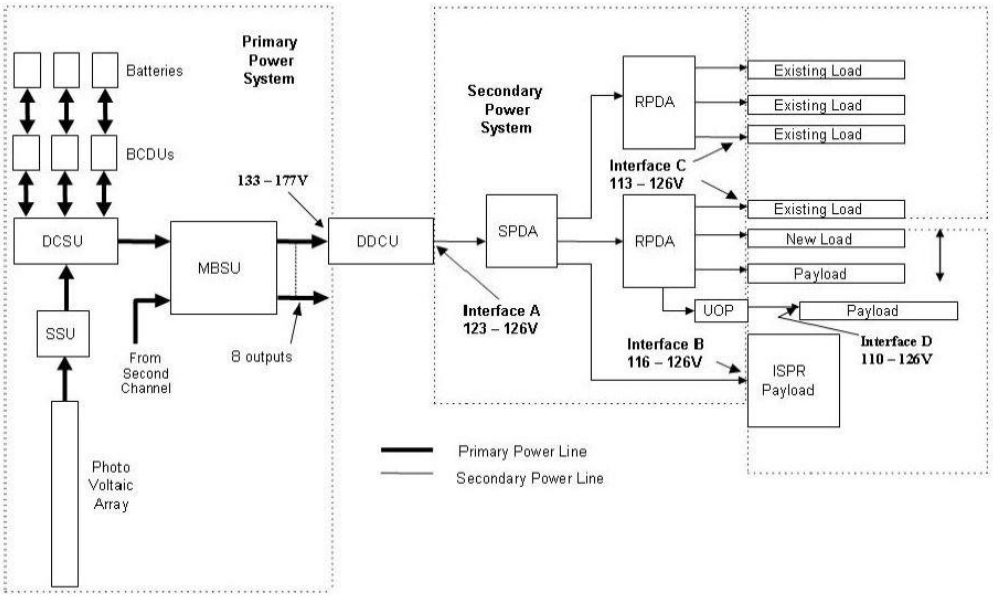

Figure 5 - ISS electrical power distribution overview

2.1.1 Primary Power System

The primary power system is responsible for the power generation, storage and distribution.

Power sources

There are mainly four power sources type used for space applications.

- Photovoltaic solar cells
- Static power sources
- Dynamic power sources
- Thermionic power sources

The most important one is photovoltaic solar cells. It converts incident solar radiation into electrical energy directly. Static systems rely mainly on thermoelectric convertors and nuclear sources. Dynamic systems start from a heat source also (nuclear or concentrated solar radiation) and use a Bryton, Stirling or Rankine cycle to convert it into electricity. Static and dynamic systems will be discussed in depth in Chapter 4. The thermionic energy conversion produces electricity thanks to a hot and cold electrode producing electrons flow from one to another, across ionized gas. Everything is inside a sealed enclosure.
Another power source that is becoming more popular is the fuel cell. It converts the chemical energy of a fuel (hydrogen) into electrical energy thanks to an oxidiser (generally oxygen). The related energy storage is hydrogen production.

Energy storage

Energy storage plays an important role in EPS systems. It must provide power for short missions (time mission less than one week) or back-up power for missions lasting more than one week. A further fundamental function consists in covering peak-power demand and supplying the spacecraft power need when the other sources are not available (e.g. during eclipses). A key role is played by electrochemical batteries, the most widely system used till now. The can be primary or secondary. The first ones convert chemical energy into electrical energy but it's not possible to reverse the reaction. They are typically used for shot time missions or only as a second source of energy. The most common are: Silver Zinc (AgZn), Lithium Manganese Dioxide (LiMnO2) and Lithium Sulfur dioxide (LiSO2).
The second ones are rechargeable batteries, with the advantage of being more cost efficient over long term. On the other hand, they have lower capacities, energy density and initial voltage, higher self-discharge rates and varying performance during charge/discharge cycles. The most commonly used are: Nickel Cadmium (NiCd), Nickel Hydrogen (NiH2) and Lithium Ion (Li-ion).
Energy can also be stored in mechanical form (kinetic) in flywheels. They are under development to support or substitute batteries in the next future.

Primary power distribution

The primary power distribution system is the interface between power generation and storage. The design is function of source characteristics, load requirements and subsystems functions.

ISS Primary Power system components

Referring to Figure 5, the ISS primary power system components are:

- Photovoltaic Assembly (PVA)
- Beta Gimbal Assembly (BGA)
- Sequential Shunt Unit (SSU)
- Direct Current Switching Unit (DCSU)
- Battery Charge/Discharge Unit (BCDU)
- Batteries
- Main Bus Switching Unit (MBSU)

The power is produced by a photovoltaic array. BGA is the hardware providing for array orientation and rotation around its long axis to track the Sun and maximize the power production. The PVA output voltage must be regulated, due to the performance characteristic of the solar cells. This function is performed by the SSU, that receives power from the PVA and maintains the output voltage within a specified range, defined as "primary power voltage". The BCDU is responsible for batteries' state of charge control. The primary power distribution is performed by DCSU: it provides fault protection for many EPS Orbital Replacement Units (ORUs) and support functions.

2.1.2 Secondary Power System

The conversion of primary power and its distribution to equipments, payloads, experiments, etc. belongs to secondary power system. These functions are implemented by means of Dc/Dc Converter Unit (DDCU) and Secondary/Remote Power distribution Assembly (SPDA/RPDA). The DDCU provides electrical isolation between the primary and the secondary power system. It is also responsible for DC power conversion through a transformer. The secondary power is therefore distributed to a network of ORUs called SPDA or RPDA.

2.1.3 Support Systems

In addition to power production, storage, conversion, and distribution functions, other supporting functions must be incorporated into the architecture to maintain the Power System:

- Thermal Control
- Command and control
- Systems Interfaces
- Harness

Thermal Control

PVAs are designed with their own Thermal Control System, composed of cooling devices (e.g. radiators) to dissipate the generated heat or sunshields to improve the protection level. Equipment (i.e. boxes) requires either heating devices (e.g. passive MLI blankets, powered heaters) or cooling systems (e.g. conduction toward a metallic surface, cold-plates with forced water loop) depending on their physical location.

Command & Control

Behind all of the Power System functions, C&C units/applications work to monitor and control the system operations. C&C is provided by software applications and hardware which provides system monitoring and reconfiguration capabilities from both on-board and the ground.

Systems Interfaces

The Power System has interfaces with other systems, both to provide power or receive necessary services (e.g. Guidance & Navigation Control to orient the Solar array wings, On Board Computers for command, monitoring, and data processing, STRUCTURE for physical installation).

Harness

Wiring/cabling and connectors are provided to allow the interconnections within the Power System and with the users to perform the power supply function. The design is specific for each project, based on the functional links and the physical layout.
Materials are selected from space-quality specifications (i.e. NASA SSQ, ESA SCC).

2.2 Power Conditioning and Regulation

Power conditioning and regulation functions are usually performed by a unique electronic unit, that is the PCDU (Power Conditioning and Distribution Unit). In addition. It has to provide power to the loads, managing the batteries, the EPS bus protection (over-voltage, Over-current, Under voltage, etc.) and the heating system, provide the command to the Electro-Explosive device (EED), used for example to deploy/detach items. PCDU's main functions are:

- To condition the power provided by the solar array
- To manage and survey the battery and power bus
- To provide power to the loads

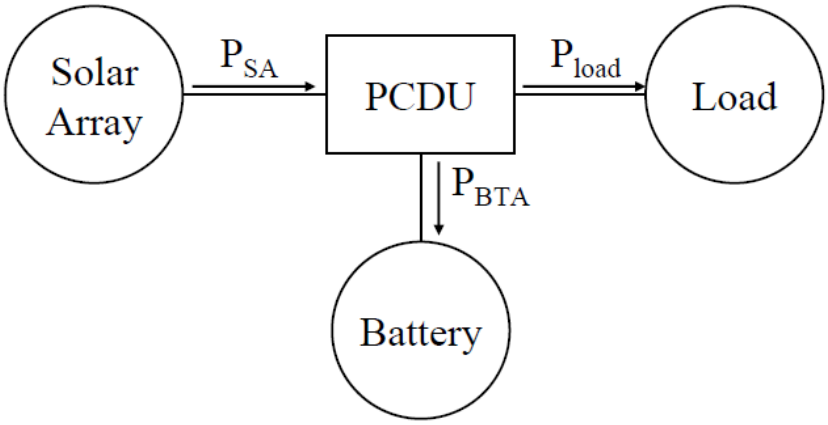

Figure 6 - EPS general layout

There are three main power distribution modes:

- Regulated (V_{bus} is constant)
- Sun-regulated (V_{bus} constant in sunlight and variable in eclipse phases)
- Unregulated (V_{bus} variable)

The fully regulated bus implies that all sources generated power is regulated. The Sun-regulated mode provides a regulated voltage bus during sunlit, while V_{bus} is determined by battery's voltage when system is in shade. In the last case, the bus voltage is determined by the battery. Each of these architectures presents pros and contra and a trade-off between them is usually performed during the preliminary phases of a project to evaluate which is the best design choice based on the specific mission.

2.3 Power system design process

The power system architecture definition is influenced by the following aspects:

- Mission operational modes
- Operative environment
- User needs
- Interfaces with other systems

The preliminary design process is composed by the following steps:

1. Identify the requirements:
   Select the mission type and the mission life; list all the electrical loads to build up the average and peak power demand profile.
2. Select and size the power source:
   From the power budget, it is possible to choose the power sources and size them at End of Life (EOL) conditions, taking into account their degradation throughout the overall mission.
3. Select and size the energy storage:
   The peak power demand and, in case of PV power source mainly, eclipse/night period determine the energy storage and its size.
4. Identify power regulation and control:
   The power sources, loads/thermal control requirements and mission life determine the PCDU architecture
5. Define the mass budget
   After the definition of the previous steps, a mass budget analysis is performed, or the total mass parameter necessary for the mission power requirements

The analysis performed in this thesis is mainly focused on the power sources and the electrical energy storage size, with the relative partial mass budget.

Chapter 3

Moon base design

The Moon is our closest neighbour. In a future prevision of a human expedition to Mars, it's necessary a deep development of instruments, technologies and techniques for long duration stay on other planetary surfaces. The Moon can become an intermediate stage and a sort of testbed for human missions.

3.1 Landing site

The south pole was chosen as mission landing site, and in particular North Haworth. This is due to the confirmed presence of water, mostly concentrated in coldest and permanently shadowed craters. The discovery was published in the Proceedings of the National Academy of Sciences from NASA's Ames Research Center, California. Water can be an in-situ resource for the lunar base astronauts and used as propellant, if divided in its main components: hydrogen and oxygen.

3.1.1 North Haworth

North Haworth has scientific interest and a longer period of daylight illumination. The Moon rotates on its axis every 708 hours (about 29 Earth days) and, on average, day and night lasts 14 days. The tilt axis is about 1.5° from the vertical and this cause permanently shadowed area, but also site illuminated for more than 70% of the time. The maximum temperature and the duration of the night are the design parameters for North Haworth site, in particular:

- T_{max} = 300 K
- h_{night}= 180 h

The data were acquired by LRO - Diviner Lunar Radiometer Experiment. The surface temperature map of the south polar region of the Moon refers to a period between September and October 2009, when south polar temperatures were close to their annual maximum values.

3.2 Power budget

3.2.1 ISS power budget

The estimation of the power budget is based on ISS consumption to have a realistic analysis. ISS power demand is between 75 and 90 kW_e. This is supplied by solar array with a total generated power of 84-120 kW. The electrical load description is summarized in Table 8.

Electrical loads ISS			
	Number	P_{el} [kW_e]	P_{tot} [kW_e]
Battery	12	2.215	26.6
Fan	9	0.535	4.8
Atmosphere controller	2	1.2	2.4
Crew system	2	0.575	1.2
Control system	2	0.82	1.6
Communications	2	0.47	0.9
Lighting bank	9	0.36	3.2
Main PC	2	0.385	0.8
Robotic workstation	2	0.895	1.8
Canadian robotic arm	2	3.21	6.4
Air pump	2	1.15	2.3
Experiments			25.9
TOT			**78.0**

Table 8 - ISS power budget

3.2.2 Lunar base design parameters

The lunar base power budget depends on the day and night cycle. The hypotheses are presented in Table 9 and Table 10. Batteries were excluded in this initial phase and are sized in the section Power source and energy storage sizing.

Electrical loads - Day			
	Number	P_{el} [kW_e]	P_{tot} [kW_e]
Fan	9	0.535	4.8
Atmosphere controller	2	1.2	2.4
Crew system	2	0.575	1.2
Control system	2	0.82	1.6
Communications	2	0.47	0.9
Lighting bank	9	0.36	3.2
Main PC	2	0.385	0.8
Robotic workstation	2	0.895	1.8
Canadian robotic arm	2	3.21	6.4
Air pump	2	1.15	2.3
Experiments			25.9
TOT			**51.4**

Table 9 - Lunar base power budget (day)

To find the night electrical loads, the day power budget was reduced by the systems that are supposed not to be used during the night.

Electrical loads - Night			
	Number	P_{el} [kW_e]	P_{tot} [kW_e]
Fan	9	0.535	4.8
Atmosphere controller	2	1.2	2.4
Crew system	2	0.575	1.2
Control system	2	0.82	1.6
Communications	1	0.47	0.5
Lighting bank	9	0.36	3.2
Main PC	1	0.385	0.4
Air pump	2	1.15	2.3
TOT			**16.4**

Table 10 - Lunar base power budget (night)

Taking into consideration a 5% tolerance on the data above, the total electrical loads are **53.9 kW** and **17.2 kW**. The bus voltage is decided to be equal to 120 V, mainly to reduce power losses along the system harness connections. These losses, in fact, are proportional to the square of the current and then a lower bus voltage (implying a higher current according to Ohm Law) would significantly increase them. The expected life mission is considered to be a minimum of 10 years.

3.2.3 Power source

The mission duration and the electrical loads determine the power source that better suits for the purpose.

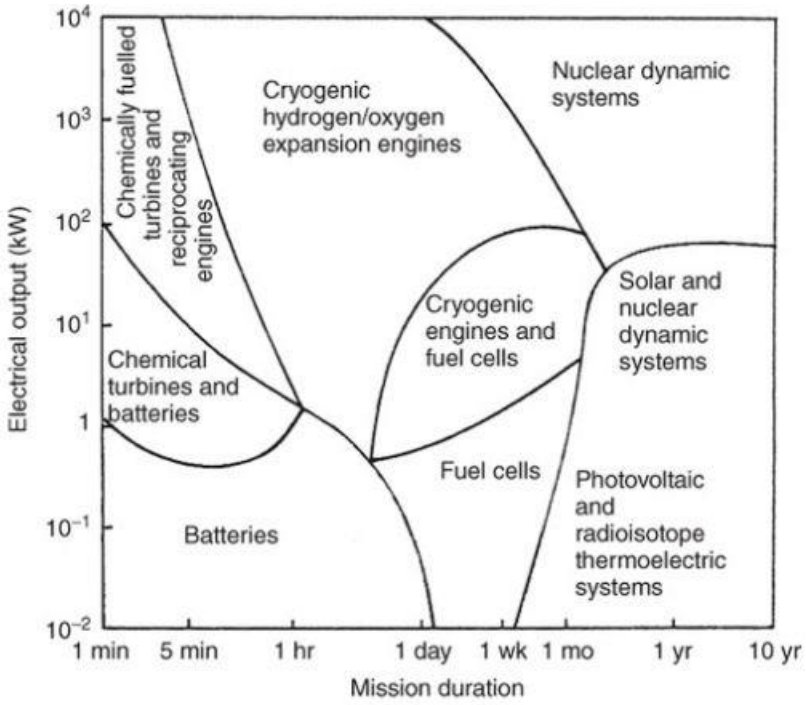

Figure 7 - Power source selection – Source: (Fortescue P., 2011)

It's possible to see from Figure 7 that, if the power budget is on the order of 10^1 kW and the duration is 10 years, the best configuration would be solar photovoltaic cells and nuclear dynamic system. This is due to their partial complementary aspects and the criticality in power supply in such a mission.

Chapter 4

Nuclear power technology

Nuclear power technology for space application is known since late 20th century and have been employed for interplanetary and lunar missions, mainly by adopting the so-called Radioisotope Power Systems (RPS). RPS systems have been used since 1961 in more than 40 US missions. They are mainly used in outer planets due to the limited solar energy available, but also in case of long mission duration, permanently shadowed craters or Sun mission because the PV panel can't reach so high temperature. To have an idea of the solar irradiance reaching different planets, it's presented a diagram of the solar flux as function of distance from the Sun in Astronomical Unit (1 AU ≈ 150 million kilometres, roughly the distance from Earth to Sun).

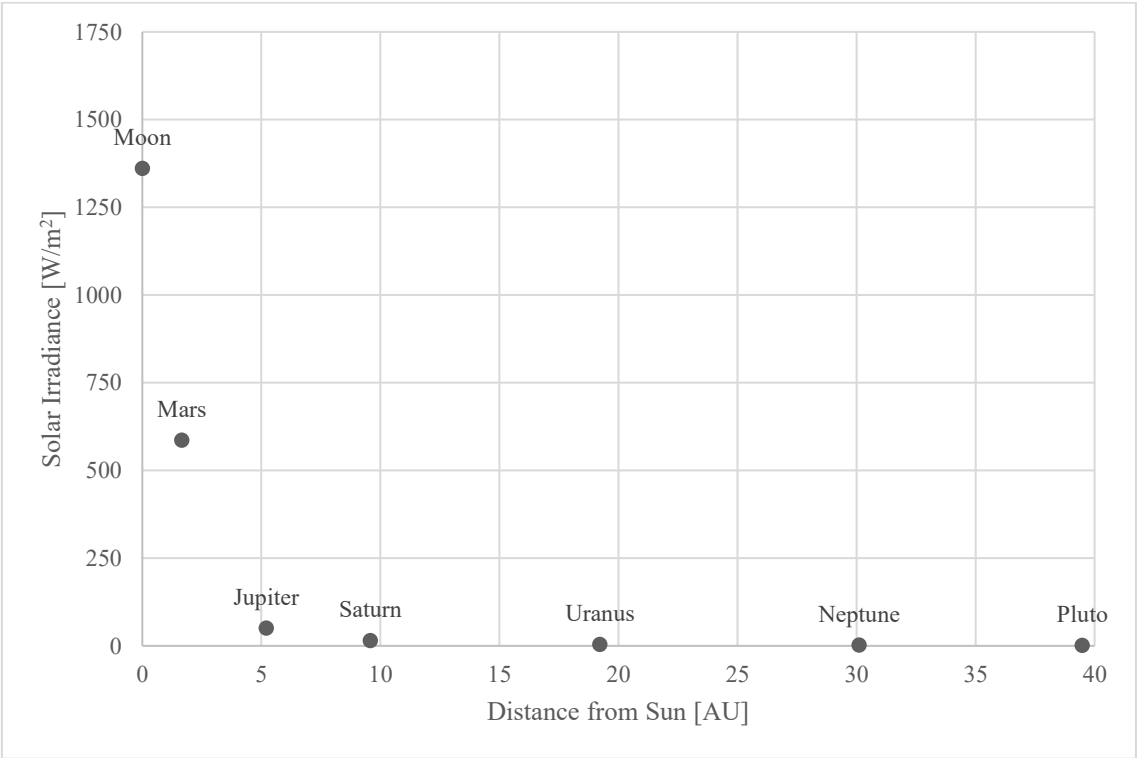

Figure 8 - Solar irradiance as function of planet's distance from sun

There are two main categories of nuclear space technology:

- Radioisotope power system (RPS)
- Fission power system (FPS)

In the first case, the source is a radioisotope material that release thermal energy by radioactive decay and is converted into electrical energy. The second one uses the heat produced by fission reaction. RPS systems are also used as simply heater and in this case are known as Radioisotope Heater Unit (RHU).

4.1 Radioisotope power system

The radioactive decay process consists in radiation emission of photons and/or elementary particles by a nucleus. The deposition of the electromagnetic or kinetic energy particles in the surrounding material, cause a heat energy release. The decay can be in three different form:

- Alpha decay
- Beta decay
- Gamma decay

The first one is the emission of Helium nucleus, and so formed by two protons and two neutrons. They have large mass, with respect to beta or gamma rays, and have low penetration depth: they can be stopped by a sheet of paper or by the skin and the nuclei travel for a few centimeters in air. They can cause serious damage if ingested through food or air. The second one generates beta particles, electrons or positron with high speed and so high energy. The relatively small mass permits the particles to travel few meters in air and could be stopped by plastic or aluminium plate. The last one evolves in gamma rays production: electromagnetic waves with the shortest wavelength, and so the highest photon energy. The radiation can travel furthest in air, losing about half energy every 150 metres. In this case, the radiation shielding must be a dense material, such as lead, concrete or steel.

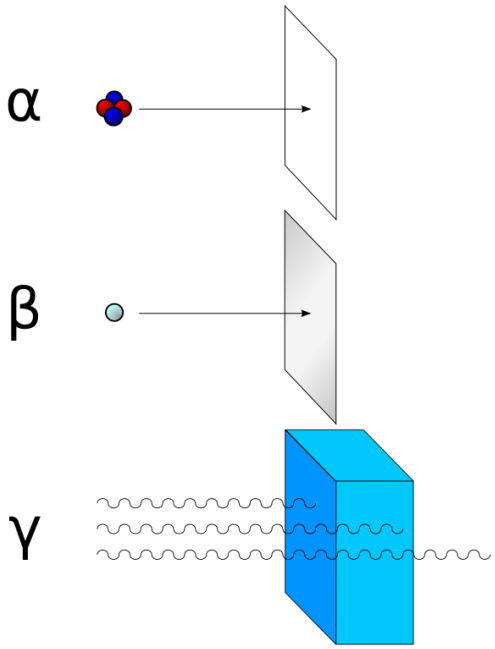

Figure 9 - Material shielding for different radioactive particles.
Source: Wikipedia

The half-life ($t_{1/2}$) is defined as the time necessary for 50% atoms to decay. The decay has an exponential form as:

$$N(t) = N_0 \cdot e^{-\lambda \cdot t} \quad [1]$$

With N(t)= number of atoms that still remain at time t
N_0= initial number of atoms
λ= decay constant (1/s)
t= time (s)

The half-life, in seconds, is therefore

$$t_{1/2} = \frac{ln(2)}{\lambda} \quad [2]$$

The specific power is defined as:

$$P_{sp} = \frac{ln(2)}{t_{1/2}} \cdot \frac{E_d}{A} \cdot N_A \quad [3]$$

With E_d= average released energy per decay
A= relative atomic mass
N_A= Avogadro's number
P_{sp}= specific power in W_{th}/g

The specific power is therefore inversely proportional to the half-life: a compromise must be found between these two parameters in order to have relative long half-life and high specific power emitted.

4.1.1 Nuclear power source

The power source module is a Department of Energy (DOE) designed system, named General Purpose Heat Source (GPHS). To minimize the contamination risk, the radioactive material is posed in modular units, with their own shielding. In particular, each module is composed by five main elements:

- Fuel
- Fuel cladding
- Graphite Impact Shell (GIS)
- Carbon Bonded Carbon Fiber Sleeve (CBCF)
- Aeroshell

Each GPHS contains four fuel pellets on form of PuO_2 with a thermal power of about 250 W and has a mass of 1,43 kg. The fuel pellet is encapsulated in an Iridium clad and put in a graphite shell. These two materials are chosen because of their heat and corrosion resistance. The fuel is stored in a ceramic form, to prevent the risk of vaporization and aerosolization.

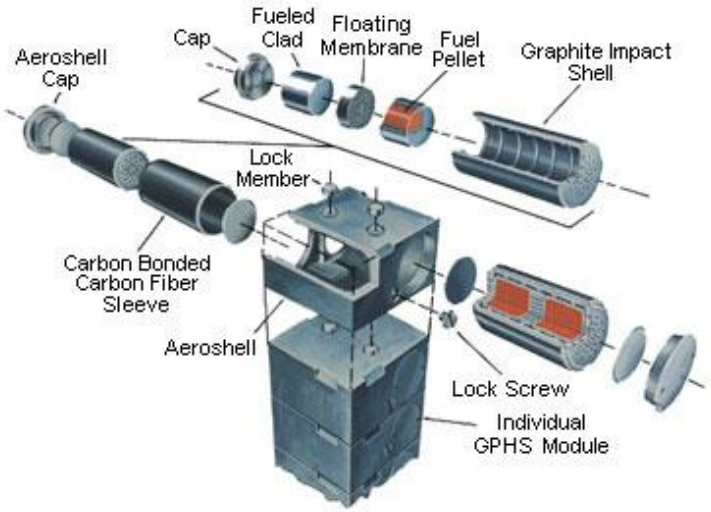

Figure 10 - General Purpose Heat Source.
Source: http://nuclear.gov/space/gphs.html

The radioactive material must have the following characteristics:

- Relatively long half-life, compared to mission duration, in order to provide power at almost constant rate
- High specific power and density
- Low radiation emission, preferably alpha decay, in order to have light shielding structure
- Easy to produce and at a reasonable cost
- Stable fuel form with high melting point

Different radioisotopes were investigated for space missions, like Strontium 90 (Sr-90), Polonium 210 (Po-210), Curium 242 (Cm-242), Curium 244 (Cm-244), and Plutonium 238 (Pu-238). A summary of the different fuel features is presented in the following section.

Isotopes characteristics

1. Sr-90 and Po-210 were considered for high powered military satellite constellation due to limited quantities of Pu-238. The missions were however cancelled and therefore they were never utilised for space missions.
2. Cm-242 has high power density and high melting point but the half-life is small (162 days).
3. Cm-244 has high power density, with high half-life. However, it's difficult to produce and has high neutron and gamma emission, that lead to important protection shielding.
4. Pu-238 has high half-life (87.7 years), high power density, low alpha emission and useful fuel form but it is limited in availability: it' s a by-product of nuclear weapons materials. The alpha particles kinetic energy is 5.544 Mev.
5. Am-241 is very similar to Pu-238. The major differences are a very high half-life (433 years), it's probably not limited in availability, coming from a by-product of nuclear reprocessing fuel, but has a power density equal to about one fifth of the Pu-238 one.

The fuel most widely used in space architectures is Pu-238, because of its long half-life, high power density (0.57 W_{th}/g), low radiation level, thermal stability, low solubility in the human body and environment. It' necessary less than 2.5 mm of lead to shield the source. It is produced from the irradiation of Neptunium 237, recovered from processing enriched uranium fuel. The availability is however limited due to restricted resources of Np-237. In the last decade, Americium 241 (Am-241) was also taken in consideration.

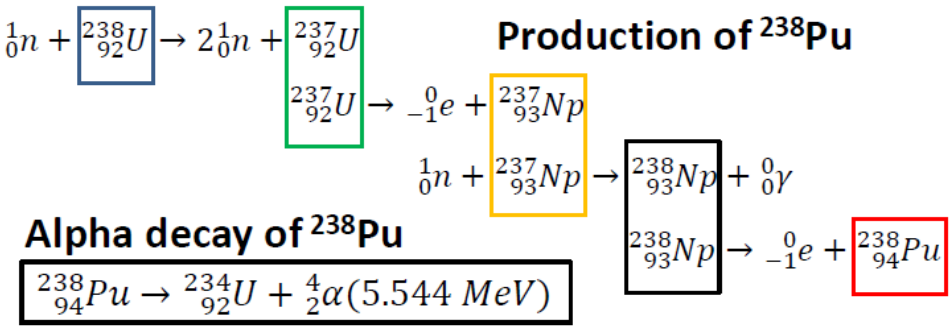

Figure 11 - Production and decay of Pu-238

4.1.2 Power conversion system

The energy conversion of RPS can be static or dynamic.

Static energy conversion

The static energy conversion, i.e. no moving parts, involves the use of thermocouples that exploit Seebeck Effect: in an electrical circuit formed by two different conductors, or semiconductors, a temperature gradient can generate a current. In this case, the system is known as RTG, or Radioisotope Thermoelectric Generator.

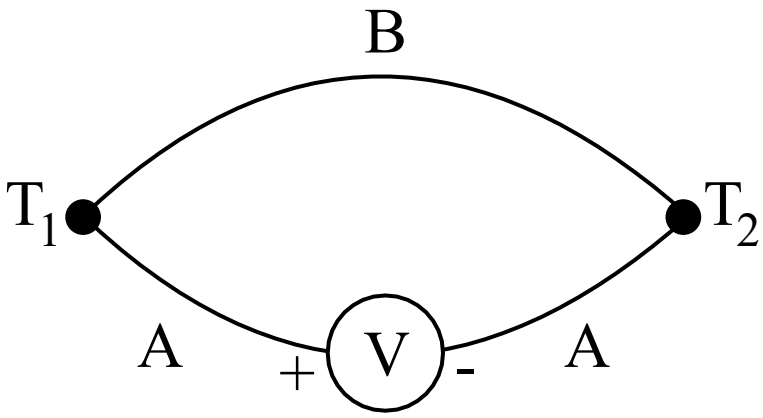

Figure 12 - Seebeck effect schematic. Source: Wikipedia

The open-circuit voltage is proportional to the temperature difference $\Delta T=T_1-T_2$ (K) between junctions and depends on the materials used, as:

$$V_{OC} = \alpha_{AB} \cdot \Delta T \qquad [4]$$

With α_{AB} (V/K) relative Seebeck coefficient, or a measure of the induced voltage per unit of temperature difference in the material.
The major figure of merit is the Z parameter (1/K), defined as

$$Z = \frac{\alpha_{AB}^2 \cdot \sigma}{\lambda} \qquad [5]$$

With σ= electrical conductivity (S/m)
λ= thermal conductivity (W/m/K)

It is proportional to the square of the Seebeck coefficient and electrical conductivity, and inversely proportional to the thermal conductivity. To have a big Z parameter, the main impacting factor is α, so it's necessary a material with high tension per unit of temperature difference created. It is also favourable a high electrical conductivity, in order to have small dissipation due to Joule effect. On the other hand, a small thermal conductivity helps to create a big temperature difference across the junction and favors the thermoelectric effect. A material is considered thermoelectric if Z is larger than 0.5e-3 K^{-1}. Multiplying Z for the absolute temperature, we can obtain a dimensionless parameter, characteristic of the material performance.
The figure of merit for the thermocouple is:

$$Z = \frac{\alpha_{AB}^2}{(\sqrt{\rho_1 \cdot k_1} + \sqrt{\rho_2 \cdot k_2})^2} \quad [6]$$

With ρ= electrical resistivity (Ω·m).
The electrical power is therefore:

$$P_{el} = (1 - \frac{T_c}{T_h}) \cdot \frac{\sqrt{1 + Z\bar{T}} - 1}{\sqrt{1 + Z\bar{T}} + \frac{T_c}{T_h}} \quad [7]$$

$$\overline{T} = \sqrt{T_h + T_c} \quad [8]$$

With T_c= Cold temperature
T_h= Hot temperature.

For space applications, the thermocouples can be formed by the following materials:

- Lead Telluride (PbTe)
- Tellurides of Antimony, Germanium and Silver (TAGS)
- Lead Tin Telluride (PbSnTe)
- Silicon Germanium (SiGe)

The operative temperature is increasing from the top to the bottom list. The first three materials are limited by a maximum hot junction temperature of 500 °C, the last one of 1000 °C.
The thermal efficiency is defined as

$$\eta_{th} = \frac{P_{el}}{\dot{Q}_{th}} \quad [9]$$

Where P_{el} is the electrical power output and $\dot{Q}_{th}$ is the thermal power input. The conversion efficiencies are comparable and relatively low, smaller than 10 %.

Dynamic energy conversion

The dynamic energy conversion involves the use of a working fluid and a heat engine. The heat is converted into mechanical energy and then into electricity. The most used thermodynamic cycles are Rankine, Bryton or Stirling. In space application, Stirling cycle is the most common, and the system is named therefore Stirling Radioisotope Generator (SRG). The working fluid is Helium and the cycle is showed in Figure 13.

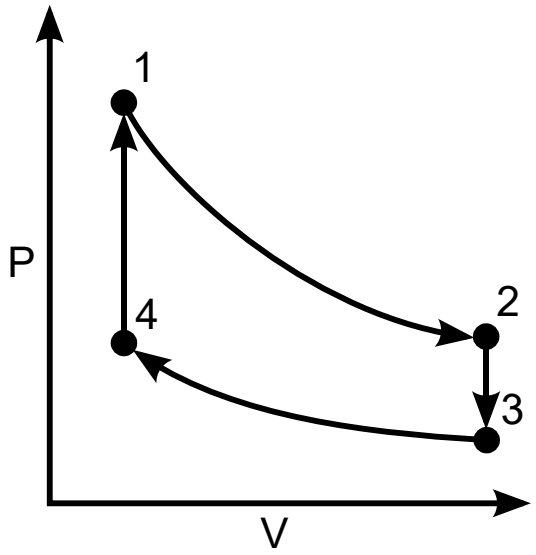

Figure 13 - Stirling cycle

The gas expands isothermally, absorbing heat from the source (1-2). Then it releases heat, passing through the regenerator, at constant volume (2-3). The helium is then compressed from stage 3 to 4 isothermally and heated up at constant volume (4-1) thanks to the regenerator. The rapid expansion and compression cause the piston movement that, coupled with an alternator, can generate electric current.

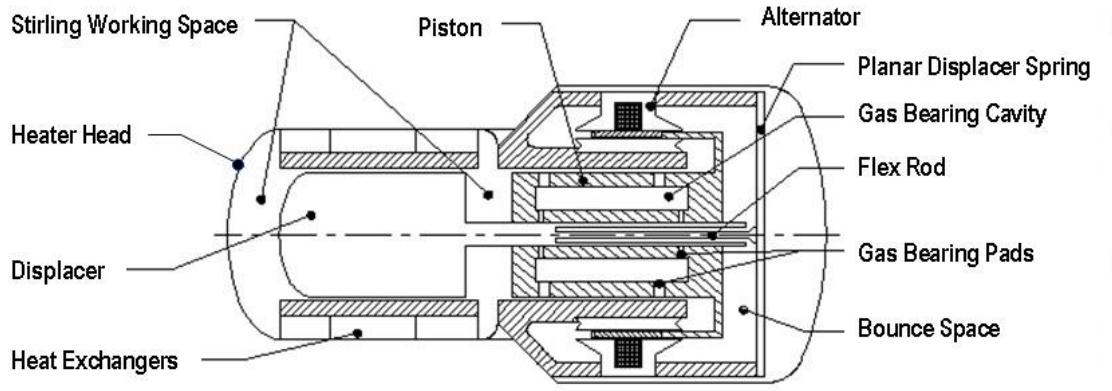

Figure 14 - Advanced Stirling Convertor (ASC). Courtesy Sunpower

The maximum theoretical efficiency is the ratio between the electrical power output and the thermal power input. It is equal to the Carnot efficiency if operating between the same thermal sources.

$$\eta_{th} = 1 - \frac{T_{min}}{T_{max}} \quad [10]$$

The larger the difference between the hot and cold temperature, the higher the efficiency. The overall efficiency is the product of thermal and alternator efficiency.
Independently from the conversion method adopted for RPS systems, the non-converted heat can be used to keep in temperature the spacecraft's payload or must be rejected into the space vacuum through radiators. Therefore, the operating temperature are limited on the hot side by the source and the system conversion materials, on the cold side by weight and size of the radiators. The research is moving towards systems with higher efficiency conversion technology to have a reduction in fuel use, mass and cost.

4.1.3 Radioisotope Thermoelectric Generator

RTG has been the dominant technology till now: it's reliable and not sensible to vibration environment experienced during the launch. The first RTGs were employed for space and military use in the frame of the Systems Nuclear Auxiliary Power (SNAP) program, in late 20th century. The first systems had a relatively small efficiency, on the order of 4-5 %. In 1977 started Voyager 1 and Voyager 2 missions and the spacecrafts were powered with Multihundred-Watt Radioisotope Thermoelectric Generator (MHW RTG), reaching 6.5 % efficiency. It was then developed the General Purpose Heat Source RTG (GPHS RTG), optimized for use in vacuum, used for Ulysses, Galileo, Cassini-Huygens and New Horizons missions. The efficiency is like MHW RTG. The newest RTG, named Multi Mission RTG (MMRTG), was designed by NASA and DOE. The design permits the operation both in vacuum and in planetary atmospheres. The efficiency is between 5-6 %. It was launched in 2011 with Curiosity rover on Mars and is still in operation. The future of the MMRTG is the e-MMRTG: there is an increase in electrical power output due to the replacement of TAGS thermocouples with Skutterudite (SKD) one. The power at beginning of life is 145 W with 8 % efficiency and a specific power higher than 3.6 W/kg. A general scheme of RTG is presented in Figure 15.

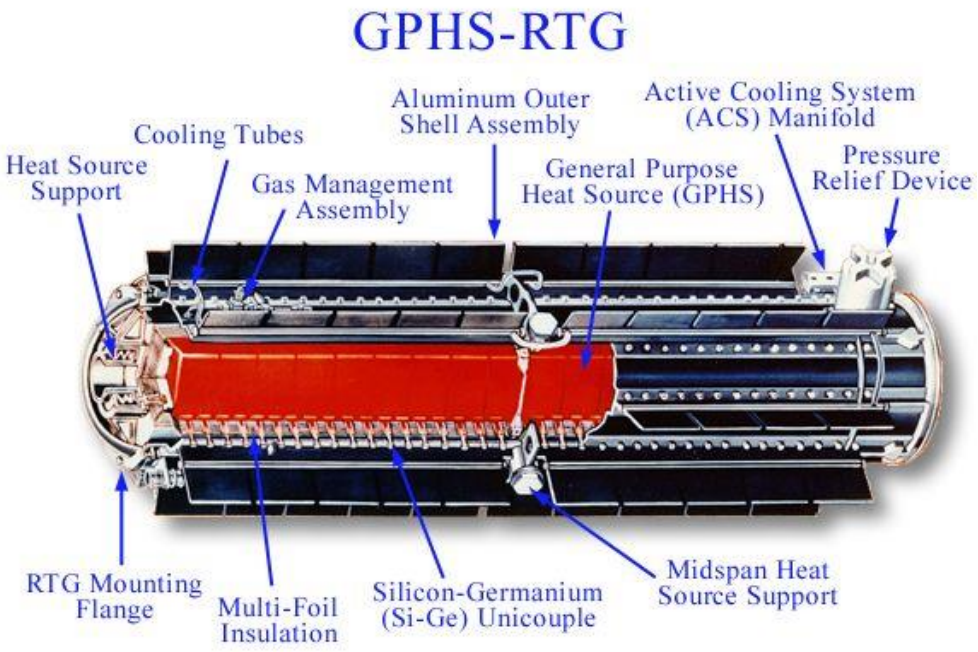

Figure 15 - General Purpose Heat Source RTG scheme. Source: NASA

In Table 11 it is presented an overview of RTG systems used for different missions. The specific power refers to electrical power density.

Mission	Planet	Power source	Thermoelectric device	Power [W]	Specific power (W/kg)	T max [°C]	Efficiency [%]
Apollo	Moon	SNAP-27	PbTe	73	3.65	550	4.9
Viking	Mars	SNAP-19	PbTe	42,7	2.8	550	4.1
Voyager	Jupiter	MHW RTG	SiGe	157	4	1000	6.5
Galileo	Jupiter	GPHS RTG	SiGe	300	5	1000	6.8
Ulysses	Jupiter	GPHS RTG	SiGe	300	5	1000	6.8
Cassini	Jupiter	GPHS RTG	SiGe	3x300	5	1000	6.8
New Horizons	Pluto	GPHS RTG	SiGe	250	4	1000	6.8
Mars Science Lab	Mars	MMRTG	PbTe-TAGS	110	2.4	1000	5.5

Table 11 - RTGs overview

The main RTG advantage is the absence of moving parts, making it a compact, light and maintenance free system. On other hand, the decay heat cannot be turned off and the conversion efficiency is low.

4.1.4 Stirling Radioisotope Generator

The Stirling Radioisotope generator was developed by NASA and DOE aiming to reduce the use of Pu-238, respect to RTGs' systems. The Stirling engine has higher conversion efficiencies, that can reach 25 % and more, with a reduction in system fuel mass and consequently a higher power-to-weight ratio. This implies also a cost reduction and a decrease in emitted radiation. In particular, the system has evolved into Advanced Stirling Radioisotope Generator with incorporation of Advanced Stirling Convertor ASC by Sunpower Inc., with a declared efficiency of 38 % and T_h=850 °C and T_c=90 °C and an increase of specific power from 3.5 W/kg to 7 W/kg and beyond. The higher the rejection temperature, the lighter the radiator. Trade-off between T_c and radiator dimension must be found to obtain the power density desired.

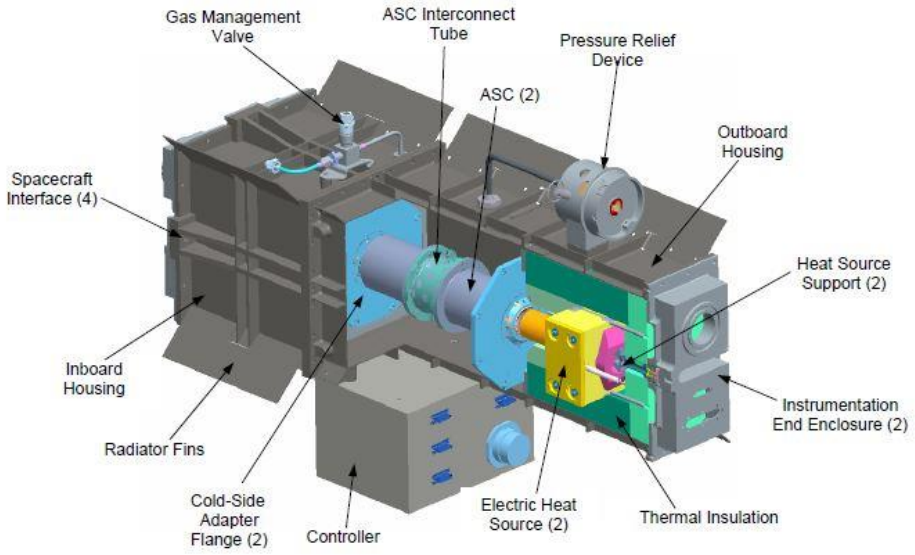

Figure 16 - ASRG layout – Courtesy of NASA

The future mission that could rely on ASRG technology are:

- Lunar Polar Volatile Explorer – NASA, 2018-2023 (Moon)
- Pathfinder – ESA, 2021 (Uranus)
- Muse – ESA, 2019 (Uranus)
- OSS mission – ESA/NASA, TBD (Neptune)

4.2 Fission power system

Nuclear fission is a reaction that involves the split of a nucleus into generally two lighter parts. It's a rare spontaneous event and can also be induced by the capture of a neutron. This can produce in turn free neutron, photons, alpha or beta particles with big energy release in form of gamma rays or kinetic energy of the by-products. The fission chain reaction is sustained only if there is the release of neutrons that can generate fission as well. This occurs with some isotopes, such as Uraniun-235, Uranium-233 and Plutonium-235.

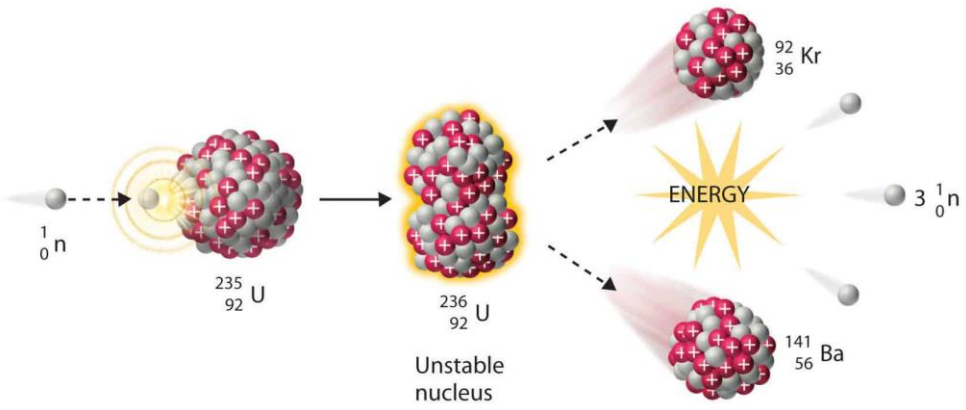

Figure 17 - Nuclear fission reaction – Source: chemwiki.ucdavis.edu

The US first and only nuclear fission reactor used in space application was SNAP-10A (System for Nuclear and Auxiliary Power), launched in 1965 into low Earth orbit altitude. It was a thermal reactor (using moderator to slow neutron) with Uranium-235 fuel in form of uranium-zirconium-hydride. The coolant is sodium-potassium eutectic alloy. The power conversion system is a thermoelectric converter using SiGe thermocouple: the temperature difference between the coolant and the cold space generate an electric potential with current generation. The reactor could generate 40 kW of thermal power and around 600 W_e, with a power density of 1.3 W_e/kg when shielded. The conversion efficiency was relatively small, around 1.83 %. The mission lasted 43 days and then it was terminated because of an electrical component failure.

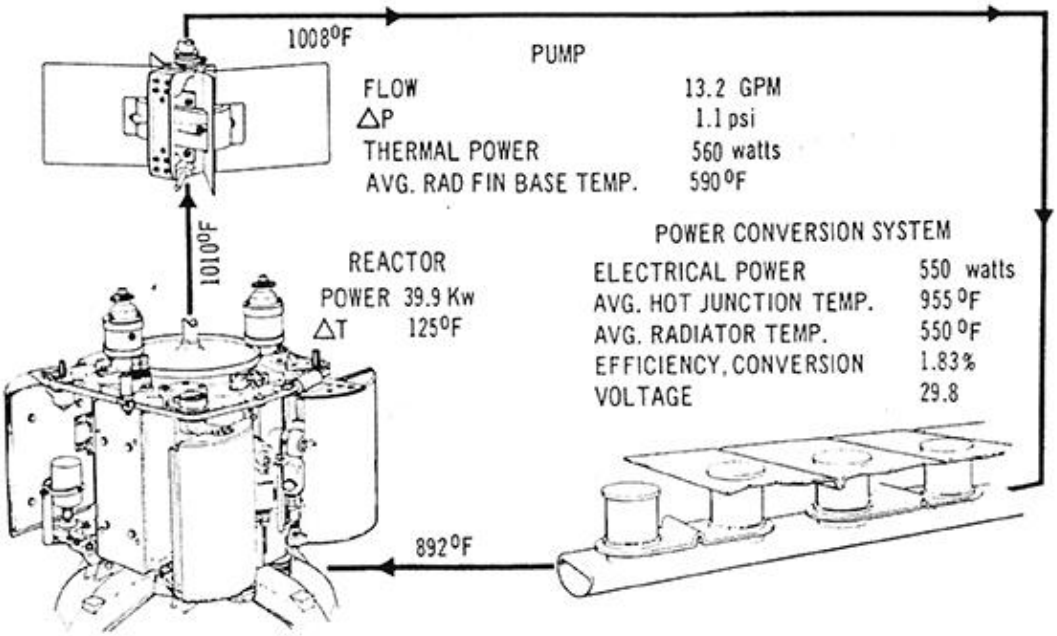

Figure 18 - SNAP-10A Thermodynamic cycle. Source: DOE

There were also produced SNAP-2 and SNAP-8 thermal reactors, NaK cooled but the power conversion system was a Rankine cycle. They never flown, also if ground-tested.

The Soviet Union reactor program history began probably in 1965. From 1967 to 1988 a number equal to 35 nuclear reactors were launched. They are mostly low-power technology, with a thermoelectric conversion system. Romashka and TOPAZ are part of this program, both fast reactors. The first used thermoelectric power conversion system. It could generate more or less the same thermal and electrical power as SNAP-10A, but with higher temperature core and hot junction. The overall efficiency is 1.5 % with a power density of 1.4 W_e/kg without shielding. TOPAZ (Thermionic Experimental Conversion in the Active Zone) was based on thermionic conversion, i.e. electron production from a hot electrode to a cold one, across a small gas-filled gap, producing useful electrical power. The coolant is NaK and it can generate from 130 to 150 kW_t and a maximum electrical power of 10 kW. The efficiency is the range 4-7 % with a power density of about 5 W_e/kg on average, excluding automatic control system, for TOPAZ-II.

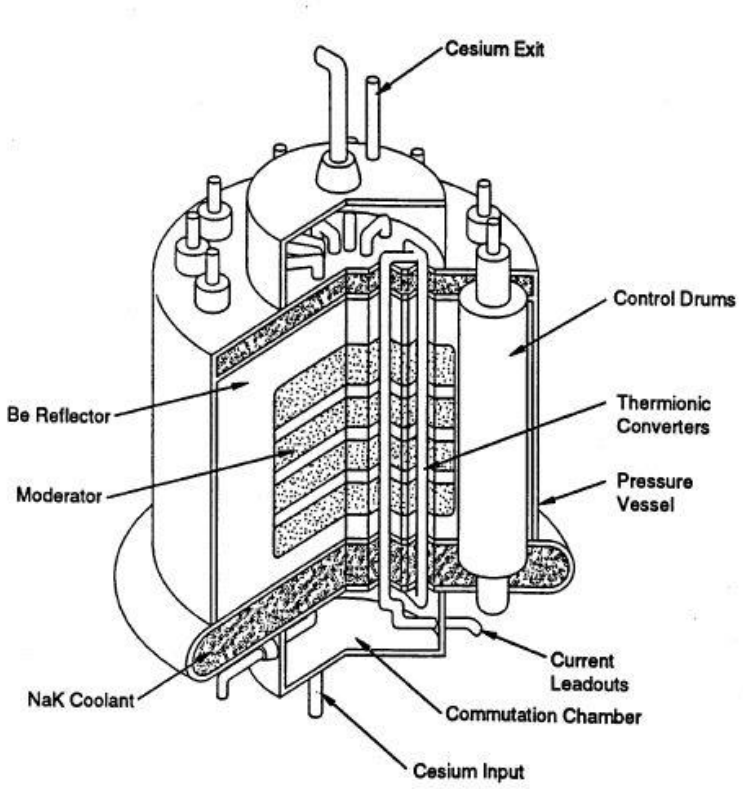

Figure 19 - TOPAZ layout – Source: Bennett, 1989

The US are studying and developing new fission system for space application, as Fission Surface Power (FSP) and KRUSTY.

4.2.1 Fission Surface Power (FSP) and Krusty

Fission Surface Power System

FSP system is a NASA project, developed primarily for lunar application. It is a fast reactor, designed to provide 40 kW electrical power output for 8 years on Moon's surface. The nuclear fuel is UO_2 with a NaK reactor cooling system. The energy conversion relies on Stirling converters with a water-loop heat rejection system. The thermal efficiency is 26 %.

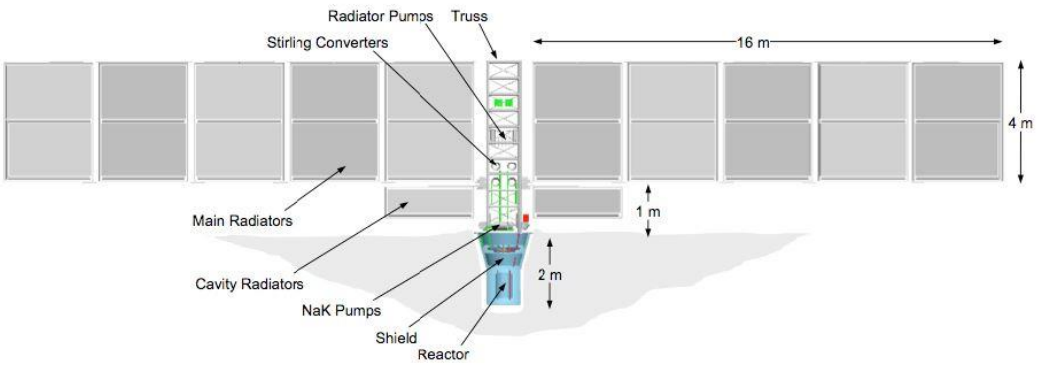

Figure 20 - FSP layout. Source: NASA

The architecture was proposed with the reactor in a 2 m depth excavation in order to use the regolith present on the lunar surface as a radiation shield. This permits a mass reduction of the entire system, due to a reduction in mass shielding. Other configurations are also possible.

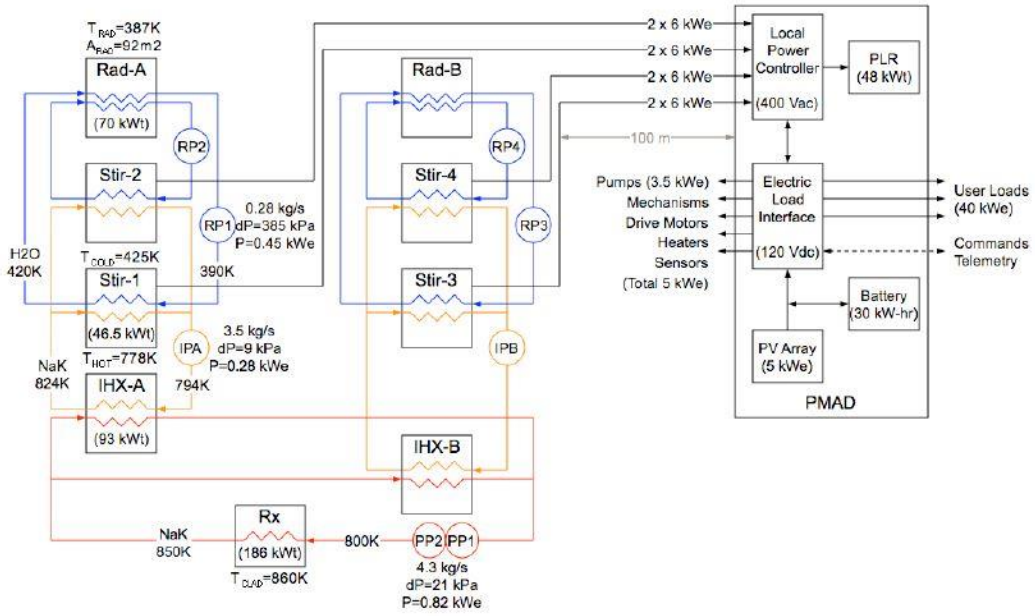

Figure 21 - FSP Scheme. Source: NASA/DOE

Legend:

- Rx= Reactor
- IHX= Intermediate Heat Exchanger
- PP= Primary Pumps
- IP= Intermediate Pump
- Stir= Stirling Convertor
- PMAD= Power Management and Distribution
- LPC= Local Power Controller
- PV= Photovoltaic
- Rad= Radiators

PV array and batteries are also provided to cover start-up and back-up operations. The overall mass would be 6942 kg with a 19 % margin. The main role is played by the radiation shield (30 %), followed by the reactor module (27 %). The power density is therefore 5.8 W_e/kg.
For further information see (Fission Surface Power Team, 2010).

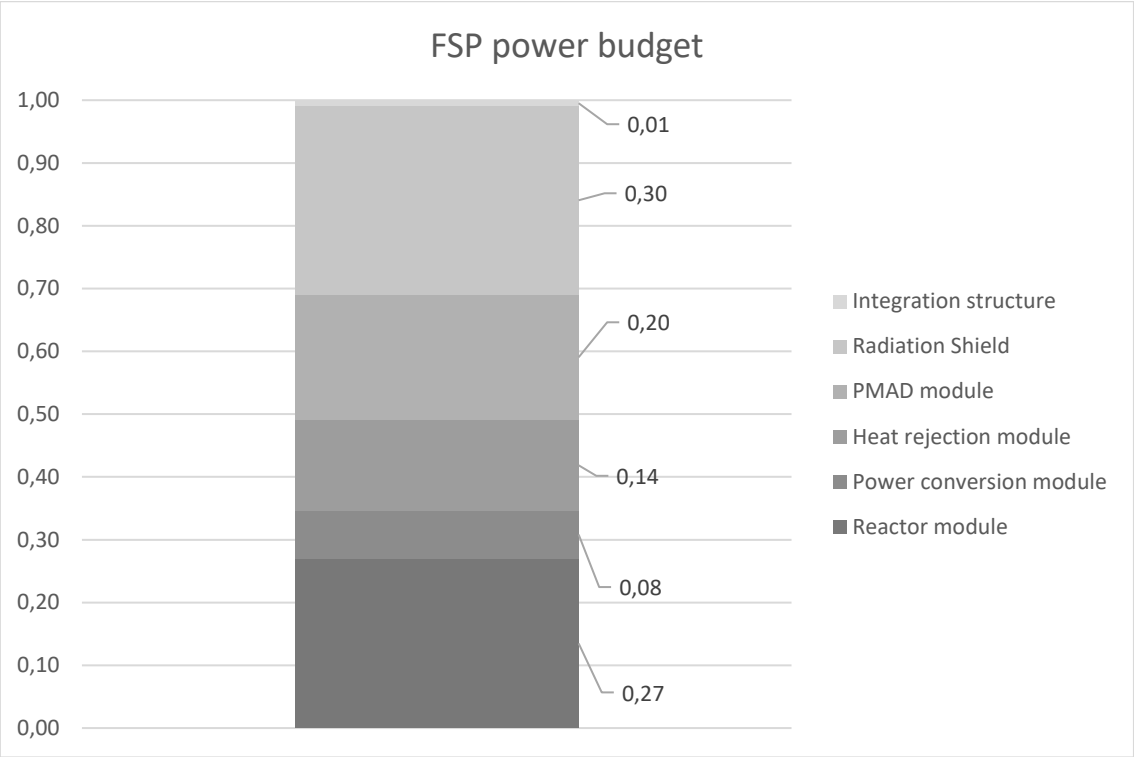

Figure 22 - Fission surface power system mass percentage breakdown

KRUSTY System

Kilopower Reactor Using Stirling Technology, or KRUSTY, is a NASA's Space Technology Mission Directorate's Game Changing Development (GCD) program, which is managed by NASA's Langley Research Center. The scope is to cover the gap between RPS and FSP systems, with a power range of 1-10 kW_e. KRUSTY is like FSP system, but it has few moving parts, less mass and volume, easier logistics. The cooling system is based on sodium heat pipes to transfer the heat out of the reactor core instead of a pumped liquid. The power conversion unit is the Stirling engine. The fuel is a uranium-molybdenum alloy (93% enriched uranium by weight). The fast-spectrum core has a strong negative temperature reactivity coefficient with a consequent self-regulating behaviour with a single boron-carbide control rod for start-up, shut-down or major changes in power regulation. The nominal thermal power is 13 kW_{th} at 1200 K average fuel temperature. The electrical power generated is 3 kW_e, with an overall efficiency of 23 %. To shield the electronic components, different plates made of lithium-hydride and depleted uranium are provided, with a total mass of 85.7 kg. The reflector is a 70 kg structure of beryllium. The heat rejection system relies on titanium-water heat pipes, protected by carbon fiber radiator panels.

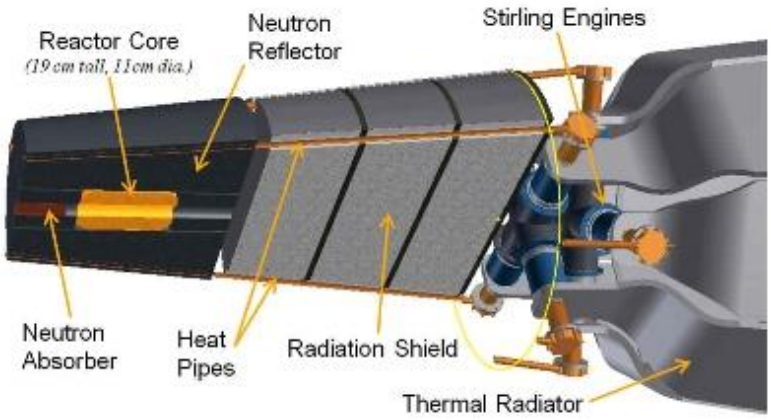

Figure 23 - KRUSTY architecture. Source: LANL

The system described reaches a power density of 4 W_e/kg, but it's possible to arrive at 6.5 W_e/kg for a 10 kW_e reactor. The KRUSTY system is 4 m height with a radius of 4 m as well.

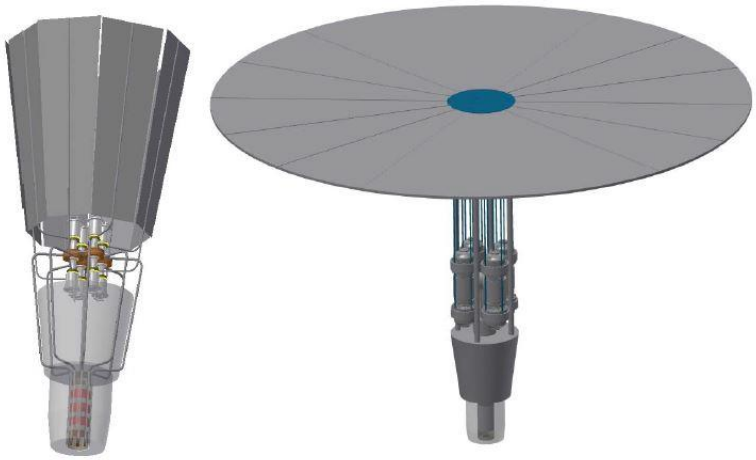

Figure 24 - KRUSTY power systems – 1 kW (left) and 10 kW (right).
Source: NASA

As for FSP systems, shielding and reactor plays a main role in mass budget analysis (see Figure 25).

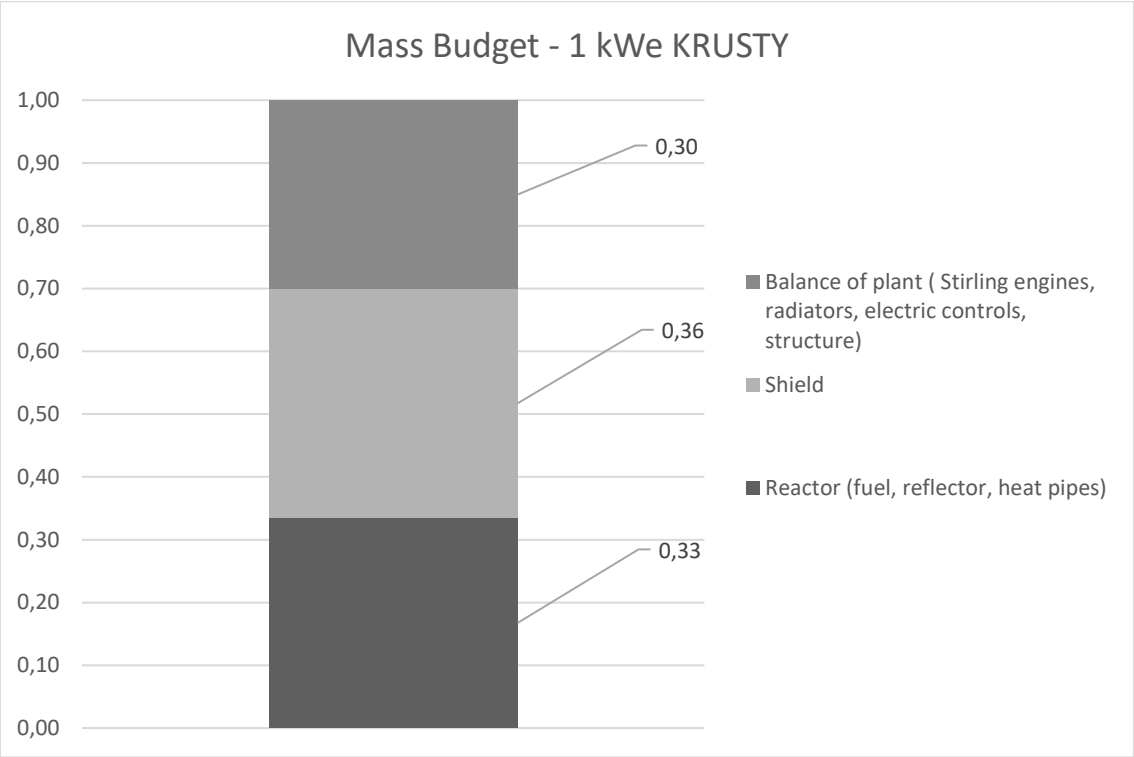

Figure 25 - KRUSTY breakdown for 1 kWe system

Increasing the power output, the core becomes less important in the mass budget, the shielding remains approximately constant and increases the balance of plant importance in percentage.

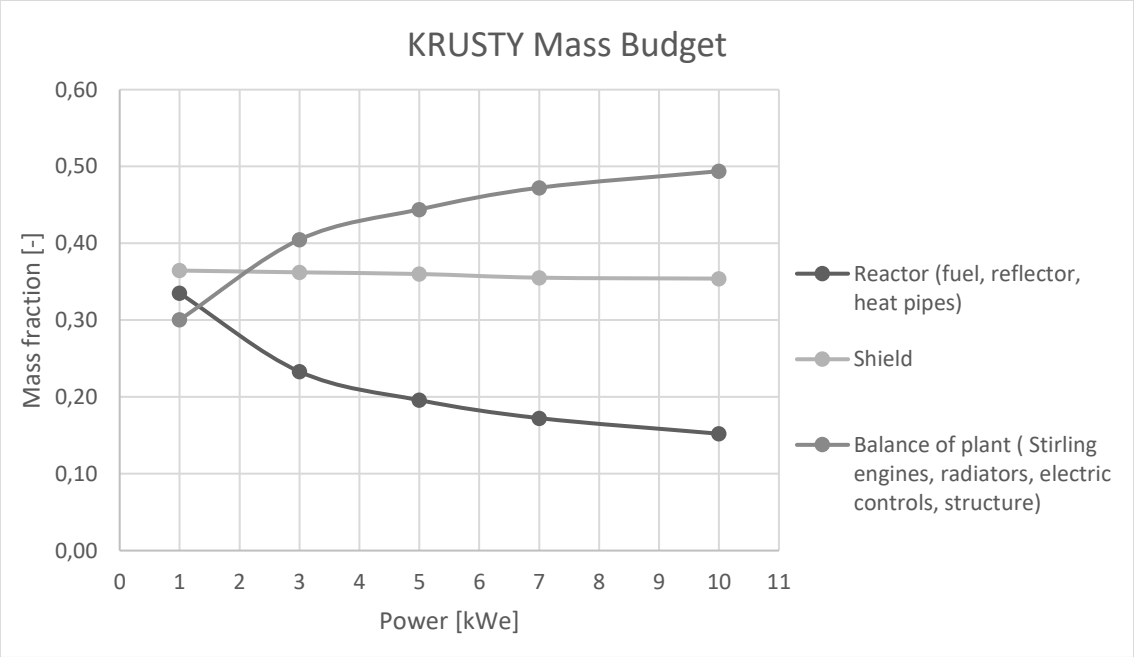

Figure 26 - KRUSTY mass budget at different power level

4.3 RHU

RHU contains a small quantity of radioactive material, generally less than 20 g. It provides thermal power, on the order of about 10 W. These heater units can substitute electrical heaters, placed where heat is necessary to keep in temperature the scientific instrumentation or any electronic device that has a limited temperature range operation, providing power budget saving.

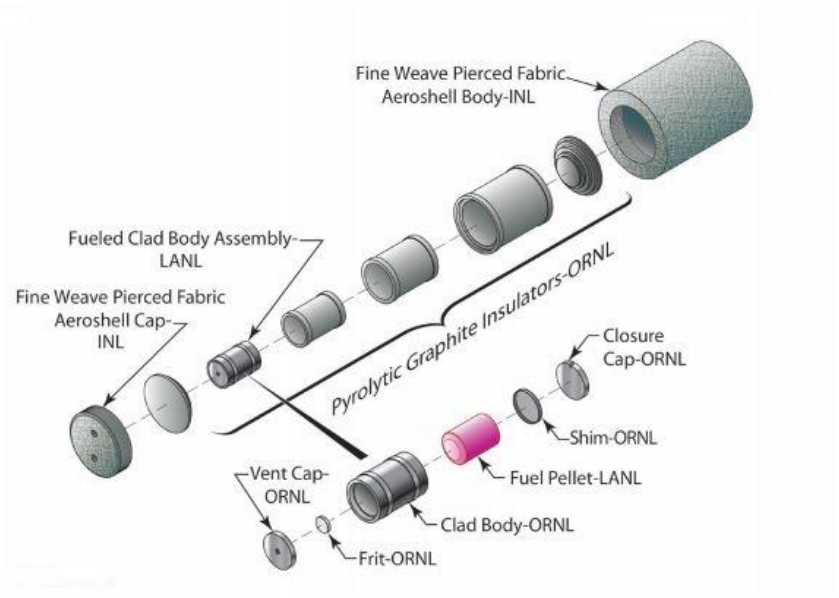

Figure 27 - RHU layout. Source: NASA

The encapsulation of the radioactive material plays an important role: it has to ensure the robustness of RHU in case of accident scenario in order to prevent any material leakage and exposure to people, instrumentations or Earth. A future ESA mission that will use RHU for thermal control will be Exomars second mission, both in the rover (2) and lander module.

4.4 Safety issues

The use of radioactive material always implies particular attention to what concern safety for workers and environment protection. It requires high safety standards and the development of procedures, systems and regulatory to manage nuclear power system, mainly during the launch phase, the most critical one. NPS research focus is risk minimization in case of accident, robust and affordable systems, with non-proliferation aspects to be considered.

4.4.1 Radiation hazards

The radiation hazard (possible release of radioactive material) in space applications, can have different types and level. The three categories are:

- Launch hazard: release of radioactive material in case of a failure during launch phase. To prevent from that, the fission reactor would be sent with a non-critical core, or the RPS with protection layers. They are however designed to prevent any accidental criticality.
- In-space hazard: humans and electronic components are protected against high radiation level in space yet. NPS don't add any relevant dose, but therefore shielding and distance prevent from any further radiation
- Re-entry hazard: release of nuclear material in re-entry phase. RPS systems are protected by different layers, nuclear reactors are put into a safe orbit in case of hazard.

4.5 Advantages and disadvantages

Nuclear power systems have the following advantages:

- Power generation independent from Sun distance
- Electrical power almost constant in time, with a reduction in mass batteries
- Long lasting and not influenced by cosmic radiation
- Compact and lightweight

The disadvantages are instead:

- Possible hazards due to launch or in other phases failure
- Radiation emission
- Complex systems and difficult to build
- Constant cooling and shielding
- Expensive technology
- Heavy radiation shielding

RPS Type		TRL	Power BOL [We]	P_s [We/kg]	Efficiency BOL [%]	Life [y]	Power degradation rate [% per year]
GPHS-RTG	SoA	9	285	5.1	6.3	>17	1.6
e-MMRTG	SoA-MMRTG	6	120	2.8	6.1	17	3.8
	Goal		120-160	4	>10	17	<2.5
ASRG-100	SoA	5	130-140	3	30	17	3.8
	Goal	6	120-160	4	12-30	17	<2.5
ARTG-500	SoA	2	250-290	5.1	6.3	>17	1.6
	Goal	6	400-600	>8	12-30	>17	<1.6
ASRG-500	SoA	3-4	250-290	5.1	6.3	>17	1.6
	Goal	6	400-600	>8	12-30	>17	<1.6

Table 12 - RPS overview

Chapter 5

Power source and energy storage sizing

5.1 Power sources

As described in Chapter 3, the best power source configuration would be solar panels and dynamic nuclear system. To size and analyse the best configuration, the proper components are chosen.

5.1.1 Photovoltaic cells

The selected PV cells are AZUR SPACE triple junction Gallium-Arsenide (GaAs), the most commonly used in satellite applications and the most performing ones in the European space market. The data sheet is presented in Appendix A. The key features are summarized in Table 13. The data refer to spectrum AM0 (Solar radiation spectrum outside Earth atmosphere) WRC=1367 W/m^2 and T=28°C.

Design parameters AZUR SPACE 3G30C- BOL	
$\mathbf{V_{oc}}$ [mV]	2700
$\mathbf{I_{sc}}$ [mA]	520.2
$\mathbf{V_{mp}}$ [mV]	2411
$\mathbf{I_{mp}}$ [mA]	504.4
$\boldsymbol{\eta}$ [%]	29.5

Table 13 - PV cells design parameters

5.1.2 ASRG

The technical data used refers to a NASA project. For more information see (Radioisotope Power Systems Committee, National Research Council, 2009). To have a great level of redundancy and fault tolerance, ASRG system is chosen instead of a single nuclear fission reactor. The power density is also bigger than FPS one, due to a higher technology readiness level and lower shielding requirements. Moreover, they can be easily packaged in landers because of the small size and mass.

Design parameters ASRG - BOL	
Degradation/year [year^{-1}]	0.008
Power density [W_e/kg]	8

Table 14 - ASRG design parameters

5.2 Energy Storage

In the system design, lithium-ion batteries are also been provided. The reason is that they can cover peak power or can be used in case of failure of part of the system. The key features are in Table 15 and the data sheet is in Appendix B.

Design parameters Li-ion battery - SAFT MP 174565	
EOCV [V]	4.2
$\mathbf{E_{bat}}$ [Wh/kg]	175
$\mathbf{m_{cel}}$ [kg]	0.103

Table 15 - Batteries design parameters

5.3 Power flow design

The power architecture is shown in Figure 28.

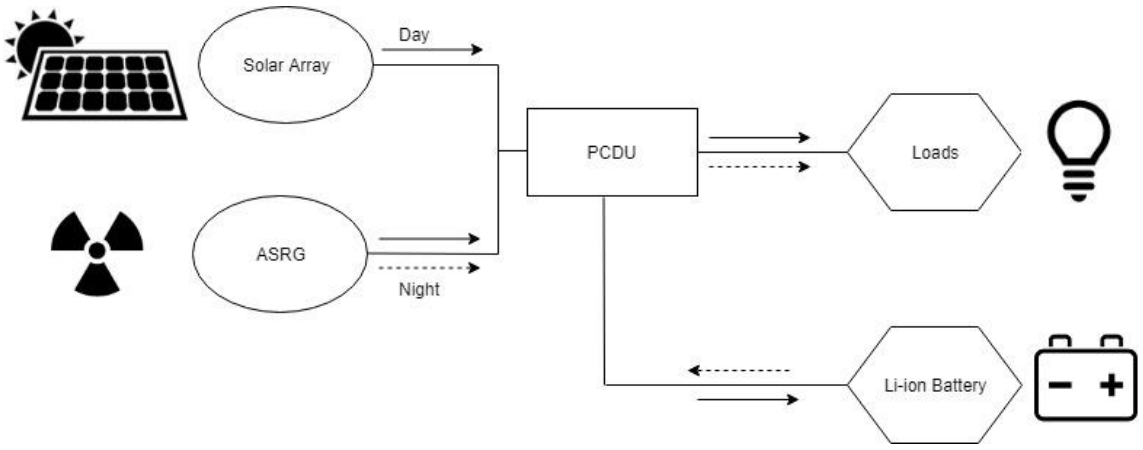

Figure 28 - Power flow design

During the day, the SA and ASRG will charge the batteries and give power to the loads. During the night the power flow is from the batteries and ASRG to the electrical loads, always through the PCDU component.

5.4 Mass budget and power sizing case

One of the most important figures of merit in space applications is the mass of the system, and for each project the maximum launchable mass is established by the capability of the chosen launcher. In terms of power system dimensioning, the sizing case for the selected mission profile is represented by the power demand of the overall system during the night period, due to the fact that the solar array is not working. The analysis was performed varying the power supplied from the ASRG from 0 to 17.2 kW, which represents the night maximum electrical power load required (Table 10), and calculating, consequently, the number of batteries required and the PV area. At the end, we can obtain the mass budget of the EPS power and storage.

5.4.1 Battery sizing

The battery sizing starts with the determination of the number of cells to be connected in series (forming a so-called string) as:

$$N_s = \frac{V_{bus}^{max}}{V_{cell}^{max}} \quad [11]$$

With V_{bus}^{max} = maximum bus voltage
V_{cell}^{max} = EOCV cell.

The energy that must be stored is:

$$E_{BTA} = \frac{E_{disch}^{max}}{DOD_{max}} \cdot (1 + Fade) \quad [12]$$

Where E_{disch}^{max} = maximum energy discharge and the Fade is the loss of performance of the battery due to aging. The DOD_{max} is the maximum depth of discharge considered for the mission. The batteries performance, in charging and discharging process, is considered with an efficiency of 0.81 (Wu, 2016).
If E_{cell} is the cell energy, the total number of cells are therefore:

$$N = \frac{E_{BTA}}{E_{cell}} \quad [13]$$

At the end, the number of strings to be connected in parallel is given by:

$$N_p = \frac{N}{N_s} + 1 \qquad [14]$$

The total number of cycles is the number of day/night variation during the entire mission life and was estimated to be 124 cycles. Based on the mission profile and on the relatively small number of cycles that the battery has to perform, the DOD was assumed equal to 80% and the Fade equal to 0.013%/cycle. These values are in line with the test results performed by the cells manufacturer in similar conditions. The mass of the batteries package is therefore calculated as the ratio of the total energy that has to be stored and the energy density of the cell.

5.4.2 PV sizing

To estimate the total area required to supply the desired power, it is used a simplified model. The solar array power can be calculated as:

$$P_{sa} = \frac{\frac{P_d \cdot T_d}{X_d} + \frac{P_n \cdot T_n}{X_n}}{T_d} \qquad [15]$$

With

- P_d= daylight power requirements
- P_n= night power requirements
- T_d= length of the lunar day
- T_n= length of lunar night
- X_d= conversion efficiency from the solar array to the loads
- X_n= conversion efficiency from the solar array to the batteries and then to loads

X_d is assumed to be 0.9 and X_n equals to 0.73. It's the product of battery efficiency and solar array efficiency, assumed to be 0.9 (Wu, 2016).
The ideal cell output per unit area is given by the product of cell efficiency and solar constant G in W/m^2:

$$P_0 = \eta \cdot G \qquad [16]$$

The south pole solar irradiance can be considered 1316 W/m^2 (Bussey, Spudis, & Robinson, 1999). The cell efficiency depends on temperature, but the data sheet parameters refer to 28 °C and the maximum design temperature is 27 °C. To be conservative, it's reasonable to consider the efficiency mentioned in Table 13.

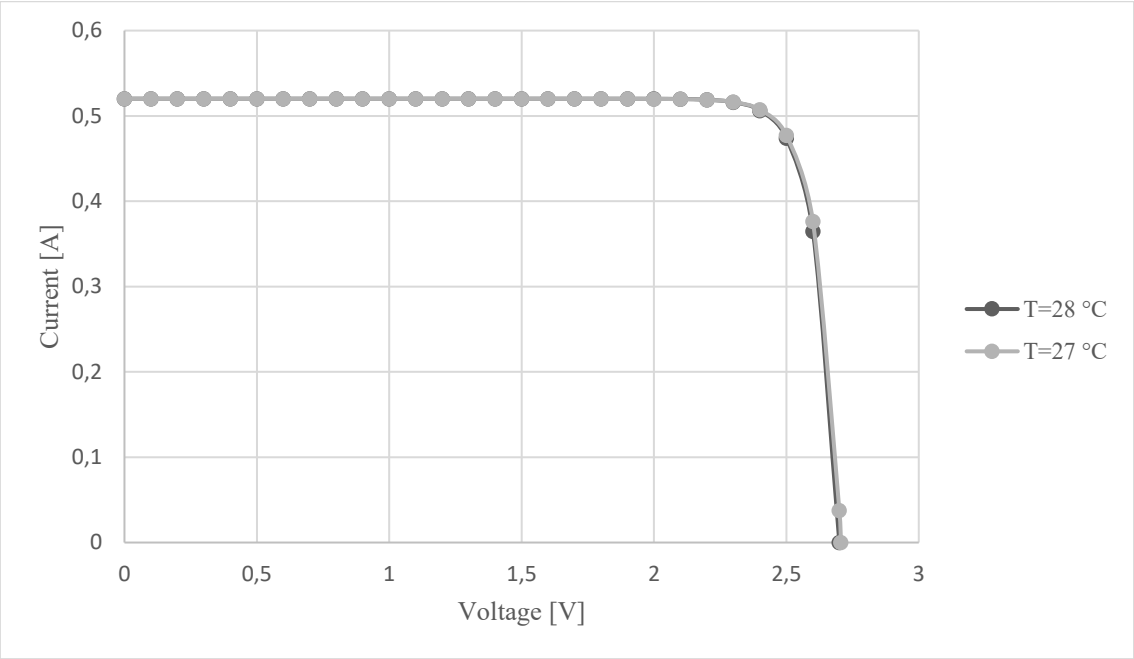

Figure 29 - PV characteristic

The losses due to solar array assembly, shadowing and temperature variations are considered by the inherent degradation I_d.

Element of Inherent Degradation	Nominal	Range
Design and Assembly	0.85	0.77-0.90
Temperature of the array	0.85	0.80-0.98
Shadowing of the cells	1.00	0.80-1.00
Inherent Degradation, Id	0.77	0.49-0.88

Table 16 - Element of Inherent degradation. Source: (Larson, 1999)

To be conservative, the lowest limits for Design and Assembly and Shadowing of the cells were considered. The coefficient due to array's temperature was set equal to 0.98. The total Id is 0.6. Therefore, it's possible to calculate the power at beginning of life as:

$$P_{BOL} = P_0 \cdot I_d \cdot cos(\theta) \quad [17]$$

Where θ is the Sun incidence angle between the normal to the panel and the Sun line. For this mission, a reasonable value is 10°. To have an estimation of the output power at the end of life of the system, the power degradation factor L_d must be considered. It can be calculated as

$$L_D = (1 - degradation/yr)^{mission\ life} \quad [18]$$

The degradation per year of a triple junction solar cell ca be assumed equal to 0.5% (Lotfy, Anis, Atalla, Halim, & Abouelatta, 2017). The end of life power output is therefore

$$P_{EOL} = L_d \cdot P_{BOL} \quad [19]$$

At the end, the solar array area and the mass can be calculated.

$$A_{sa} = P_{sa}/P_{EOL} \quad [20]$$

$$M_{sa} = k_{PV} \cdot A_{sa} \quad [21]$$

P_{sa} is the power that the solar array must provide and k_{PV} is a constant that considers for the total assembly weight of the PV array. It varies from 2.7 to 4.5 kg/m^2 (Wu, 2016) with a nominal value of 3.6 kg/m^2. The series and parallel number of cells are computed as:

$$N_s = V_{bus}/V_{mp}(T_{max}) \quad [22]$$

$$N_p = I_{SA}/(I_{mp}(T_{max}) \cdot G/G_{STD}) \quad [23]$$

Where: - V_{bus}= bus tension [V]
- $V_{mp}(T_{max})$= maximum power cell tension at T_{max} [V]
- I_{SA}= solar array current [A]
- $I_{mp}(T_{max})$= maximum power current at Tmax [A]
- G= solar irradiance landing site [W/m2]
- G_{STD}= PV test solar irradiance [W/m2]

5.5 Parametric analysis

The best configuration, in mass term, is obtained with a parametric analysis varying the nominal power from the ASRG source. The two limit cases are presented in Table 17. The ASRG has a degradation per year equal to 0.8 %/yr.

P_{ASRG} = 0 kW			**P_{ASRG} = 17,2 kW EOL**		
Batteries	N_s	29	Batteries	N_s	0
	N_p	9452		N_p	0
	m [t]	27.8		m [t]	0
PV	P_{sa} [kW]	68	PV	P_{sa} [kW]	40.8
	A_{sa} [m^2]	310		A_{sa} [m^2]	186
	N_s	50		N_s	50
	N_p	1166		N_p	700
	m [t]	1.1		m [t]	0.7
ASRG	m [t]	0	ASRG	m [t]	2.3
Total mass [t]		**29**	**Total mass [t]**		**3**

Table 17 - Limit cases power budget design

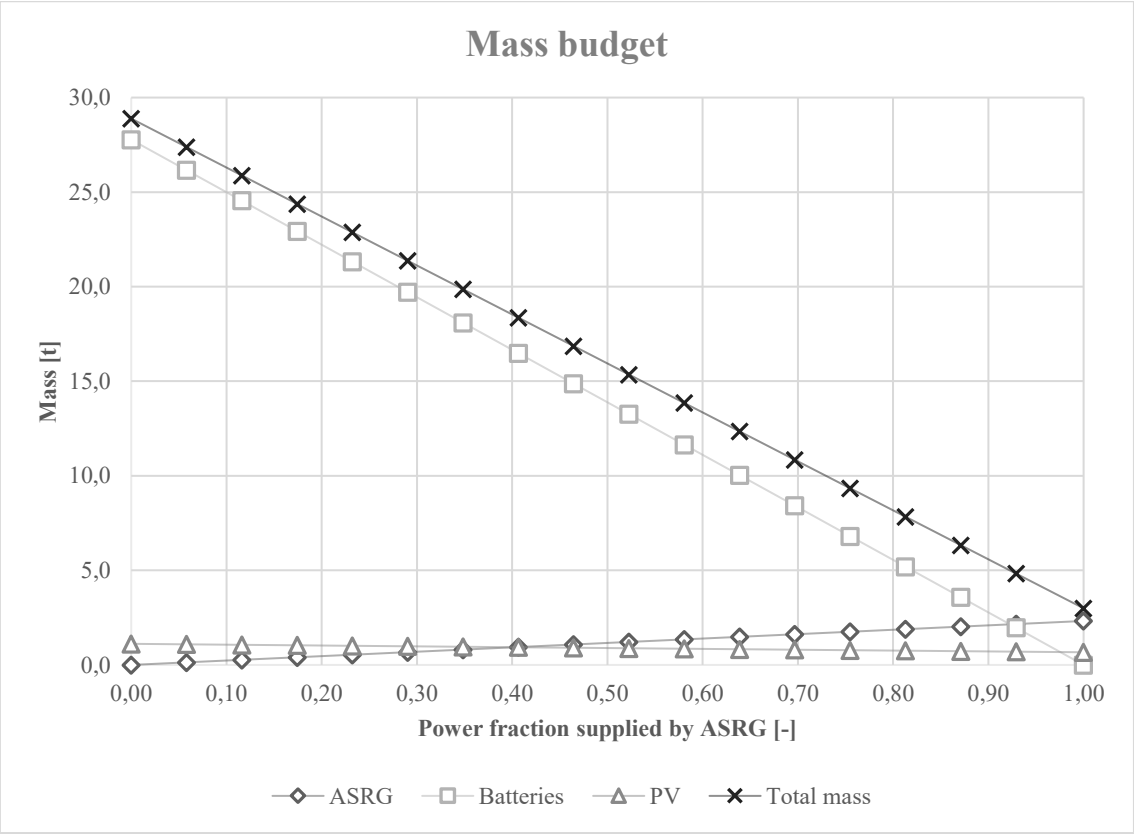

Figure 30 - Parametric analysis power supply

From Figure 30 is visible that the PV mass is almost constant and that the ASRG mass increases less than the decrease of batteries mass curve. It is clear that by taking into account only the mass as figure of merit, the best configuration would be the one without considering the presence of batteries. However, it is fundamental to highlight that the ASRG technology is relatively new for the space market, while the energy storage based on batteries has a strong heritage. These considerations bring to the conclusion that a power system design based only on ASRG without any energy storage capability would be a too risky design option. The working point considered is therefore the intersection between ASRG and batteries mass curve which represents a good compromise between the mass saving goal and the necessary presence of an energy storage system as a de-risking design choice. We consider a power fraction of 0,93 and so 16 kW_e at the end of life. The total mass is 5 tons and is distributed as in Figure 31. The specific power of Plutonium 238 is about 560 W_{th}/kg and the necessary radioisotope mass is therefore 103 kg.

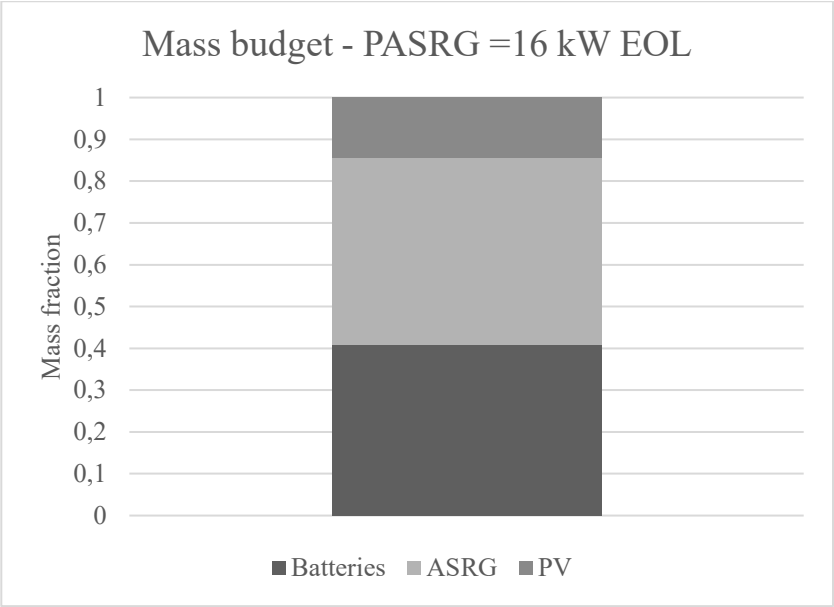

Figure 31 - Mass distribution

5.6 Battery oversizing

To consider a possible failure of the ASRG system or compensate a peak power demand, it's necessary to oversize the batteries. The hypothesis is a 20% power loss. The new total mass is now 10 tons with a distribution as in Figure 32.

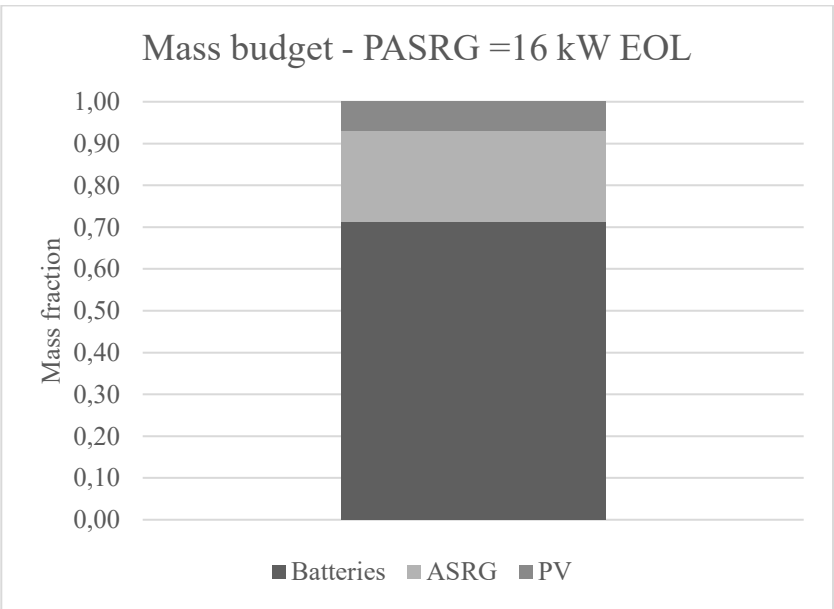

Figure 32 - Battery oversizing

5.7 Batteries advantages and disadvantages

The batteries are a consolidated technology, easy to use and implement. They need very low maintenance and have a quick response. On the other hand, they suffer self-discharge and ageing, i.e. the performance has a degradation during life. The operating temperature can vary between -20 °C and +60 °C, otherwise the performance will decrease rapidly. Another important parameter is the Depth of Discharge (DOD), or a degree at which the battery is discharged in relation to its total capacity. The bigger is the DOD, the lower number of cycle a battery can reach. It's also difficult to obtain the state of charge, due to the difficulty in measure and control the chemical reaction. Overcharge and over-discharge will reduce the battery's life.

5.8 Flywheel technology

It was investigated another energy storage technology, in order to reduce the mass budget. The flywheel stores energy in a mechanical form, putting in rotation a mass with a defined moment of inertia.

5.8.1 Basics

The stored energy depends linearly on the rotor shape, and quadratically to the angular velocity as the equation

$$\mathrm{E} = 1/2 \cdot I \cdot \omega^2 \qquad [24]$$

Where I is moment of inertia and ω is angular velocity. The moment of inertia depends on the rotational axis and the mass. It is calculated as

$$I = \int_m r^2 dm \qquad [25]$$

r is the distance of the infinitesimal mass dm from the axis. For a thin rim, where the thickness is negligible, the moment of inertia becomes:

$$I = m \cdot r^2 \qquad [26]$$

The energy density is therefore equal to

$$\mathrm{E} = 1/2 \cdot \mathrm{m} \cdot \mathrm{r}^2 \cdot \omega^2 \qquad [27]$$

The maximum energy storable depends on the maximum velocity the rotor can achieve, that is limited by the tensile strength of the material. The definition is reported in Equation 29.

$$\sigma_{max} = \rho \cdot \mathrm{r}^2 \cdot \omega^2 \qquad [28]$$

ρ is the material density. The unit of measure is $\mathrm{N/m^2}$. At the end, the energy density formula is obtained, as function of density and tensile strength.

$$E = 1/2 \cdot \frac{\sigma_{max}}{\rho} \quad [J/kg] \qquad [29]$$

For a general case, the equation becomes

$$E = k \cdot \frac{\sigma_{max}}{\rho} \quad [J/kg] \qquad [30]$$

Where *k* is a shape factor, function of the rotor used. From Equation 30, it's possible to see that the energy density is proportional to σ_{max} and inversely proportional to the density.

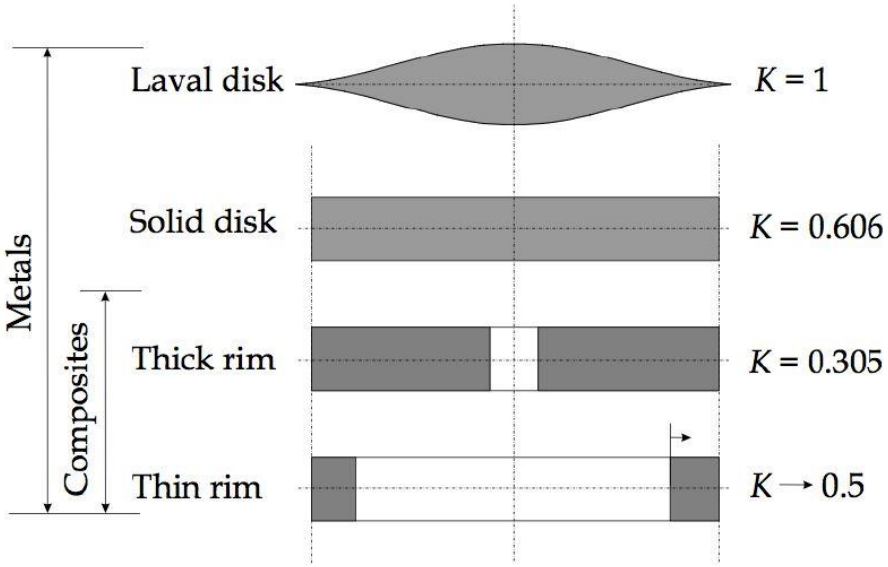

Figure 33 - Different rotor shape. Source: (Östergård, 2011)

The shape of the rotor depends on the material: if anisotropic, like fibre-reinforced composites, the best choice is a rim due to the unidirectional tensile strength. When a surplus of electrical energy occurs, the system charges the flywheel trough the electrical machine acting as motor, increasing the rotor velocity. In discharge phase, it slows down until a minimum angular velocity and the machine acts as a generator.

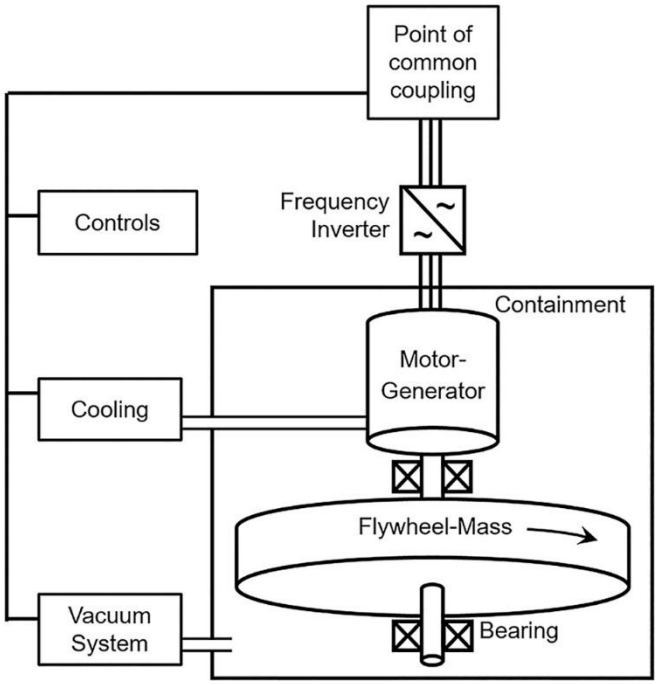

Figure 34 - Flywheel architecture. Source: (Wicki & Hansen, 2017)

In a flywheel system, the bearings and the containment are key features. Both play an important role in the system efficiency. To reduce the friction losses, magnetic bearings and vacuum housing must be used.

5.8.2 Material comparison

To have an idea of the storable energy, different materials were investigated.

Material	Density [kg/m3]	Tensile strength [GPa]
4320 Steel	7700	1.52
AISI 4340	7800	1.80
AlMnMg	2700	0.60
TiAl6Zr	4500	1.20
E-glass	200	0.10
S-glass	1920	1.40
Carbon T-1000	1520	1.95
Projected composites	1780	10

Table 18 - Material characteristic

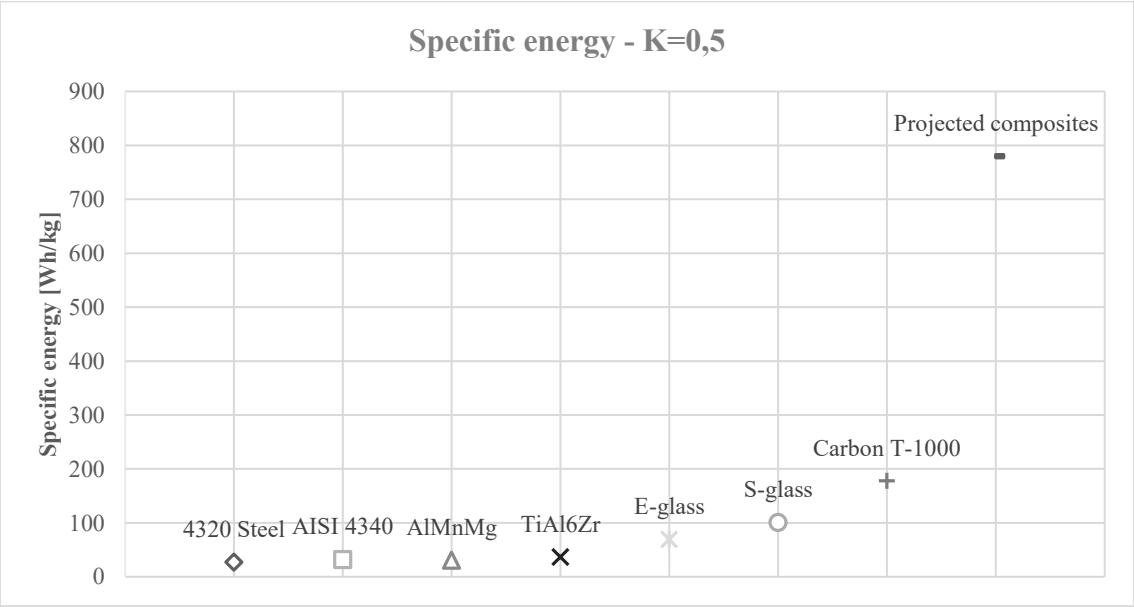

Figure 35 – Flywheel specific energy with k=0.5

Considering a projected composites material with a shape factor equal to 0.5, the maximum energy storable can reach 780 Wh/kg, that is more than four times the battery energy density.

5.8.3 Advantages and disadvantages

The main positive flywheel characteristics are:

- High power density
- Relatively high energy density
- Low capacity degradation during the charging and discharging phase
- Easy state of charge measurement, function of the rotational speed, independent from temperature and time
- Low maintenance
- Quick time response
- Low environmental impact
- Universal localization
- Long cycle life (~20 years)
- High efficiency
- Scalable technology
- Lower DOD capabilities

The disadvantages are:

- Maximum speed limited by material tensile strength
- Necessity to have magnetic bearings
- Vacuum housing has to be guaranteed
- Short discharge time

- Relatively high parasitic and intrinsic losses
- Potentially hazardous failure mode

5.8.4 Parametric analysis mass budget

The mass budget analysis is shown in Figure 36 and was carried out as for the Li-ion batteries. The two limit cases are shown in Table 19.

P_{ASRG} = 0kW			**P_{ASRG} = 17,2 kW EOL**		
FW	E_{FW} [kWh/kg]	0.78	FW	E_{FW} [kWh/kg]	0.78
	m [t]	4.2		m [t]	0
PV	P_{sa} [kW]	68.0	PV	P_{sa} [kW]	40.8
	A_{sa} [m^2]	310		A_{sa} [m^2]	186
	N_s	50		N_s	50
	N_p	1166		N_p	700
	m [t]	1.1		m [t]	0.7
ASRG	m [t]	0	ASRG	m [t]	2.3
Total mass [t]		**5**	**Total mass [t]**		**3**

Table 19 - Limit cases mass budget flywheel technology

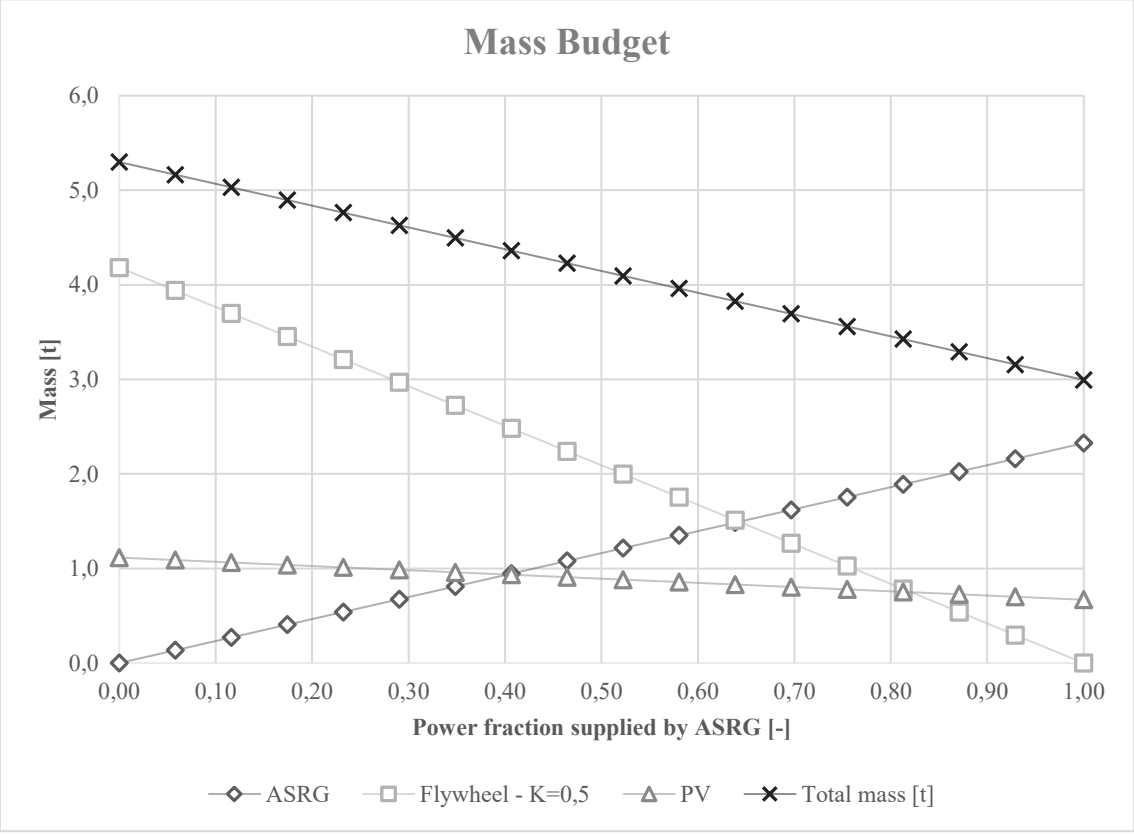

Figure 36 - Mass budget flywheel technology

The PV mass is almost constant; the ASRG and FW mass curves have the intersection in a power fraction supply of 0.63, smaller than that in Figure 30, with the implication of a reduction in power supply by ASRG. To have a mass reduction comparison and taking into account the same considerations done in Section 5.5, the working point

chosen is the same as the previous case, or 0.93 ASRG power fraction. In this point the total mass is 3 tons, distributed as Figure 37.

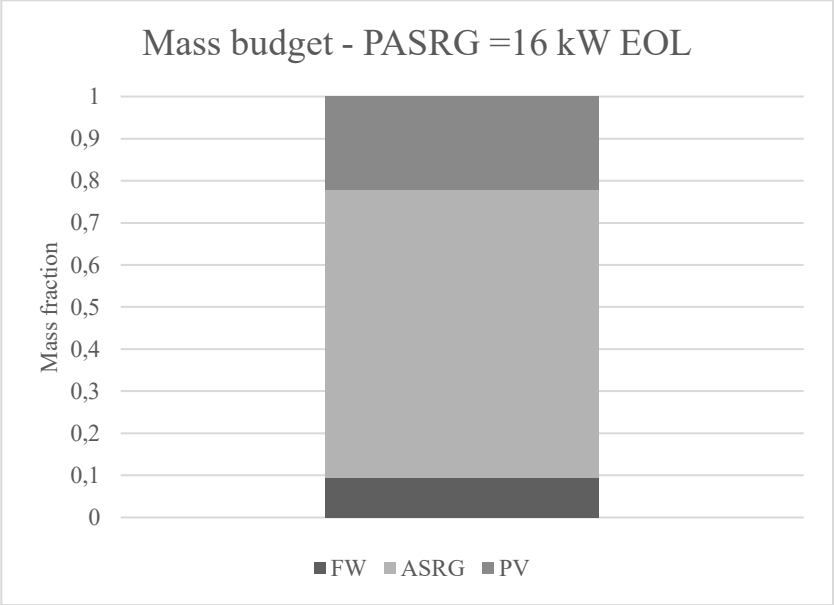

Figure 37 - Mass distribution with FW technology

5.8.5 Flywheel capacity oversizing

Also in this case, the hypothesis is the partial ASRG power loss, in particular equal to 20 %. The total mass is therefore 3.8 tons. There is a 62 % mass reduction, respect to the battery case energy storage.

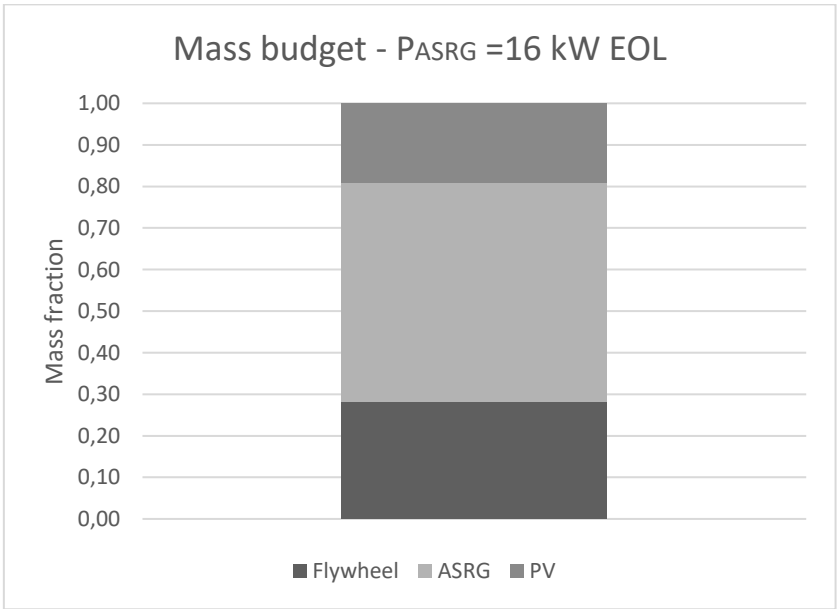

Figure 38 - Mass distribution FW oversizing

In this case, ASRG gives the major contribution to the total mass and it's more than 50 %.

5.8.6 Discharge strategy

The flywheel technology has a relatively short discharge time, and this allows its use in power quality application, less indicate for large scale usage. If they are aggregated in multiple cells configuration, it's possible to overcome the limit: each flywheel intervenes when the previous one has reached the maximum design DOD, i.e. the minimum velocity achievable.

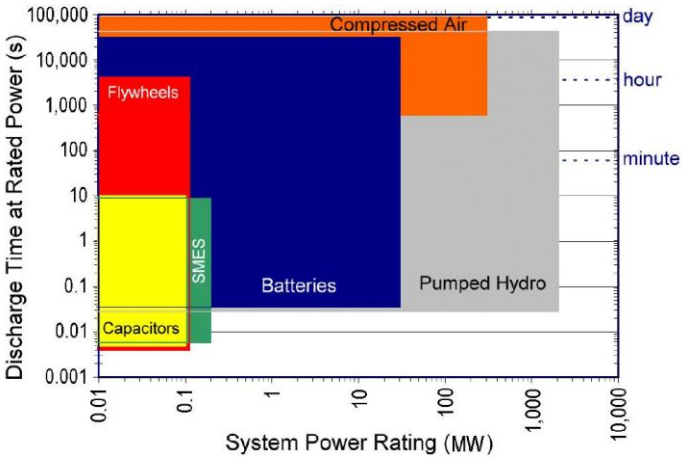

Figure 39 - System power rating and discharge time for different storage

Chapter 6

Thermal Control System

The design of the thermal control system (TCS) starts with the hypothesis of the structure that can be used for a manned mission. The TCS permits to control the base temperature and to take it in a reasonable temperature range. The modular base built is taken from a preliminary study, part of the European Space Exploration Programme AURORA.

6.1 Lunar base

The lunar base is a modular structure with a cylindrical shape, 17 m long and with an outer diameter of 6 m. The total volume must be almost equal to ISS one (935 m^3) in order to be consistent with the assumptions taken in building up the power budget. Therefore, the structure will be composed by 5 modules.

6.1.1 Structure and stratigraphy

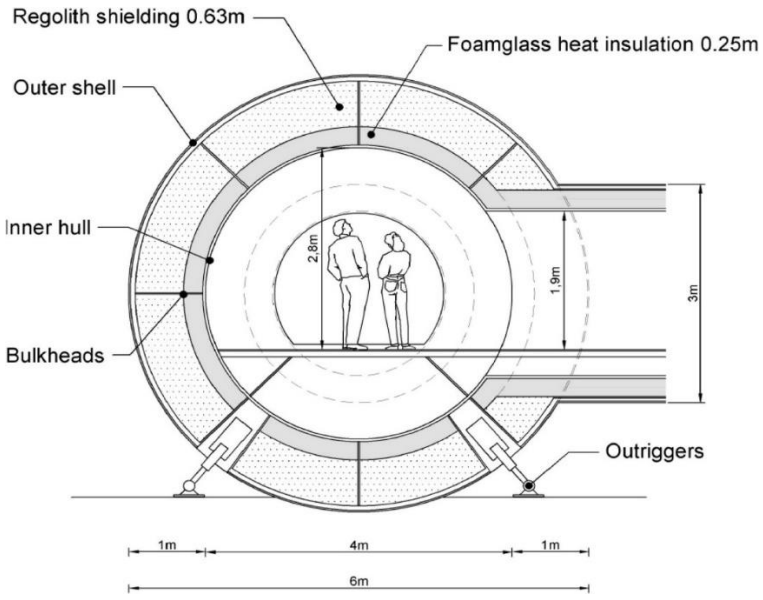

Figure 40 - Moon base structure. Source: (Grandl, 2017)

The configuration is shown in Figure 41. The modules considered are the following:

a. Energy plant module (only PV is considered in this study). The nuclear power source has been considered placed far from the living modules.
b. Living module
c. Airlock module
d. Laboratory module
e. Private room living module
f. Additional module (not considered for this study)

For further information see (Grandl, Human life in the Solar System, 2017).

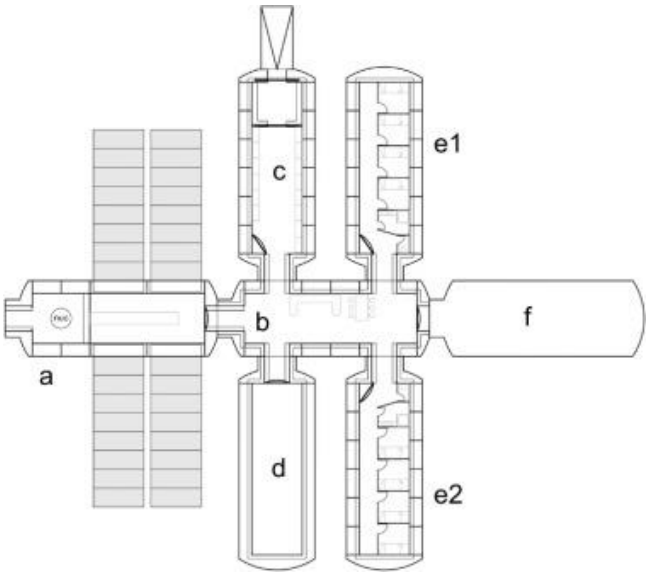

Figure 41 - Modular habitat configuration. Source: (Grandl, 2017)

To have an idea of the thermal load for the entire base, a simplified stratigraphy from (Grandl, Human life in the Solar System, 2017) was considered.

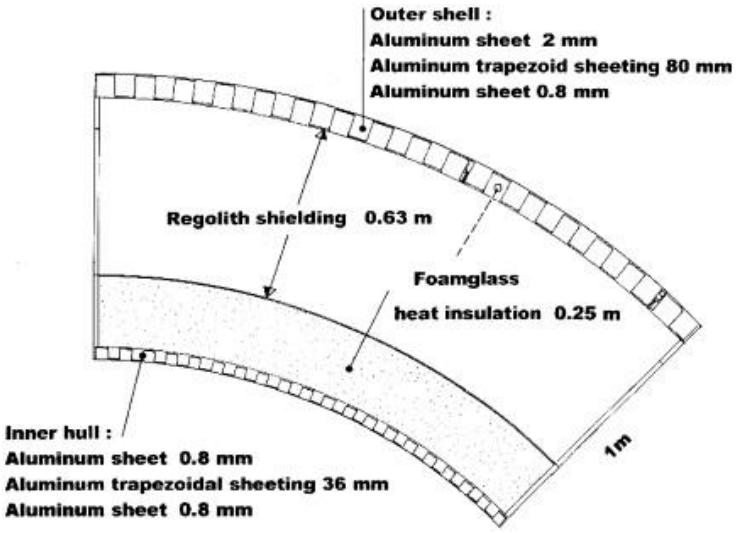

Figure 42 - Module stratigraphy. Source: (Grandl, 2007)

In particular, from inside to outside, the following materials were assumed:

- Internal aluminium sheet (37.2 mm)
- Foamglass heat insulation (250 mm)
- Regolith shielding (630 mm)
- External aluminium sheet (82.8 mm)

The total thickness will be 1 m. The internal and external aluminium sheets weren't considered to be trapezoidal: this hypothesis is conservative because probably the trapezoidal sheet has a lower thermal conductivity due to air or Foamglass presence. Furthermore, it simplifies the model.

6.1.2 Landing site and internal temperature conditions

The lunar surface temperature varies mainly with latitude and the angle that the Sun forms with the horizon (Simonsen, Debarro, & Farmer, 1992).

$$T_m = 373.9 \cdot cos(\Phi)^{0.25} \cdot sin(\vartheta)^{0.167} \quad [\text{K}] \qquad [31]$$

Where Φ= latitude (deg)
θ=Sun's angle with the horizon

For North Haworth, the latitude is 86.3 S and therefore the model used is the following: (Mottaghi & Benaroya, 2014)

$$T_m = \begin{cases} 161.607 \cdot [sin(11.4786 \cdot d + 9.6495)]^{1/6} & for\ 0 \le d \le 14 \\ 120 & for\ 14 < d \le 28 \end{cases} \quad [\text{K}] \qquad [32]$$

Where d= Earth days.
Equation 31 was developed for 88° S, that is almost landing site latitude.

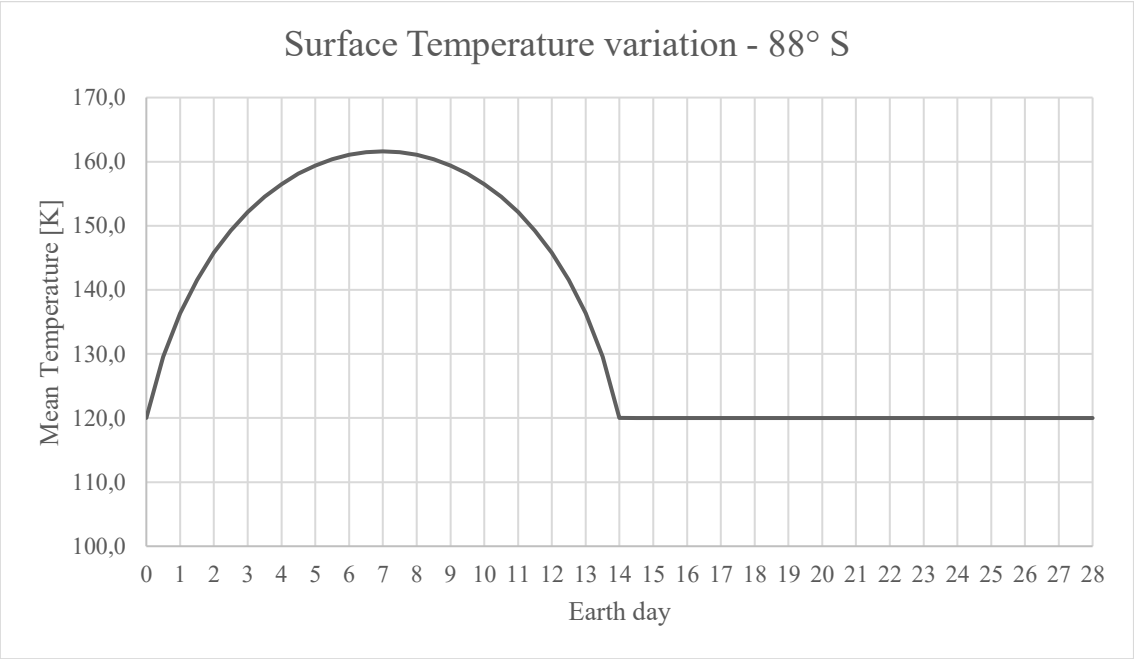

Figure 43 - Surface temperature variation at landing site

The model assumes a fast cooling after sunset with a temperature of 120 K constant during the lunar night. The internal temperature condition is set at 23 °C, or 296 K.

6.1.3 Thermal properties

The material properties are summarized in Table 20 and considered constant with temperature. To sustain this assumption, the worst-case values has been taken into account, as described below.

Material	Thermal conductivity [W/m/K]
Aluminium	302
Foamglass	0.042
Regolith	0.011

Table 20 - Material properties modules

Aluminium

In the range 100-300 K, the aluminium thermal conductivity decreases as the temperature increases. Therefore, it was considered at 120 K (worst case possible) to be conservative and it was obtained with a linear interpolation between 100 and 150 K.

Aluminium	
T [K]	k [W/m/K]
100	302
150	248
200	237
250	235
300	237

Table 21 - Aluminium thermal conductivity

Foamglas

The thermal conductivity of the foamglas varies with the temperature and the trend is shown in Figure 44. It was chosen the value at 23 °C for the same conservative reasons. The linear interpolation between 10 and 24 °C gives k=0.042 W/m/K approximately.

THERMAL CONDUCTIVITY (λ) VALUES AT SELECT MEAN TEMPERATURES (ASTM C518, C177)														
TEMPERATURE	°C (°F)	204 (400)	149 (300)	93 (200)	38 (100)	24 (75)	10 (50)	-18 (0)	-46 (-50)	-73 (-100)	-101 (-150)	-129 (-200)	-157 (-250)	-165 (-265)
ASTM C552[3]	W/m K (BTU in/hr °F ft²)	0.084 (0.58)	0.069 (0.48)	0.058 (0.40)	0.048 (0.33)	0.045 (0.31)	0.043 (0.30)	0.039 (0.27)	0.035 (0.24)	0.030 (0.21)	0.027 (0.19)	0.025 (0.17)	0.023 (0.16)	N/A
FOAMGLAS® ONE™ Insulation[4]	W/m K (BTU in/hr °F ft²)	0.078 (0.54)	0.066 (0.46)	0.054 (0.38)	0.044 (0.31)	0.042 (0.29)	0.040 (0.28)	0.036 (0.25)	0.032 (0.22)	0.029 (0.20)	0.026 (0.18)	0.023 (0.16)	0.021 (0.14)	0.020 (0.14)

Figure 44 - Foamglass thermal conductivity

Regolith

The regolith thermal conductivity was estimated from Apollo missions' experiments. It's on the order of 10^{-3} W/m/K in the upper soil layer (~ 2cm) and then varies in the range 0.009-0.013 W/m/K. A nominal value of 0.011 W/m/K was chosen.

6.2 Heating loads

The TCS design was performed for a lunar night (worst case). For the lunar day, in case heat dissipation would be necessary, it's reasonable to consider the presence of radiators. The absence of atmosphere on the Moon implies conduction and radiative heat transfer only. To calculate the heating load, it's necessary to set up a template that considers how the physic works. The highest temperature gradient is in radial direction, so it is possible to consider a 1D radial model. A more accurate calculation could be done with a 3D simulation tool. The module's external layer will exchange heat mainly by radiation with external ambient at T_{amb}. Inside the module the presence of air favours convection with h_{in} heat transfer coefficient at internal temperature T_{in}.

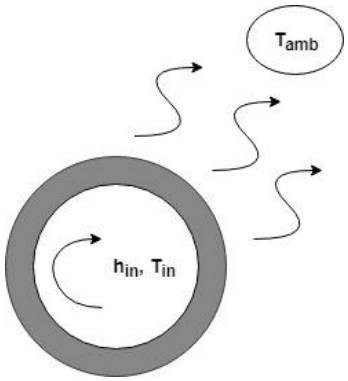

Figure 45 - Module's boundary conditions

The external temperature is 120 K, h_{in} is considered equal to 10 W/m^2/K and T_{in} is set at 23 °C, or 296 K. Performing a heat balance, it is possible to connect the three thermal fluxes: convective, conductive and radiative.

The equations are:

$$\left|\dot{Q}_{conv}\right| = h_{in} \cdot (T_{in} - T_{w,i}) \cdot A_{int} \quad [33]$$

Where $T_{w,i}$= internal wall temperature [K]
A_{int}= internal surface [m^2]

$$\left|\dot{Q}_{tr}\right| = 2 \cdot \pi \cdot L \cdot (T_{w,i} - T_{w,o})/R_{tot} \quad [34]$$

Where $T_{w,o}$= outer wall temperature [K]
L= module's length [m]
R_{tot}= total conductive resistance [m·K/W]

$$\left|\dot{Q}_{rad}\right| = \varepsilon \cdot \sigma \cdot ({T_{w,o}}^4 - {T_{amb}}^4) \cdot A_{ext} \quad [35]$$

Where σ = Stefan-Boltzmann constant [$W/m^2/K^4$]
A_{ext}= external surface [m^2]
ε= Aluminium emissivity [-]

In cylindrical geometries, with multiple layers

$$R_{tot} = \sum_{i=1}^{n} 1/k_i \cdot ln(r_{i+1}/r_i) \quad [36]$$

Where k_i= thermal conductivity of i-th layer [W/m/K]
r= radius [m]
n= number of layers [-]

The unknowns are $T_{w,i}$ and $T_{w,o}$. To solve this nonlinear problem, the Newton's method can be used. To do this, it is necessary to reformulate the three equations into a single function. Firstly, Equations. 33 and 34 are combined and $T_{w,i}$ is explicated as function of $T_{w,o}$.

$$h_{in} \cdot (T_{in} - T_{w,i}) \cdot r_{int} = (T_{w,i} - T_{w,o})/R_{tot}$$

$$T_{w,i} = \frac{r_i \cdot h_{in} \cdot T_{in} + T_{w,o}/R_{tot}}{r_i \cdot h_{in} + 1/R_{tot}} \quad [37]$$

Then, combining equation 33 with 35 and substituting equation 37 I obtain:

$$r_i \cdot h_{in} \cdot (T_{in} - \frac{r_i \cdot h_{in} \cdot T_{in} + T_{w,o}/R_{tot}}{r_i \cdot h_{in} + 1/R_{tot}}) = \varepsilon \cdot \sigma \cdot r_e (T_{w,o}^4 - T_{amb}^4) \quad [38]$$

Equation 38 is only a function of $T_{w,o}$ and rewriting it in the form $f(T_{w,o})=0$ the result is:

$$r_i \cdot h_{in} \cdot T_{in} - r_i \cdot h_{in} \cdot \frac{r_i \cdot h_{in} \cdot T_{in} + T_{w,o}/R_{tot}}{r_i \cdot h_{in} + 1/R_{tot}} - \varepsilon \cdot \sigma \cdot r_e \cdot T_{w,o}^4 + \varepsilon \cdot \sigma \cdot r_e \cdot T_{amb}^4 = 0 \quad [39]$$

To solve this equation, it was implemented a MATLAB® routine (Appendix C). The result is $T_{w,o}$= 126.65 K with a relative error of 1e-4. With ε=0.8 the specific radiative power is therefore:

$$q = \varepsilon \cdot \sigma \cdot ({T_{w,o}}^4 - {T_{amb}}^4) = 2.26\ W/m^2 \quad [40]$$

The view factor was considered equal to 1. The temperature profile in the stratigraphy is:

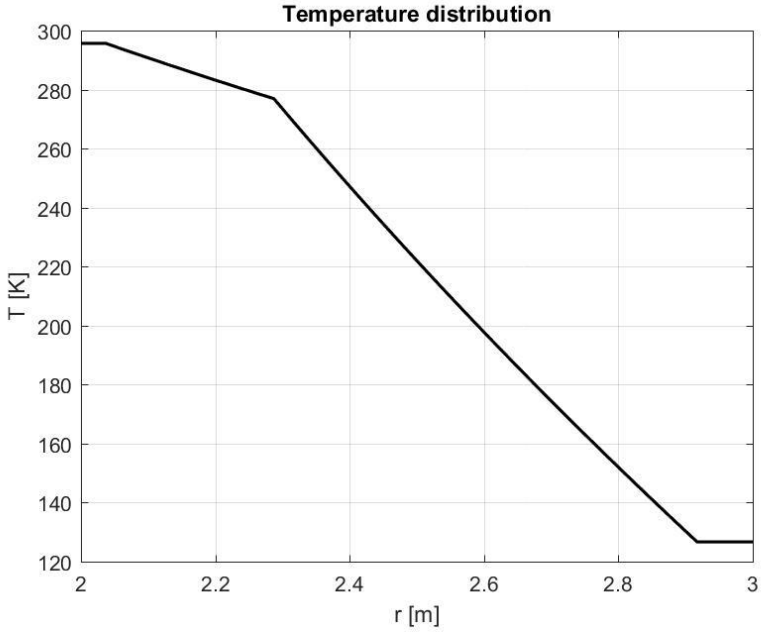

Figure 46 - Module's temperature profile

The total external surface area of the 5 modules is:

$$A_{ext} = 2 \cdot \pi \cdot r_o \cdot L \cdot 5 = 1602\ m^2 \quad [41]$$

The power dissipated is therefore:

$$\dot{Q}_{th} = 3629\ W = 3.6\ kW \quad [42]$$

It is also relevant the thermal load contribution through the cylinder basis. Therefore, the total power load becomes:

$$\dot{Q}_{th} = 4.3\ kW \quad [43]$$

The internal heat gains (persons, computers and any other electronic instruments) and solar gains were neglected to have a conservative and worst-case result.

6.3 Heat transfer system layout

The nuclear waste heat can be a thermal power source for the lunar base. The Stirling cycle of the ASRG has a hot junction temperature of 850 °C and a cold junction temperature of 90 °C. The EPS was sized with 16 kWe coming from ASRG at EOL. Considering an overall ASRG efficiency of 30 %, the heat that must be rejected is about 37 kW. The hypothesis is to transfer the 50 % of this power and see if it can cover totally or partially the heat load required. To do this, it was hypothesized a 100 m distance between ASRG power plant and the living modules due to safety issues. This distance implies an active thermal control system choice. Further considerations must be done in order to correctly quantify this value.

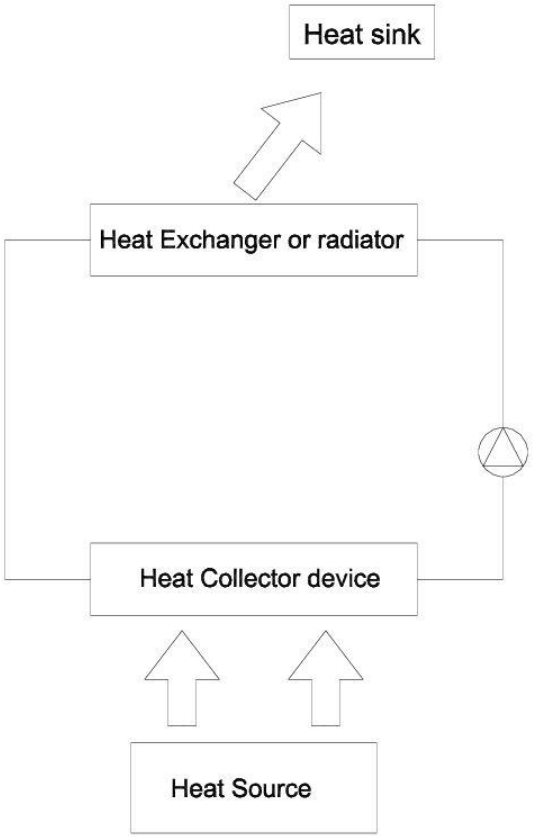

Figure 47 – Active Thermal control system general layout

6.3.1 Piping

The hypothesis is that the heat transfer pipe is made of stainless steel covered with Multi-Layer Insulation (MLI). The pipe has the following characteristics:

Stainless steel	
k_{steel} [W/m/K]	52
steel thickness [m]	7.1e-4
Di [m]	0.01905
MLI (20 layers)	
k_{MLI} [W/m^2/K]	0.0424
MLI thickness [m]	3e-3
ε [-]	0.05

Table 22 - Pipe characteristics

The MLI data were taken from a Thales Alenia Space specification. In particular, the "thermal conductivity" value is obtained from laboratory test and semiempirical correlations. It corresponds to the power transfer through a 20 layers MLI per unit area and per unit temperature difference. This characteristic is function of the temperature, but to simplify the calculation, it was chosen the value at -40 °C, mean temperature between the inlet heat transfer fluid temperature (80 °C) and the sink temperature 120 K. The main problem is to calculate, at that distance from the source, the temperature gradient and understand the feasibility of the solution. To do that, it was implemented a lumped parameter model of the pipe.

6.3.2 Multi-layer Insulation (MLI)

Multilayer insulation is one of the main components in passive thermal control system for space applications or cryogenic storage. It permits the reduction of heat leak due to radiative heat transfer. MLI consists of a series of reflective foils, stacked up to form a blanket. The principle is to thermally insulate thanks to radiation heat transfer barriers.

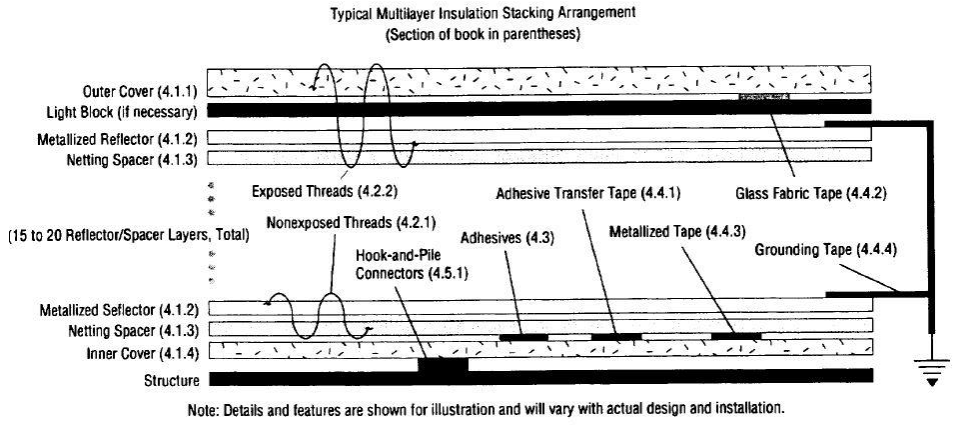

Figure 48 - MLI cross section – Source: NASA

The foils are generally made of plastic material, such as Kapton or Mylar, coated with highly reflective metal on both sides. They are placed between two surfaces and separated by insulating layers, such as silk or nylon. Another solution is to omit the insulation layer and provide only contact points between the surfaces in order to minimize thermal conduction.

Figure 49 – MLI closeup – Source: Wikipedia

The heat transfer coefficient scales as 1/(N+1), with N the number of MLI layers. The outer layer is generally a reinforced material to provide protection for the system that need to be insulated, for example beta cloth. It is a light weight system, with only few millimetres thickness, capable to support hundreds of degrees of temperature gradient.

6.3.3 Lumped parameter model

The lumped parameter model consists in discretizing the continuous geometry into a network of nodes. The nodes are linked to each other through conductors, or the heat transfer rate between 2 nodes at different temperature. The method derives from the analogy with electrical model, where the temperature difference is the voltage drop on a component and the heat flux is the current. The result is a series of algebraic equations that can be solved to obtain a numerical solution. Once discretized the geometry, the nodal heat balance must be solved:

$$C_i \cdot \frac{dT_i}{dt} = \sum_i GL_{ij} \cdot (T_j - T_i) + \sum_i \sigma \cdot GR_{ij} \cdot (T_j^4 - T_i^4) + Q_i \qquad [44]$$

Where:

- C_i= Capacitance [J/K]
- T_i= Temperature of node i [K]
- T_j= Temperature of adjacent node j [K]
- GL_{ij}= Linear/fluidic conductor between i-th and j-th node [W/K]
- GR_{ij}= Radiative conductor [m^2]
- Q_i= Nodal heat generation [W]
- σ= Stefan-Boltzmann constant [$W/m^2/K^4$]

The capacitance is the product of the mass [kg] and heat capacity c_p [J/kg/K]. The linear conductors are conductive, convective and fluidic. The convective GL is:

$$GL_{ij} = h \cdot A \quad [45]$$

Where:

- h= convective heat transfer coefficient [W/m^2/K]
- A= convective area [m^2]

The conductive GL is:

$$GL_{ij} = 1/R_{th} \quad [46]$$

Where:

- R_{th}= thermal conductive resistance [K/W]

In cylindrical geometry it is:

$$R_{th} = \frac{1}{2 \cdot \pi \cdot L} \cdot \sum_i \frac{1}{k_i} \cdot ln(r_{i+1}/r_i) \quad [47]$$

Where:

- k= thermal conductivity i-th layer [W/m/K]
- L= pipe length [m]
- r= radius [m]

The fluidic conductor is:

$$GL_{ij} = \dot{m} \cdot c_p \quad [48]$$

Where:

- ṁ= mass flowrate [kg/s]
- cp= specific heat [J/kg/K]

The radiative conductor is the product of the following parameters:

$$GR_{ij} = \varepsilon_i \cdot \ \varepsilon_j \cdot A_i \cdot F_{ij} \quad [49]$$

Where:

- ε= emissivity [-]
- A_i= Radiative area [m^2]
- F_{ij}= View factor between node i and j [-]

The calculus was done in steady state conditions, with a view factor equal to one. As first approach, the scheme applied is the following:

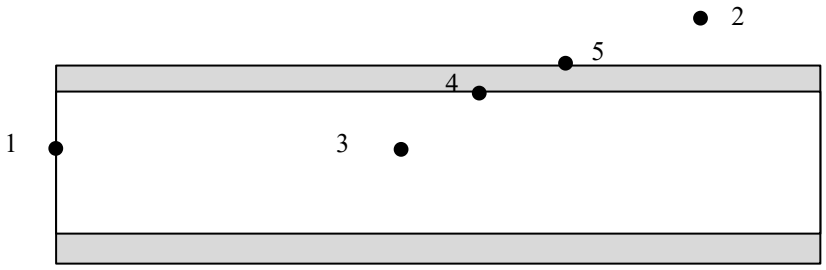

Figure 50 - Pipe scheme

The node 1 in the fluid inlet and the node 2 represents the sink (vacuum). Then node 3 is the fluid, 4 is the internal pipe layer and 5 is the external. Temperature in node 1 and 2 are imposed and they are T_1= 80 °C (353 K) and T_2= -153 °C (120 K). The nodes are linked as follows:

- 1-3 fluidic conductor
- 3-4 convective conductor
- 4-5 conductive conductor
- 5-2 radiative conductor

This is the model for an ideal 100 m long pipe. In reality, the pipe is divided into sections, the insulation layer is interrupted and then they are connected through a metallic junction. To consider the thermal losses linked to this phenomenon, an additional conductive conductor between the fluid and the external environment was considered, and in particular 0.1 W per linear meter per unit temperature difference. This value is extremely conservative and derives from internal Thales Alenia Space laboratory tests. The results obtained are:

Node i	**Node j**	**GL_{ij} [W/K]**
4	5	3.53E-01
3	2	1.00E+01

Table 23 - Linear conductors

Node i	**Node j**	**GR_{ij} [m^2]**
5	2	4.16E-01

Table 24 - Radiative conductors

The linear conductors from node 1 to 3 and from 3 to 4 depend on the mass flowrate and from the convective heat transfer coefficient, but also from the fluid used in TCS.

The analysis was performed in a parametric way, as function of the flowrate and of three different fluids. The total flowrate changes from 300 to 1300 kg/h, but only the 95% is used as heat transfer fluid. The reason is explained in paragraph 6.3.4. The Nusselt number, and so the convective heat transfer coefficient, was calculated with the Dittus-Boelter equation for fully developed turbulent flow. In particular, in case of cooling:

$$Nu_D = 0.0265 \cdot Re_D^{4/5} \cdot Pr^{(0.3)} \quad [50]$$

The range of validity is:

$$0.6 \leq Pr \leq 160$$
$$Re_D \geq 10000$$
$$L/D \geq 10$$

In case of non-turbulent flow, the convective coefficient was calculated with Equation 50 however, conscious that it was overestimated. This permits a conservative approach.
The solution of the model was obtained thanks to an internal Thales Alenia Space Excel worksheet, with and absolute error of 1e-7 °C. The problem was also been simulate with C&R Thermal Desktop® and 300 nodes and the error is smaller than 1% between the two models. Different fluids can be investigated. The most commonly used for space applications are:

- Water
- Water and glycol
- Ammonia
- Ethoxy-nonafluorobutane (HFE)

In this study I have analysed the first two fluids. Ammonia was excluded do to its toxicity and its boiling point at ambient pressure (-33.34 °C), that will let to a pressurized circuit. HFE was also not considered because boils at 76 °C at 1 atm.

Water

Water can be a coolant fluid, easy to find on some South polar craters of the Moon and therefore utilized for this purpose. It has a high specific heat, chemically stable and intrinsically safe (it' s not toxic, flammable or explosive). On the other hand, the temperature range of the liquid state varies from 0 °C to 100 °C, at ambient pressure. It can create problems if there is a failure in the system and the temperature goes under 0 °C. In this case can be used electrical heaters to prevent water solidification with a consequent increase in volume. I have analysed two pipe configurations, one with the pipe on the ground, exposed to the vacuum, and one in which the pipe was considered buried.

Ground pipe

The pipe scheme is the same as in Figure 50. The fluid temperature variation inside the pipe is between 70 and 80 °C. To be conservative, the physical properties were taken at 80 °C and this gives a higher convective heat transfer coefficient.

Water	
ρ [kg/m^3]	971.8
μ [Pa·s]	3.55E-04
c_p [J/kg/K]	4194
k_{H2O} [W/m/k]	0.656
Pr [-]	2.266

Table 25 - Water thermal properties

The convective coefficient and the temperature obtained are presented in the following Tables. It was then calculated the convective power loss Q_{tot}, the radiative one (Q_{rad}) and the loss due to metal junction between sections Q_{lin}. From the calculus obtained, it's possible to see that the about 98 % of the losses is due to the effect of the junctions between pipe section. The total power loss, in absolute value, varies from 2.31 kW to 2.36 kW and the curve is shown in Figure 51. The specific power per pipe meter is therefore in the range 23.1 to 23.6 W/m.

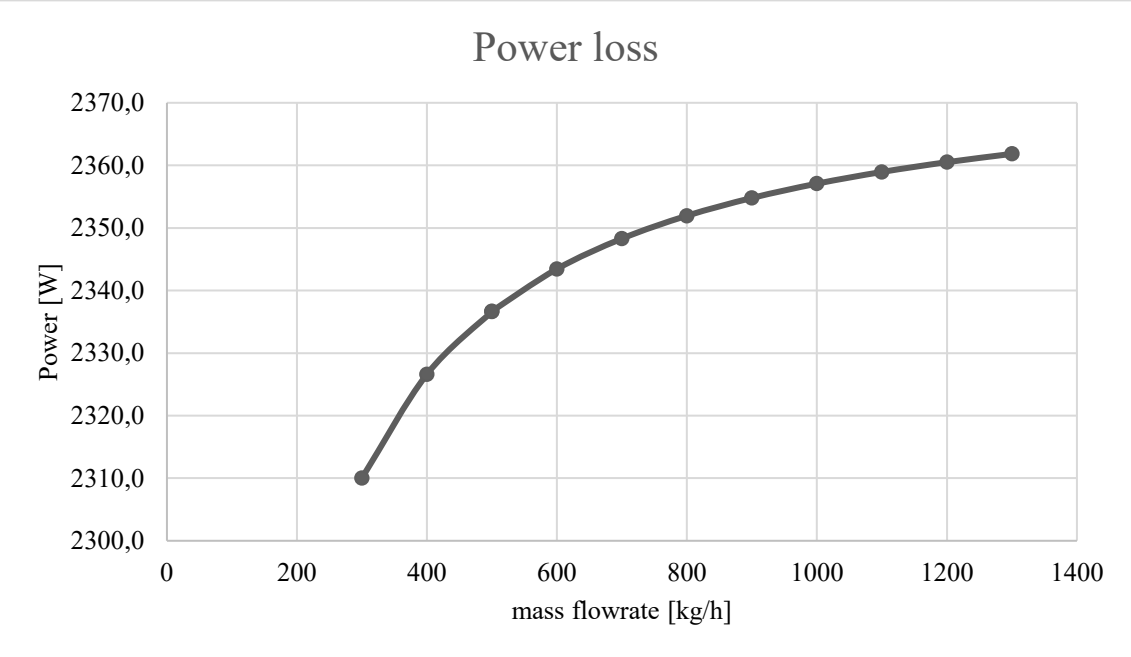

Figure 51 - Power loss ground pipe (Water)

Ground pipe Water											
$\dot{m}$ [kg/h]	1300	1200	1100	1000	900	800	700	600	500	400	300
v [m/s]	1.30	1.20	1.10	1.00	0.90	0.80	0.70	0.60	0.50	0.40	0.30
Re [-]	6.8E+04	6.3E+04	5.8E+04	5.2E+04	4.7E+04	4.2E+04	3.7E+04	3.1E+04	2.6E+04	2.1E+04	1.6E+04
Nu [-]	2.5E+02	2.3E+02	2.2E+02	2.0E+02	1.9E+02	1.7E+02	1.5E+02	1.3E+02	1.2E+02	9.7E+01	7.7E+01
h [$W/m^2/K$]	8.6E+03	8.0E+03	7.5E+03	7.0E+03	6.4E+03	5.8E+03	5.2E+03	4.6E+03	4.0E+03	3.3E+03	2.7E+03
$T_{f,o}$ °C	78.4	78.3	78.2	78.0	77.8	77.5	77.1	76.6	76.0	75.0	73.4
$T_{MLI,e}$ °C	-56.1	-56.1	-56.2	-56.2	-56.3	-56.3	-56.4	-56.6	-56.7	-57.0	-57.4
Q_{rad} W	47	47	47	47	47	47	47	47	47	47	46
Q_{lin} W	2314	2313	2312	2310	2308	2305	2301	2296	2290	2280	2264
Q_{tot} W	2362	2361	2359	2357	2355	2352	2348	2343	2337	2327	2310
%lin	0.98	0.98	0.98	0.98	0.98	0.98	0.98	0.98	0.98	0.98	0.98
%rad	0.02	0.02	0.02	0.02	0.02	0.02	0.02	0.02	0.02	0.02	0.02

Table 26 - Ground pipe water results

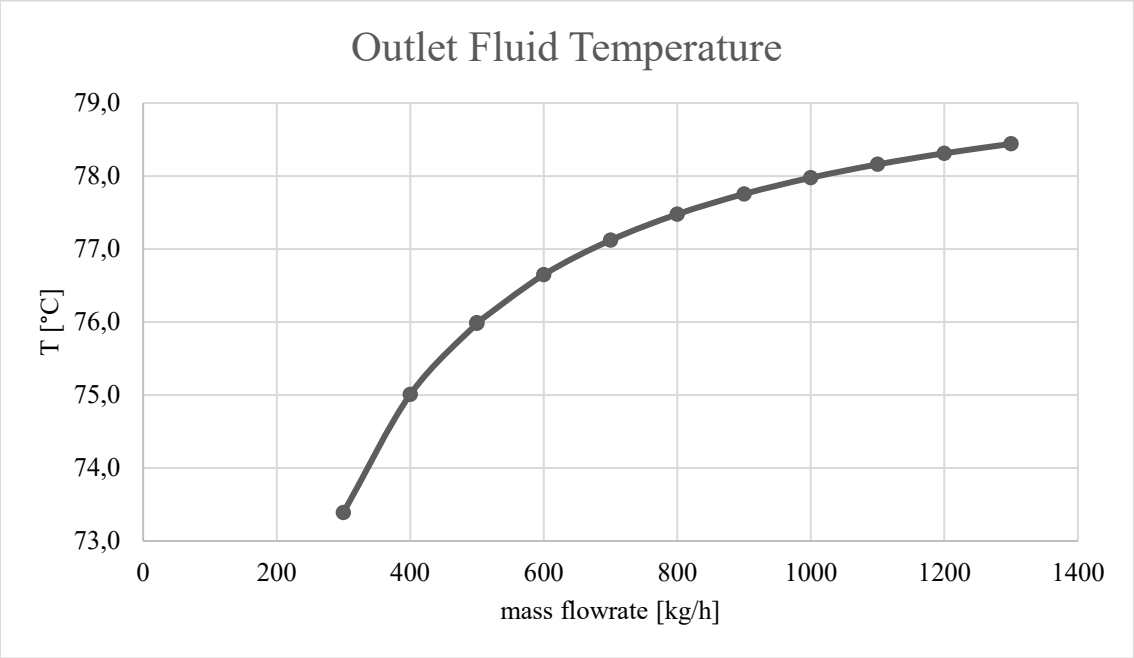

Figure 52 - Outlet fluid temperature (Water)

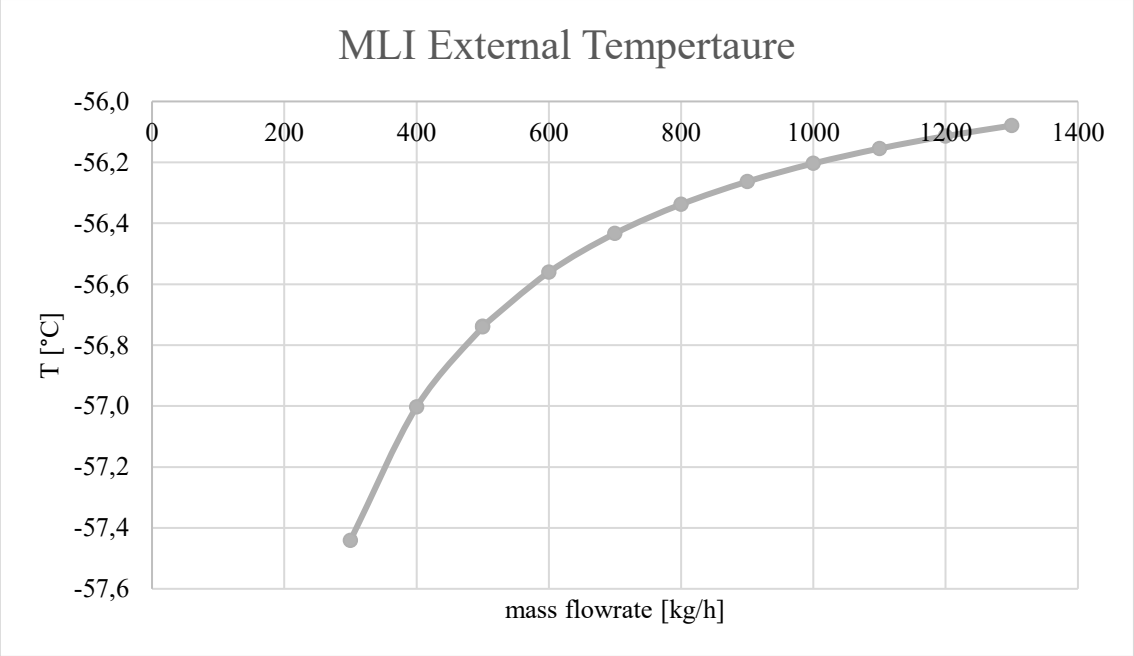

Figure 53 - MLI External Temperature (Water)

The outlet fluid temperature $T_{f,o}$ and the MLI one, increase as the mass flowrate increases, and the maximum temperature variation on $T_{f,o}$ is 6.6 °C.

Buried pipe

In the buried pipe case, the reference scheme is always Figure 50, but in these conditions it's not present node 2 (sink) and node 5 is a boundary node with imposed temperature. In particular, it was considered equal to 250 K at a depth of 50 cm. The scope is to see what the difference respect to the previous case is. In Figure 54 it's possible to see that the fluid temperature variation between inlet and outlet varies from 77.0 to 79.3 °C about. The maximum temperature variation between inlet and outlet is 3 °C.

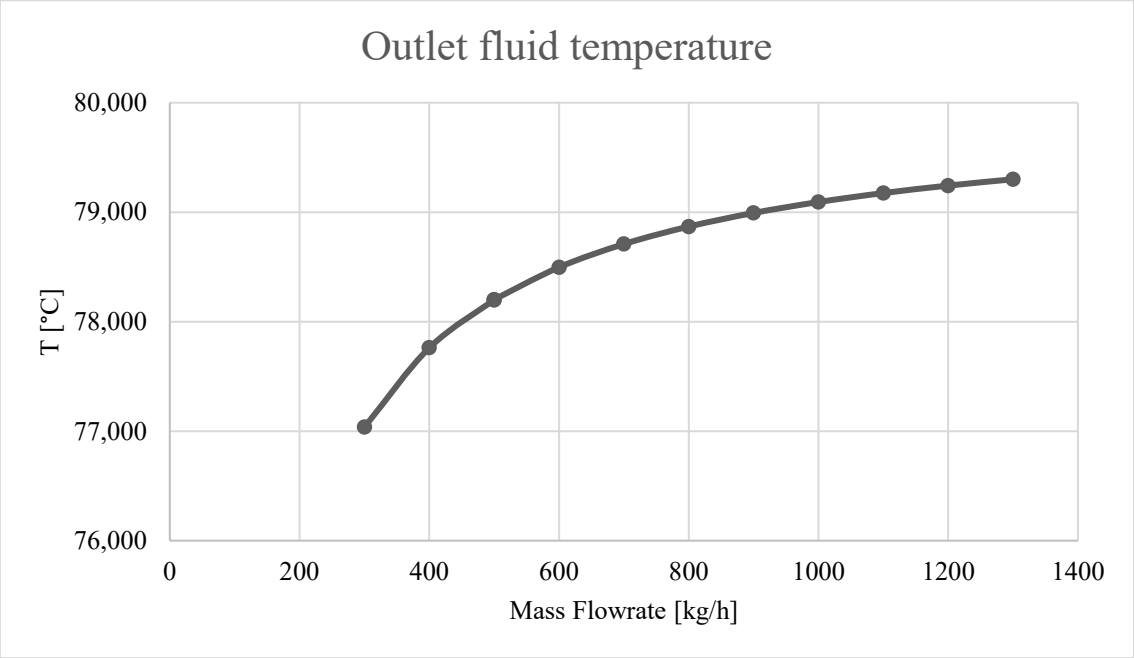

Figure 54 - Outlet fluid temperature buried pipe (Water)

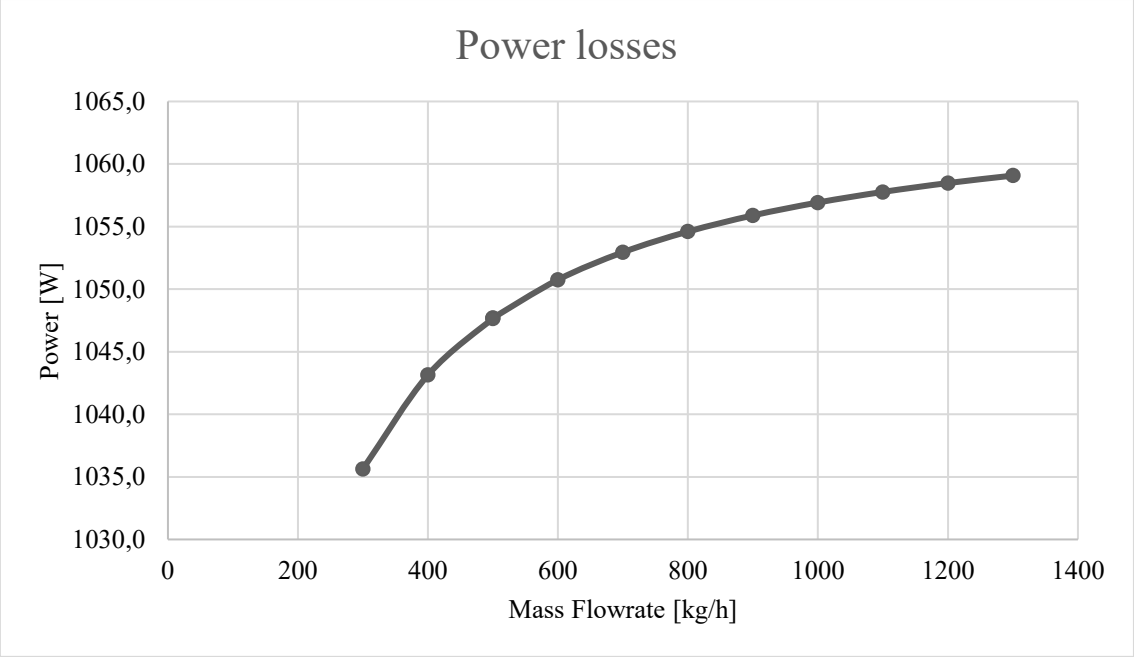

Figure 55 - Power losses buried pipe (Water)

Buried pipe Water											
$\dot{m}$ [kg/h]	1300	1200	1100	1000	900	800	700	600	500	400	300
v [m/s]	1.30	1.20	1.10	1.00	0.90	0.80	0.70	0.60	0.50	0.40	0.30
Re [-]	6.8E+04	6.3E+04	5.8E+04	5.2E+04	4.7E+04	4.2E+04	3.7E+04	3.1E+04	2.6E+04	2.1E+04	1.6E+04
Nu [-]	2.5E+02	2.3E+02	2.2E+02	2.0E+02	1.9E+02	1.7E+02	1.5E+02	1.3E+02	1.2E+02	9.7E+01	7.7E+01
h [W/m^2/K]	8.6E+03	8.0E+03	7.5E+03	7.0E+03	6.4E+03	5.8E+03	5.2E+03	4.6E+03	4.0E+03	3.3E+03	2.7E+03
$T_{f,o}$ °C	79.301	79.243	79.175	79.093	78.993	78.868	78.709	78.497	78.201	77.761	77.037
$Tss_{,i}$ °C	79.300	79.242	79.174	79.092	78.992	78.867	78.708	78.495	78.200	77.760	77.035
Q_{cond} W	36.1	36.0	36.0	36.0	36.0	35.9	35.9	35.8	35.7	1043.1	1035.6
Q_{lin} W	1023.0	1022.4	1021.7	1020.9	1019.9	1018.7	1017.1	1015.0	1012.0	35.5	35.3
Q_{tot} W	1059.1	1058.5	1057.8	1056.9	1055.9	1054.6	1052.9	1050.8	1047.7	1007.6	1000.4
%lin	0.03	0.03	0.03	0.03	0.03	0.03	0.03	0.03	0.03	0.03	0.03
%cond	0.97	0.97	0.97	0.97	0.97	0.97	0.97	0.97	0.97	0.97	0.97

Table 27 -Buried water pipe results

The power losses are lower and varies from 1.04 to 1.06 kW, with a specific power of 10.4 to 10.6 W/m. In this case, the flowrate variation has no relevant influence on outlet fluid temperature and specific power. As for ground pipe, the main power loss is due to metal junction between sections. The main disadvantage of this configuration is the accessibility of the pipe in case of maintenance or failure of the system. Therefore, this configuration was no longer considered.

Mixture of water and glycol

To have a higher temperature range, mainly for negative temperatures, it was implemented also a solution that uses as coolant fluid a mixture of water and glycol. In particular, it was considered with 47 % in volume mixture of 1,2-Propylenglycol $C_3H_6(OH)_2$. The temperature range in which it is in a fluid state varies from -57 to 187.4 °C at ambient pressure. Water glycol fluid is not corrosive for stainless steel, it's stable under normal conditions but it has a low degree of toxicity. As for water, the physical properties are taken at 80 °C.

Water and glycol	
ρ [kg/m^3]	999
μ [Pa·s]	1.1E-03
c_p [J/kg/K]	3450
k [W/m/k]	0.391
Pr [-]	9.7

Table 28 - Water and glycol thermal properties

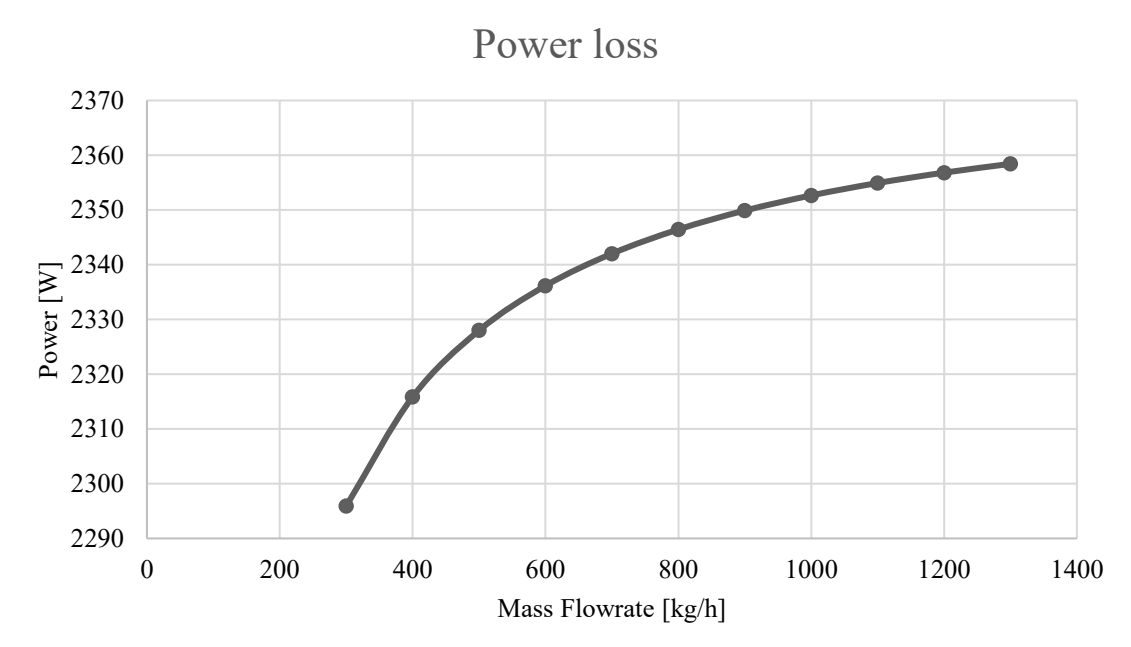

Figure 56 - Power loss (Water and glycol)

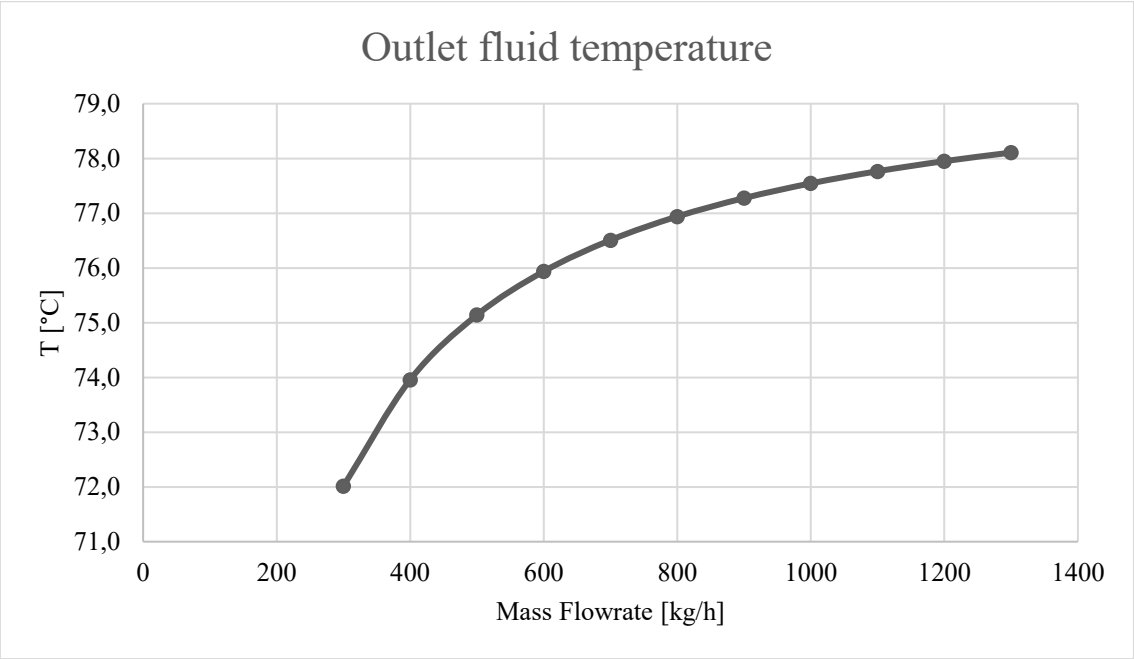

Figure 57 - Outlet fluid temperature (Water and glycol)

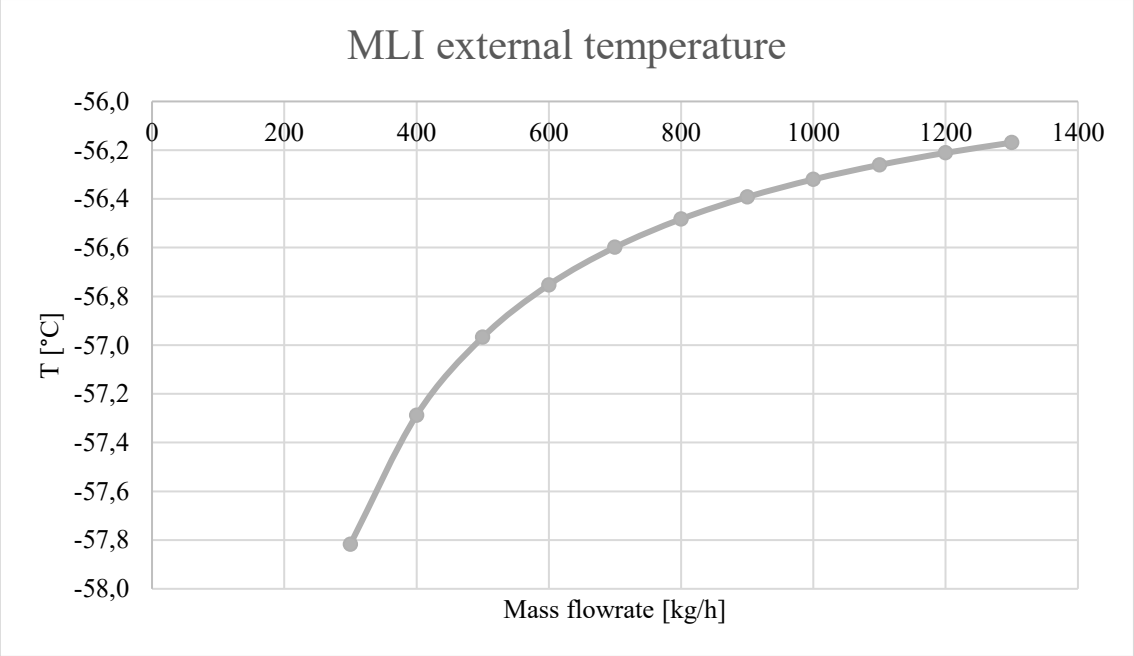

Figure 58 - MLI external temperature (Water and glycol)

The maximum temperature variation is 8 °C and the power losses are in the range 2.3 and 2.4 kW with therefore a medium specific power 23.5 W/m.

Water and glycol											
$\dot{m}$ [kg/h]	1300	1200	1100	1000	900	800	700	600	500	400	300
v [m/s]	1.27	1.17	1.07	0.98	0.88	0.78	0.68	0.59	0.49	0.39	0.29
Re [-]	2.2E+04	2.0E+04	1.9E+04	1.7E+04	1.5E+04	1.4E+04	1.2E+04	1.0E+04	8.4E+03	6.8E+03	5.1E+03
Nu [-]	1.6E+02	1.5E+02	1.4E+02	1.3E+02	1.2E+02	1.1E+02	9.5E+01	8.4E+01	7.3E+01	6.1E+01	4.8E+01
h [$W/m^2/K$]	3.2E+03	3.0E+03	2.8E+03	2.6E+03	2.4E+03	2.2E+03	1.9E+03	1.7E+03	1.5E+03	1.2E+03	9.9E+02
$T_{f.o}$ [°C]	78.1	78.0	77.8	77.5	77.3	76.9	76.5	75.9	75.1	74.0	72.0
$T_{MLI,ext}$ [°C]	-56.2	-56.2	-56.3	-56.3	-56.4	-56.5	-56.6	-56.8	-57.0	-57.3	-57.8
Q_{rad} [W]	47.4	47.3	47.3	47.2	47.2	47.1	47.0	46.8	46.6	46.3	45.8
Q_{lin} [W]	2311.1	2309.5	2307.7	2305.5	2302.8	2299.4	2295.1	2289.4	2281.4	2269.6	2250.1
Q_{tot} [W]	2358.4	2356.8	2354.9	2352.7	2349.9	2346.5	2342.0	2336.2	2328.0	2315.9	2295.9
%lin	0.98	0.98	0.98	0.98	0.98	0.98	0.98	0.98	0.98	0.98	0.98
%rad	0.02	0.02	0.02	0.02	0.02	0.02	0.02	0.02	0.02	0.02	0.02

Table 29 - Water and glycol results

A comparative table is presented as follows.

	H2O	H2O+glycol
T_{in} [°C]	80.0	80.0
$T_{out,wc}$ [°C]	73.4	72.0
ΔT_{max} [°C]	6.4	8

Table 30 - Fluids comparison

As the fluids' performances are almost the same, to have a bigger margin for negative temperature, the water glycol fluid was chosen.

6.3.4 System layout

The previous calculations were done in order to understand if the base thermal load can be totally or partially satisfied with the ASRG "waste" heat. A layout of the system is presented in Figure 59.

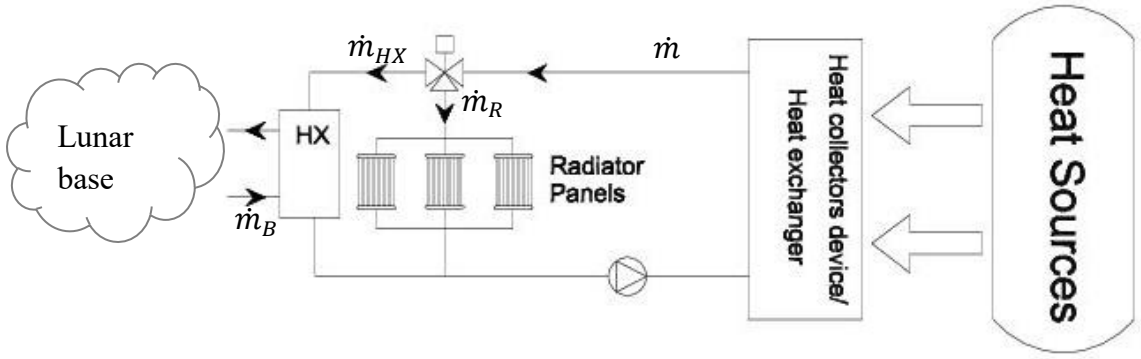

Figure 59 – TCS layout

Where:

- $\dot{m}$= total mass flowrate
- $\dot{m}_R$= radiators mass flowrate
- $\dot{m}_{HX}$= heat exchanger mass flowrate
- $\dot{m}_B$= base mass flowrate
- HX= heat exchanger

The primary circuit is from the heat collector device to the heat exchanger HX. The secondary circuit is the one that provides heat to the lunar base. The primary circuit has two loops. The first one is used to transfer heat from the source to the base, and the second one links the source with the radiators. This is because, in case it was not necessary to supply thermal power to the lunar base, the heat must be removed from the source however. For this reason, as a minimum flowrate has to circulate through the radiators, a first approximation can reasonably be 5 % of the total mass flowrate. Further considerations should be made to quantify this value. This is necessary to prevent fluid from freezing inside the pipe. The radiators should be sized to cool down the entire flowrate.

With these assumptions, and with the hypothesis of a 10 °C temperature gradient in the heat exchanger, it was calculated the thermal power yielded to the cold fluid in case of adiabatic heat exchanger, at various mass flowrate value Q_{HX} (See Table 31).

Heat exchanger power											
$\dot{m}$ [kg/h]	1300	1200	1100	1000	900	800	700	600	500	400	300
Q_{HX} [kW]	11.8	10.9	10.0	9.1	8.2	7.3	6.4	5.5	4.6	3.6	2.7

Table 31 - Heat exchanger power

In order to minimize also the power that the pump has to provide to overcome the pressure loss in the loop, it is necessary to work with low flowrate. The best configuration would be probably to work in the range 400-600 kg/h. With these hypotheses, knowing that the worst case base thermal load is 4.3 kW, it was analysed in what percentage it is possible to cover the power requirements.

$\dot{m}$ [kg/h]	Q_{HX} [kW]	%covered	% margin
400	3.6	85 %	-15 %
500	4.6	100 %	6 %
600	5.5	100 %	27 %

Table 32 - Power requirements analysis

With 500 and 600 kg/h, the power requirement is totally satisfied and there is a certain margin that can take into account the power loss in the distribution due to real system, and not ideal. In case of a flowrate of 400 kg/h, about 85 % of the thermal load is covered. Working with 600 kg/h, the inlet temperature in the heat exchanger is 75.9 °C and therefore, with a 10 °C temperature gradient, the fluid will exit at 65.9 °C.

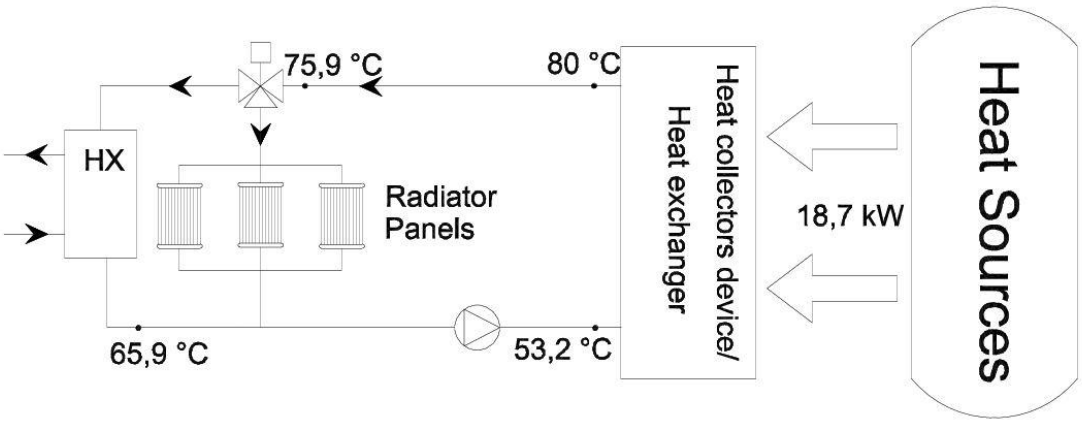

Figure 60 - Final TCS layout

The radiator panels are considered to be near the base heat exchanger in order to minimize the size and so the mass. This because they have to guarantee a 10 °C temperature difference (instead of about 27 °C) and exploit the further heat exchange in the return pipe. The return pipe should be size in order to guarantee the proper exit temperature.

Chapter 7

Conclusion

This is a preliminary study of a lunar base system design. Next steps of TCS design should be:

- Calculate the pump electrical power
- Size the heat exchanger as function of the heat transfer fluid exit temperature in the primary circuit
- Choose the secondary heat transfer fluid (air/water), see the operative outlet temperature and, in case it is not acceptable, change the minimum radiators flow rate
- Size the return pipe in order to permit an established heat transfer so that it will be possible to remove all ASRG excess heat
- Size the radiator panels at the nominal flow rate
- Investigate operative temperature range of the electronic equipment and provide thermal power in case of necessity
- Do the mass and power budget for the TCS

Further considerations on safety and reliability of the system must be done. Some assumptions have to be confirmed with other investigations, for example the presence of water and its distribution at South pole. Therefore, this is possible only with Moon exploration and data collection. Surely, in the next future, technologies will improve mainly in energy and power density with a consequent significant mass reduction. This thesis can represent a starting point in Moon manned missions. Other power configurations must be studied in order to understand what the best solution is.

References

Advanced stirling convertor. (s.d.). Tratto da Sunpower Inc.: https://sunpowerinc.com/it/benvenuto/

Advanced Stirling Radioisotope Generator (ASRG). (2018). Tratto da NASA: https://rps.nasa.gov/resources/65/advanced-stirling-radioisotope-generator-asrg/

Apollo 14 Press Kit. (1971). Tratto da NASA: https://history.nasa.gov/

Apollo 15 Mission Report. (1971). Tratto da NASA: www.nasa.gov

Apollo 16 Press Kit. (1971). Tratto da NASA: https://history.nasa.gov/

Apollo Lunar Module - Electrical Power System overviw. (s.d.). Tratto da NASA: https://www.nasa.gov/

Arridge, C. S. (s.d.). *Possible mission to the ice giants.* Tratto da Mullard Space science laboratory.

Arridge, C. S. (s.d.). *Uranus Pathfinder: Exploring the Origins and Evolution of Ice Giant Planets.* Tratto da Mullard Space Science Laboratory: https://www.mssl.ucl.ac.uk/planetary/missions/uranus/downloads/up_expastron_submitted.pdf

Beagle 2 lander. (s.d.). Tratto da ESA: http://www.esa.int/Our_Activities/Space_Science/Mars_Express/Beagle_2_lander

Beasley, D., Agle, D., & Tune, L. (2005). *Deep Impact Comet Encounter.* Tratto da Jet Propulsion Laboratory - NASA: https://www.jpl.nasa.gov/news/press_kits/deep-impact-encounter.pdf

Bennett, G. L. (1989). Energy Conversion Engineering Conference. *A LOOK AT THE SOVIET SPACE NUCLEAR POWER* (p. 1187-1194 vol.2.). IECEC-89. Proceedings of the 24th Intersociety. Tratto da Energy Conversion Engineering Conference.

Bennett, G. L. (2006). 4th International Energy Conversion Engineering Conference and Exhibit (IECEC) . *Space Nuclear Power: Opening the Final Frontier.* San Diego, California: American Institute of Aeronautics and Astronautics.

Berner, C., Bourillet, L., Casteren, J. v., Ellwood, J., Kasper, M., Kletzkine, P., . . . Bond, P. (2002). *Rosetta.* Tratto da ESA: http://www.esa.int/esapub/bulletin/bullet112/chapter1_bul112.pdf

Bibring, J., Rosenbauer, H., Boehnhardt, H., Ulamec, S., Biele, J., Espinasse, S., . . . Wittmann, K. (2007). THE ROSETTA LANDER ("PHILAE") INVESTIGATIONS. *Space Science Reviews*, 205-220.

Boeing's Rocketdyne Propulsion and Power division. (s.d.). *International Space Station Electric Power System (EPS).* Tratto da https://www.alternatewars.com/BBOW/Energy/ISS_EPS.pdf

Brinton, H. C., Mitchell, R. T., & Matson, D. L. (s.d.). *Cassini*. Tratto da Nasa Space Science Coordinated Archive: https://nssdc.gsfc.nasa.gov/planetary/planets/jupiterpage.html

Brown, D., Agle, D. C., & Friedlander, B. (2011). *Stardust-NEXT.* Tratto da NASA: www.nasa.gov

Bussey, D. B., Spudis, P., & Robinson, M. S. (1999). Illumination conditions at the lunar South Pole. *Geophysical Research Letters*.

Chan, J., Wood, J. G., & Schreiber, J. G. (2007). *Development of Advanced Stirling Radioisotope Generator for Space Exploration.* Tratto da NASA: https://ntrs.nasa.gov/search.jsp?R=20070021756

Chang'e. (2018, October). Tratto da ESA: https://earth.esa.int/web/eoportal/satellite-missions/c-missions/chang-e-1

Christophe, B., Spilker, L., Anderson, J., & Andrè, N. (2012). *OSS (Outer Solar System): A fundamental and planetary physics mission to Neptune, Triton and the Kuiper Belt.* Tratto da Cornell University: https://arxiv.org/pdf/1106.0132.pdf

Clausen, K. C., Hassan, H., Verdant, M., Couzin, P., Huttin, G., Brisson, M., & Sollazzo, C. (2002). THE HUYGENS PROBE SYSTEM DESIGN. *Space Science Reviews*, 155-189.

Crawford, I. A., & Joy, K. H. (2014). *Lunar exploration: opening a window into the history and evolution of the inner Solar System.* Tratto da Phil. Trans. R. Soc. A: http://rsta.royalsocietypublishing.org/

Daubar, I. (s.d.). MUSE - Mission for Uranus Science and Exploration. University of Arizona.

Douglas, I., & O'Donnell, F. (1997). *Mars Pathfinder - Press kit.* NASA.

Eckroad, S. (2003, December). Final report. *EPRI-DOE Handbook of Energy Storage for Transmission & Distribution Applications*. Washington, DC 20585: U. S. Department of Energy.

Electrical power system. (1969). In *Apollo operations handbook* (Vol. 1). NASA.

Emily Baldwin, S. C. (2016, October). *ExoMars - EUROPE'S NEW ERA OF MARS EXPLORATION.* Tratto da ESA: http://exploration.esa.int/exomars-2016-media-kit-landing

Enhanced Multi-Mission Radioisotope Thermoelectric Generator (eMMRTG) Concept. (s.d.). Tratto da NASA - Radioisotope power system: https://rps.nasa.gov/power-and-thermal-systems/power-systems/future/

European Space Agency. (2011). *JUICE - Exploring the emergence of habitable worlds around gas giants.* Tratto da ESA: https://www.esa.int/ESA

Fimmel, R., Willett, J., Dyal, P., & Jones, V. (s.d.). *Pioneer 10*. Tratto da NASA Space Science Coordinated Archive: https://nssdc.gsfc.nasa.gov/planetary/planets/jupiterpage.html

Fimmel, R., Willett, J., Dyal, P., & Jones, V. (s.d.). *Pioneer 11*. Tratto da NASA Space Science Coordinated Archive: https://nssdc.gsfc.nasa.gov/planetary/planets/jupiterpage.html

Finckenor, M., & Dooling, D. (1999). *Multilayer Insulation Material Guidelines.* Tratto da NASA.

Fission Surface Power Team. (2010). *Fission Surface Power System Initial Concept Definition.* Tratto da National Aeronautics and Space Administration and Department of Energy: https://ntrs.nasa.gov/search.jsp?R=20100033102

Fortescue P., S. G. (2011). *Spacecraft Systems Engineering.* John Wiley & Sons.

Garcia, M. (2017, August). *About the Space Station Solar Arrays*. Tratto da NASA: https://www.nasa.gov/mission_pages/station/structure/elements/solar_arrays-about.html

General Purpose Heat Source. (s.d.). Tratto da NASA: http://nuclear.gov/space/gphs.html

Gibson, M. A., Mason, L., Bowman, C., Poston, D. I., McClure, P. R., Creasy, J., & Robinson, C. (2014). *Development of NASA's Small Fission Power System for Science and Human Exploration.* Tratto da NASA Technical Report Service: https://ntrs.nasa.gov/search.jsp?R=20140017750

Grandl, W. (2007). Lunar Base 2015 Stage 1 - Preliminary Design Study. *Acta Astronautica*, 554-560.

Grandl, W. (2017). Human life in the Solar System. *REACH - Reviews in Human Space Exploration*, 9-21.

Hansen, C., Banfield, D., Bierhaus, E., Brown, M., & Colwell, J. (s.d.). *Neptune Mission Concept - A voyage through the outer solar system.*

Incropera, F. P., Dewitt, D. P., Bergman, T. M., & Lavine, A. S. (s.d.). *Introduction to heat transfer.* JOHN WILEY & SONS, INC.

Isbell, D., O'Donnell, F., & Hutchison, A. (1995). *Galileo Jupiter Arrival.* NASA.

ISEE (International Sun-Earth Explorer) Program. (s.d.). Tratto da ESA: https://earth.esa.int/web/eoportal/satellite-missions/i/isee

Jet Propulsion Laboratory - California Institute of Technology. (s.d.). *Juno Mission to Jupiter.* Tratto da NASA: www.nasa.gov

Jet Propulsion Laboratory - California Institute of Technology. (s.d.). *Jupiter Orbit Insertion - Press Kit.* Tratto da NASA: www.nasa.gov

Jet Propulsion Laboratory - California Institute of Technology. (s.d.). *Mars Science Laboratory Landing.* Tratto da NASA: www.nasa.gov

Jet Propulsion Laboratory - California Institute of Technology. (s.d.). *Mars Science Laboratory/Curiosity.* Tratto da NASA: www.nasa.gov

KRUSTY: FIRST OF A NEW BREED OF REACTORS, KILOPOWER PART II. (2017). Tratto da BEYOND NERVA - Nuclear Propulsion for humanity's expanse into the cosmos: https://beyondnerva.wordpress.com/

Kulcinski, G. L. (s.d.). *History of TOPAZ reactors.* Tratto da http://fti.neep.wisc.edu/neep602/SPRING00/lecture35.pdf

Landis, G. A. (2016). *A Hopper for Exploring Neptune's moon Triton.* Tratto da NASA: https://www.lpi.usra.edu/sbag/meetings/jun2016/presentations/oleson-landis.pdf

Landis, S. R. (2017). Triton Hopper: Exploring Neptune's Captured Kuiper Belt Object. *Planetary Science Vision 2050 Workshop 2017*.

Larson, W. J. (1999). *Space mission analysis and design.* Torrance CA (USA): Microcosm, Inc.

Lotfy, A., Anis, W. R., Atalla, M., Halim, J., & Abouelatta, M. (2017). Design an Optimum PV System for the Satellite Technology using High Efficiency Solar Cells. *International Journal of Computer Applications*.

Lu, J. Y. (2014). Thesis. *Uranus Orbiter and Probe Mission - Project Upsilon*. Austin: University of Texas.

(s.d.). *Mars Exploration Rover.* Pasadena CA: Jet Propulsion Laboratory - California Institute of Technology.

(s.d.). *Mars Pathfinder.* Pasadena CA: Jet Propulsion Laboratory - California Institute of Technology.

Mason, L., Gibson, M., & Poston, D. (2013). *Kilowatt-Class Fission Power Systems for Science and Human Precursor Missions.* Tratto da NASA: https://ntrs.nasa.gov/search.jsp?R=20140010823

Michael, M. (2009). Thesis. *Design of flywheel for improved energy storage*. Rourkela: Department of Mechanical Engineering - National Institute of Technology.

Ming Li, Z. S. (s.d.). Overview of China Chang'e-3 Mission and Development of Follow-on Mission.

Miotla, D. (2008). *Assessment of Plutonium-238 Production Alternatives.* Tratto da Energy.gov: https://www.energy.gov/sites/prod/files/NEGTN0NEAC_PU-238_042108.pdf

Mottaghi, S., & Benaroya, H. (2014). Design of a Lunar Surface Structure. I: Design Configuration and Thermal Analysis. *Journal of Aerospace Engineering*.

NASA Roadmap. (s.d.).

National Astronautics and Space Administration. (2015). *NASA Technology Roadmaps - TA 3: Space Power and Energy Storage.* Tratto da NASA: www.nasa.gov

NEAR mission profile. (2000). Tratto da NASA Space Science Data Coordinated Archive : https://nssdc.gsfc.nasa.gov/planetary/mission/near/near_traj.html

Neptune Orbiter. (s.d.). Tratto da Wikipedia: https://en.wikipedia.org/wiki/Neptune_Orbiter

New Horizons - The first Mission to Pluto and the Kuipier Belt: Exploring Frontier Worlds. (2006). Tratto da NASA: https://www.nasa.gov/pdf/139889main_PressKit12_05.pdf

Nuclear Power in Space. (s.d.). Tratto da https://web.archive.org/web/20080619143130/http://www.totse.com/en/technology/space_astronomy_nasa/spacnuke.html

Oh, D., Collins, S., Goebel, D., Hart, B., Lantoine, G., Snyder, S., . . . Rotlisburger, L. (2017). *Development of the Psyche Mission for NASA's Discovery Program.* Tratto da https://iepc2017.org/sites/default/files/speaker-papers/iepc-2017-153_psyche_mission_overview_final_0.pdf

OSIRIS-REx (Origins, Spectral Interpretation, Resource Identification, and Security–Regolith Explorer). (s.d.). Tratto da https://eoportal.org/web/eoportal/satellite-missions/pag-filter/-/asset_publisher/8jbNpfmcMhvK/content/osiris-rex?redirect=https%3A%2F%2Feoportal.org%2Fweb%2Feoportal%2Fsatellite-missions%2Fpag-filter%3Fp_p_id%3D101_

Östergård, R. (2011, December). Thesis . *Flywheel energy storage - a conceptual study*. Uppsala University.

Paige, D. A. (2010). Diviner Lunar Radiometer Observations of Cold Traps in the Moon's South Polar Region. *Science*, 479-482.

Palac, D., Gibson, M., Mason, L., Houts, M., McClure, P., & Robinson, R. (2016). *Nuclear Systems Kilopower Overview.* Tratto da NASA: https://www.nasa.gov/directorates/spacetech/game_changing_development/index.html

Phoenix. (2018). Tratto da NASA: https://solarsystem.nasa.gov/missions/phoenix/in-depth/

Pisacane, V. L. (2005). *Fundamentals of Space Systems.* Oxford University Press.

Radioisotope Power Systems Committee, National Research Council. (2009). *Radioisotope Power Systems: An Imperative for Maintaining U.S. Leadership in Space Exploration.* Tratto da The national academies press: http://www.nap.edu/catalog/12653.html

Ravera, F. (2017). *ExoMars - Rover module design report.* Thales Alenia Space.

Rayman, M. D., Varghese, P., Lehman, D. H., & Livesay, L. L. (1999). RESULTS FROM THE DEEP SPACE 1 TECHNOLOGY VALIDATION MISSION. *Acta Astronautica*, p. 475.

SAFT Batteries. (s.d.). Tratto da https://www.saftbatteries.com/

Saikia, S. J. (2014). A NEW FRONTIERS MISSION CONCEPT FOR THE EXPLORATION OF URANUS. *45th Lunar and Planetary Science Conference*.

Saikia, S. J. (2016). Oceanus Mission Concept Study. Purdue University.

Salh, H. (2014). Improving the Overall Efficiency of Radioisotope Thermoelectric Generators. *Advances in Energy and Power 2*, 21-26.

Savage, D., Webster, G., & Brand, D. (2004). *Mars Exploration.* NASA.

Schmidt, G., Sutliff, T., & Dudzinski, L. (2011). Radioisotope Power: A Key Technology for Deep Space Exploration. In N. Singh, *Radioisotopes - Applications in Physical Sciences* (p. 419-456). InTech.

Schmitz, P. C., & Partners, V. (2014). *Parametric System Model for a Stirling Radioisotope Generator.* Tratto da NASA: https://ntrs.nasa.gov/search.jsp?R=20150011441

Shearer, C., & Tahu, G. (s.d.). *Lunar Polar Volatiles Explorer (LPVE) - Mission concept study.* NASA.

Simonsen, L. C., Debarro, M. J., & Farmer, J. (1992). Conceptual design of a lunar base thermal control system. *The Second Conf. on Lunar Bases and Space Activities of the 21st Century*, 579-591.

Soil Temperatures on the Moon. (s.d.). Tratto da http://biocycle.atmos.colostate.edu/shiny/Moon/

Solar energy for space exploration. (s.d.). (NASA) Tratto da NASA: www.nasa.gov

Sorensen, T. C., & Spudis, P. D. (2005). The Clementine mission - A 10-year perspective. *Journal of Earth System Science*, 645-668.

SPACE Solar Cells. (s.d.). Tratto da AZUR SPACE: http://www.azurspace.com/index.php/en/

Stephenson, K., & Blancquaert , T. (2008). *NUCLEAR POWER TECHNOLOGIES FOR DEEP SPACE AND PLANETARY.* Tratto da ESA: http://emits.sso.esa.int/emits-doc/ESTEC/AO6233-SoW-RD1.pdf

Stone, E., Massey, E. B., Brunk, W. E., & Merwarth, A. C. (s.d.). *Voyager 1*. Tratto da NASA Space Science Coordinated Archive: https://nssdc.gsfc.nasa.gov/planetary/planets/jupiterpage.html

Stone, E., Massey, E. B., Brunk, W. E., & Merwarth, A. C. (s.d.). *Voyager 2*. Tratto da NASA Space Science Coordinated Archive: https://nssdc.gsfc.nasa.gov/planetary/planets/jupiterpage.html

Summerer, L., Gardini, B., & Gianfiglio, G. (2007). *ESA's approach to nuclear power sources for space applications.* Tratto da ESA.

Sutheesh, P., & Chollackal, A. (s.d.). *Thermal performance of multilayer insulation: A review.* Tratto da IOP Conference Series: Materials Science and Engineering: http://iopscience.iop.org/article/10.1088/1757-899X/396/1/012061/meta

Taranovich, S. (2014, January). *International Space Station (ISS) power system*. Tratto da EDN Network: https://www.edn.com/design/power-management/4427522/International-Space-Station--ISS--power-system

Tatsuaki Hashimoto, T. H. (2017). *Lunar polar exploration mission.* Tratto da Japan Aerospace Exploration Agency.

Thales Alenia Space. (2009). *NEXT.* Torino.

Thales Alenia Space. (2016). *Sample and return mission.* Torino.

The CONTOUR Spacecraft. (2002). Tratto da Spaceflight Now: https://spaceflightnow.com/delta/d292/020628contour.html

Thermal Conductivity: Aluminum. (s.d.). Tratto da efunda: http://www.efunda.com/materials/elements/TC_Table.cfm?Element_ID=Al

Travers, F. (2018, September). *Ice Confirmed at the Moon's Poles*. Retrieved from https://moon.nasa.gov/news/59/ice-confirmed-at-the-moons-poles/

Ulysses - Electrical power. (2006). Tratto da ESA: http://sci.esa.int/ulysses/31016-engineering/?fbodylongid=639

Ulysses - Thermal control. (2006). Tratto da ESA: http://sci.esa.int/ulysses/31016-engineering/?fbodylongid=643

Vale, S. C. (2015). Thesis. *Thermoelectric generator from space to automotive sector model and design for commercial and heavy duty vehicles*. Lisbona: Instituo Superior Tecnico.

VEGA PROJECT. (s.d.). Tratto da http://what-when-how.com/space-science-and-technology/vega-project/

Viking 1 Lander. (s.d.). Tratto da NASA: https://www.jpl.nasa.gov/missions/viking-1/

(1988). *Viking Mission to Mars.* Pasadena CA: Jet Propulsion Laboratory - California Institute of Technology.

Webster, J. L. (2006, March 28). *Cassini Spacecraft Engineering Tutorial.* Tratto da JPL: https://saturn.jpl.nasa.gov

Weisend, J. (2010). *Multilayer Insulation*. Tratto da Criogenic Society of America, Inc.: https://cryogenicsociety.org/resources/defining_cryogenics/multilayer_insulation/

Wicki, S., & Hansen, E. (2017). Clean energy storage technology in the making: An innovation systems perspective on flywheel energy storage. *Journal of Cleaner Production*, 1118-1134.

Williams, D. (s.d.). *Jupiter Fact Sheet*. Tratto da NASA Space Science Data Coordinated Archive: https://nssdc.gsfc.nasa.gov/planetary/factsheet/jupiterfact.html

Williams, D. (s.d.). *Mars Fact Sheet*. Tratto da NASA Space Science Data Coordinate Archive: https://nssdc.gsfc.nasa.gov/planetary/factsheet/marsfact.html

Williams, D. (s.d.). *Moon Fact Sheet*. Tratto da NASA Space Science Data Coordinate Archive: https://nssdc.gsfc.nasa.gov/planetary/factsheet/moonfact.html

Williams, D. R. (2003). *Hayabusa*. Tratto da NASA Space Scince Coordinated Archive: https://nssdc.gsfc.nasa.gov/planetary/planets/asteroidpage.html

Williams, D. R. (s.d.). *Moon Fact Sheet.* Tratto da NASA: www.nasa.gov

Williams, D. R. (s.d.). *Neptune Fact Sheet.* Tratto da Nasa Space Science Coortdinated Archive: https://nssdc.gsfc.nasa.gov/planetary/factsheet/neptunefact.html

Williams, D. R. (s.d.). *Pluto Fact Sheet.* Tratto da NASA Space Science Coordinated Archive: https://nssdc.gsfc.nasa.gov/planetary/factsheet/plutofact.html

Williams, D. R. (s.d.). *Saturn Fact Sheet.* Tratto da Nasa Space Science Coordinate Archive: https://nssdc.gsfc.nasa.gov/planetary/factsheet/saturnfact.html

Williams, D. R. (s.d.). *Uranus Fact Sheet.* Tratto da Nasa Space Science Coordinated Archive: https://nssdc.gsfc.nasa.gov/planetary/factsheet/uranusfact.html

Williams, D. R. (s.d.). *Viking Mission to Mars*. Tratto da NASA Space Science Data Coordinated Archive: https://nssdc.gsfc.nasa.gov/planetary/viking.html

Wilson, A. (2005). Giotto. *ESA Achievements*, p. 114-119.

Wu, S. (2016). *Satellite System Engineering - Power System Design.* Tratto da 1st APSCO & ISSI-BJ Space Science School.

Yoshimitsu, T., Kubota, T., & Nakatani, I. (s.d.). *MINERVA rover which became a small artificial solar satellite*. Tratto da Institute of Space and Astronautical Science - JAXA: https://digitalcommons.usu.edu/cgi/viewcontent.cgi?article=1554&context=smallsat

Appendix A

AZURSPACE
SOLAR POWER GMBH

30% Triple Junction GaAs Solar Cell
Type: TJ Solar Cell 3G30C - Advanced (80µm)
Best in Class EOL-Values!

This cell type is a GaInP/GaAs/Ge on Ge substrate triple junction solar cell (efficiency class 30% advanced and thickness 80µm). The end-of-life version of the 3G30C solar cell offers best EOL-performance values and should be combined with an external bypass diode protection.

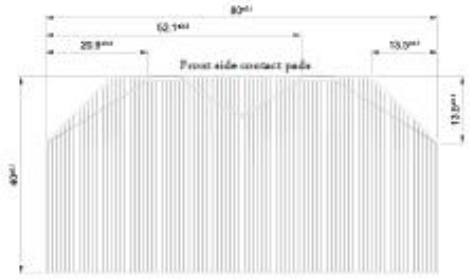

3G30C - Advanced (80µm)

Space

30% Triple Junction GaAs Junction Solar Cell
Type: TJ Solar Cell 3G30C - Advanced (80µm)

Design and Mechanical Data

Base Material	GaInP/GaAs/Ge on Ge substrate
AR-coating	TiO_x/Al_2O_3
Dimensions	40 x 80 mm ± 0.1 mm
Cell Area	30.18 cm²
Average Weight	≤ 50 mg/cm²
Thickness (without contacts)	80 ± 20 µm
Contact Metallization Thickness (Ag/Au)	3 – 10 µm
Grid Design	Grid system with 2 contact pads

Electrical Data

		BOL	2,5E14	5E14	1E15
Average Open Circuit V_{oc}	[mV]	2700	2616	2564	2522
Average Short Circuit I_{sc}	[mA]	520.2	518.5	514.0	501.9
Voltage at max. Power V_{mp}	[mV]	2411	2345	2290	2246
Current at max. Power I_{mp}	[mA]	504.4	503.2	500.6	486.6
Average Efficiency $\eta_{Zero\ (1367\ W/m^2)}$	[%]	29.5	28.6	27.8	26.5
Average Efficiency $\eta_{Zero\ (1353\ W/m^2)}$	[%]	29.8	28.9	28.1	26.8

Standard: CASOLBA 2005 (05-20MV1, etc); Spectrum: AMO WRC = 1367 W/m²; T = 28 °C @fluence 1MeV [e/cm²]

Acceptance Values

Voltage V_{op}	2350 mV
Min. average current $I_{op\ avg}$ @ V_{op}	505 mA
Min. individual current $I_{op\ min}$ @ V_{op}	475 mA

Temperature Gradients

			BOL	2E14	5E14	1E15
Open Circuit Voltage	$\Delta V_{oc}/\Delta T\uparrow$	[mV/°C]	- 6.2	- 6.5	- 6.6	- 6.7
Short Circuit Current	$\Delta I_{sc}/\Delta T\uparrow$	[mA/°C]	0.36	0.33	0.35	0.38
Voltage at max. Power	$\Delta V_{mp}/\Delta T\uparrow$	[mV/°C]	- 6.7	- 6.8	- 7.1	- 7.2
Current at max. Power	$\Delta I_{mp}/\Delta T\uparrow$	[mA/°C]	0.24	0.20	0.24	0.28

@fluence 1MeV [e/cm²]

Threshold Values

Absorptivity	≤ 0.91 (with CMX 100 AR)
Pull Test	> 1.6 N at 45° welding test (with 12.5µm Ag stripes)

3G30C - Advanced (80µm)

Space

Issue date:
2016-08-19

DB 0004148-00-01
Page 2 of 2

AZUR SPACE Solar Power GmbH
Theresienstr. 2
74072 Heilbronn
phone: +49 7131 67 2603
telefax: +49 7131 67 2727
e-mail: info@azurspace.com
website: www.azurspace.com

Certified Company

ISO 9001
ISO 14001
OHSAS 18001

Appendix B

Rechargeable lithium-ion battery
MP 174565 Integration™

High performance
Medium Prismatic cell

Saft always supplies MP cells in assemblies or as customized battery system constructions

Benefits

- Enhanced capacity
- Broad operating temperature range
- Extended autonomy and life for mobile systems
- Recommended for ruggedized designs
- Easy integration into compact and light systems
- Used in potentially explosible atmospheres
- High reliability
- Aluminium casing
- Very high energy density *(423 Wh/l and 175 Wh/kg)*
- Unrivalled low temperature performance

Key features

- Excellent charge recovery after long storage, even at high temperature
- Maintenance-free
- Long cycle life *(over 70 % initial capacity after 600 cycles, C charge rate, C/2 rate 100 % DoD at 20°C)*
- Non-restricted for transport/ Non-assigned to Class 9 according to the UN Recommendations on the transport of dangerous goods – Model Regulations
- Compliant with IEC 61960 standard and IEC 60079-11 intrinsic safety standard *(class T4 assignment between -20°C to +40°C)*
- Underwriters Laboratories *(UL)* Component Recognition

Main applications

- Mobile asset tracking
- Rack-mount telecom batteries
- Small UPS
- Future soldier equipment
- Portable radios
- Portable defibrillators
- Professional portable lighting
- Electric bikes and personal mobility

Electrical characteristics

Nominal voltage (1 A rate at 20°C)	3.75 V
Typical capacity 20°C (at 1 A 20°C 2.5 V cut-off)	4.8 Ah
Nominal energy	18 Wh

Mechanical characteristics (sleeved 100 % charged cell)

Thickness after 600 cycles *(Thickness tends to increase with cycling. Consult Saft)* *(At beginning of life 18.1 mm)*	19.7 mm
Width max	45.5 mm
Height max (including protection circuit)	70 mm
Typical weight (including protection circuit)	103 g
Lithium equivalent content	1.44 g
Volume	42.50 cm³

Operating conditions

Charge method	Constant Current/Constant Voltage
End charge voltage	4.20 +/– 0.05 V
Maximum recommended charge current**	5.0 A (~C rate)
Charge temperature range*	–20°C to +60°C
Charge time at 20°C	To be set as a function of the charge current: C rate → 2 to 3 h; C/2 rate → 3 to 4 h; C/5 rate → 6 to 7 h
Maximum continuous discharge current**	10 A
Pulse discharge current at 20°C	up to 20 A (~4C rate)
Discharge cut-off voltage	2.5 V
Discharge temperature range*	–50°C to +60°C

* *For optimized charging below 0°C, 60°C and discharging at –50°C, consult Saft.*
** *Electronic protection circuits within battery packs may limit the maximum charge/discharge current allowable. Consult Saft.*

saft

September 2009

MP 174565 Integration™

Battery assembly

In order to operate properly, individual Li-ion cells are mechanically and electrically integrated in battery assemblies specific to each application. The battery assembly incorporates electronics for performance, thermal and safety management.

Technology

- Graphite-based anode
- Lithium Cobalt oxide-based cathode
- Electrolyte: organic solvents
- Built-in redundant safety protections *(shutdown separator, circuit breaker, safety vent)*
- Batteries assembled from MP cells feature an electronic protection circuit

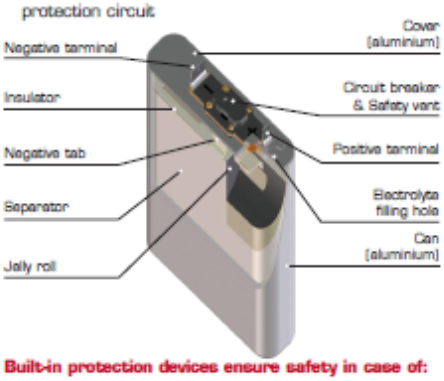

Built-in protection devices ensure safety in case of:

- Exposure to heat
- Exposure to direct sunlight for extended periods of time
- Short circuit
- Overcharge
- Overdischarge

When handling Saft MP batteries:

- Do not disassemble
- Do not remove the protection circuit
- Do not incinerate

Transportation and storage:

- Store in a dry place at a temperature preferably not exceeding 30°C
- For long-term storage, keep the battery within a 30 ± 15 % state of charge

Capacity versus current at 20°C

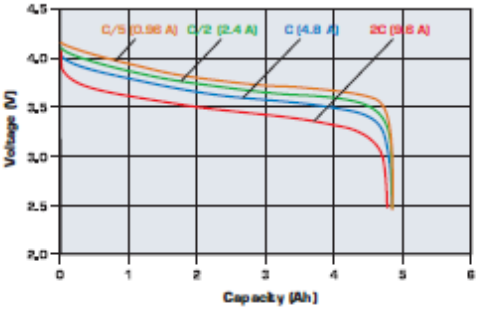

Typical discharge profiles (0.96 A - C/5 rate)

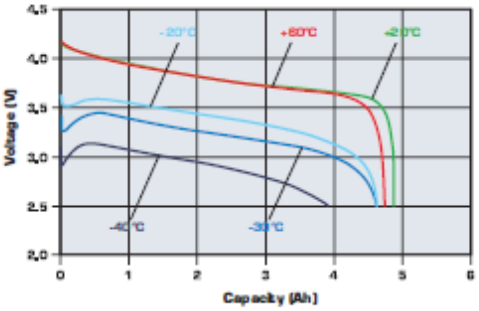

Charge characteristics to 4.2 V at +20°C

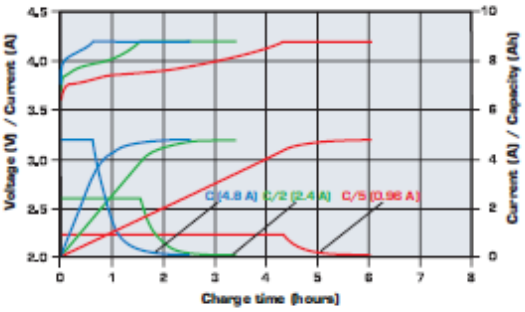

Saft
Specialty Battery Group
12, rue Sadi Carnot
93170 Bagnolet - France
Tel.: +33 (0)1 49 93 19 18
Fax: +33 (0)1 49 93 19 69

313 Crescent Street
Valdese, NC 28690 - USA
Tel.: +1 (828) 874 41 11
Fax: +1 (828) 879 39 81

www.saftbatteries.com

Doc. N° 54065-2-0809

Published by the Communications Department.

Photo credit: Saft.

Société anonyme au capital de 31 944 000 €
RCS Bobigny B 383 703 873

Produced by Arthur Associates Limited.

Appendix C

```
clear
close all
clc

%Material data input
LL=17; %[m]
rint=2; %[m]
r1=rint+37.2e-3; %[m]
k1=280; %[W/m/K]
r2=r1+.25; %[m]
k2=0.042; %(W/m/K)
r3=r2+.63; %[m]
k3=0.011; %(W/m/K)
r4=r3+82.8e-3; %[m]
k4=237; %(W/m/K)

RR=1/k1*log(r1/rint)+1/k2*log(r2/r1)+1/k3*log(r3/r2)+1/k4*log(r4/r3);

eps=0.8;
sigma=5.670373e-8;          %Stephan-Boltzmann constant [W m^-2 K^-4]
hh=10;                      %Convective int HTC [W m^-2 K]
Tp=120;                     %sink temperature [K]
Ti=23+273;                  %internal temperature [K]


Tfun=@(Tout)(hh*rint*Ti-hh*rint*(hh*Ti*rint+Tout/RR)/(hh*rint+1/RR)-
eps*sigma*r4*Tout^4+eps*sigma*r4*Tp^4);

tol=1e-4;
dx=1e-5;
[Tface,err,NN]=fzero_Newton(Tfun,dx,500,tol,500);
% Tout=(kk/ss*Tface+hh*Tw)/(hh+kk/ss);
qq=eps*sigma*(-Tp^4+Tface^4);
fprintf('The temperature of the wall on the sink side is %.2f K, the
heat load %.2f W/m^2.\n',Tface,qq);
Twi=(rint*hh*Ti+Tface/RR)/(hh*rint+1/RR);

Aext=2*pi*r4*LL;
Abase=pi*r4^2*2;
Atot=5*(Aext+Abase);
QQ=qq*Atot;
%% Temperature profile

dr=1e-4;

rr=(rint:dr:r4)';
kk=k1*(rr<=r1)+k2*(rr>r1 & rr<=r2)+k3*(rr>r2 & rr<=r3)+k4*(rr>r3 &
rr<=r4);

help1=ones(length(rr),1);
maindiag=-2/dr^2*help1;
diag_up=1./(2*rr(1:end-1)*dr)+1/dr^2;
diag_low=-1./(2*rr(2:end)*dr)+1/dr^2;
```

```
aux=[[0;diag_up] maindiag [diag_low;0]];
AA=spdiags(aux,[1 0 -1],length(rr),length(rr));
AA=full(AA);
bb=zeros(length(AA),1);

% Boundary conditions
AA(1,1)=+k1/dr/hh+1;
AA(1,2)=-k1/dr/hh;
bb(1)=Ti;

AA(end,end-1)=0;
AA(end,end)=1;
bb(end)=Tface;

N1=round((r1-rint)/dr)+1;
N2=round((r2-rint)/dr)+1;
N3=round((r3-rint)/dr)+1;

AA(N1,N1-1)=-k1/dr;
AA(N1,N1)=k1/dr+k2/dr;
AA(N1,N1+1)=-k2/dr;
bb(N1)=0;

AA(N2,N2-1)=-k2/dr;
AA(N2,N2)=k2/dr+k3/dr;
AA(N2,N2+1)=-k3/dr;
bb(N2)=0;

AA(N3,N3-1)=-k3/dr;
AA(N3,N3)=k3/dr+k4/dr;
AA(N3,N3+1)=-k4/dr;
bb(N3)=0;

%System solution
TT=AA\bb;

figure(1)
plot(rr,TT,'k-','linewidth',1.5)
grid on
box on
xlabel('r [m]')
ylabel('T [K]')
xlim([rint r4])
title('Temperature distribution')
print -depsc -f1 TempDistr
print -djpeg -f1 TempDistr
```

```
function [xx,err,num_iter,residual] =
fzero_Newton(funct,h,x0,tol,nmax)
    %NEWTON

    num_iter=0;
    err=tol+1;
    xx=x0;
    fun=feval(funct,xx);
    residual = norm(fun);

    while (err(end)>tol || residual>tol)

        deltax=-numericalJacobian(funct,xx,h)\fun;
        xx=xx+deltax;
        num_iter=num_iter+1;
        err(num_iter)=norm(deltax);
        fun=feval(funct,xx);
        residual=norm(fun);
        if num_iter>nmax
            error('Convergence not reached: choose a larger precision
or a better x0')
        end
    end

end

function numJac = numericalJacobian(func,pos,step)

    n=length(pos);
    numJac=zeros(n,n);
    %Evaluation of the derivative or jacobian of the function through
finite differences
    for j=1:n
        xx_up=pos;
        xx_up(j)=xx_up(j)+step/2;
        xx_dw=pos;
        xx_dw(j)=xx_dw(j)-step/2;
        f_up=feval(func,xx_up);
        f_dw=feval(func,xx_dw);
        numJac(:,j)=(f_up-f_dw)/step;
    end

end
```